Application of Fe(III)-EDDS complex in advanced oxidation processes : 4-ter-butylphenol degradation

Yanlin Wu

N° d'ordre : D.U. 2455

UNIVERSITE BLAISE PASCAL

U.F.R. Sciences et Technologies

ECOLE DOCTORALE DES SCIENCES FONDAMENTALES

N° 786

THESE

Présentée pour obtenir le grade de

DOCTEUR D'UNIVERSITE
Spécialité : Chimie Physique

Par Yanlin WU

Application of Fe(III)-EDDS complex in advanced oxidation processes : 4-tert-butylphenol degradation

---

Soutenue publiquement le 16 mai 2014 devant la commission d'examen.

Rapporteurs :

Pr. Feng WU (Université de Wuhan, Chine)
Pr. Jean-Marc CHOVELON (Université de Lyon 1, France)

Examinateurs :

Dr. Hongjing LI (Université de Fudan, Chine)
Dr. Marcello BRIGANTE (Université Blaise Pascal, France)
Pr. Wenbo DONG (Université de Fudan, Chine)

Pr. Gilles MAILHOT (Université Blaise Pascal, France)

<u>Invités</u> :

Pr. Khalil HANNA (Ecole Nationale Supérieure de Chimie de Rennes, France)

Abstract

Advanced Oxidation Processes (AOPs) have been proved to be successfully applied in the treatment of sewage. It can decolorize the wastewater, reduce the toxicity of pollutants, convert the pollutants to be a biodegradable by-product and achieve the completed mineralization of the organic pollutants. The Fenton technologies which are performed by iron-activated hydrogen peroxide (H_2O_2) to produce hydroxyl radical ($HO^{\bullet}$) has been widely investigated in the past few decades. Recently, Sulfate radical ($SO_4^{\bullet-}$) which was produced by the activation of persulfate ($S_2O_8^{2-}$) is applied to the degradation of organic pollutants in water and soil. It is a new technology recently developed. It is also believed to be one of the most promising advanced oxidation technologies.

In this study, a new iron complex is introduced to the traditional Fenton reaction. The ferric iron (Fe(III)) and Ethylene diamine-*N,N'*-disuccinic acid (EDDS) formed the complex named Fe(III)-EDDS. It can overcome the main disadvantage of traditional Fenton technology, which is the fact that traditional Fenton technology can only perform high efficiency in acidic condition. Simultaneously, EDDS is biodegradable and it is one of the best environment-friendly complexing agents. On the other hand, the transition metal is able to activate $S_2O_8^{2-}$ to generate $SO_4^{\bullet-}$. Therefore, Fe(III)-EDDS will also be applied to activate $S_2O_8^{2-}$ in the present study.

4-tert-Butylphenol (4-t-BP) has been chosen as a target pollutant in this study. It is widely used as a chemical raw material and is classified as endocrine disrupting chemicals due to the estrogenic effects. The 4-t-BP degradation rate ($R_{4\text{-t-BP}}$) is used to

indicate the efficiency of the advanced oxidation processes which are based on Fe(III)-EDDS utilization. The main contents and conclusions of this research are shown as follows:

In the first part, the chemical structure and properties of Fe(III)-EDDS and the 4-t-BP degradation efficiency in UV/Fe(III)-EDDS system were studied. The results showed that Fe(III)-EDDS was a stable complex which was formed by the Fe(III) and EDDS with the molar ratio 1:1. From the photoredox process of Fe(III)-EDDS, the formation of hydroxyl radical was confirmed including that $HO^{\bullet}$ is the main species responsible for the degradation of 4-t-BP in aqueous solution. Ferrous ion (Fe(II)) was also formed during the reaction. With the increasing Fe(III)-EDDS concentration, 4-t-BP degradation rate increased but is inhibited when the Fe(III)-EDDS concentration was too high. Indeed, Fe(III)-EDDS is the scavenger of $HO^{\bullet}$. pH value had a significant effect on the degradation efficiency of 4-t-BP that was enhanced under neutral or alkaline conditions. On the one hand, Fe(III)-EDDS presented in the FeL^{-}, $Fe(OH)L^{2-}$, $Fe(OH)_2L^{3-}$, $Fe(OH)^{4-}$ four different forms under different pH conditions and they had different sensitivity to the UV light. On the other hand, pH value affected the cycle between Fe(III) and Fe(II). The formation of hydroperoxy radicals ($HO_2^{\bullet}$) and superoxide radical anions ($O_2^{\bullet-}$) ($pk_a = 4.88$) as a function of pH was also one of the reasons. It was observed that O_2 was an important parameter affecting the efficiency of this process. This effect of O_2 is mainly due to its important role during the oxidation of the first radical formed on the pollutant.

The second part of the research mainly investigated the mechanism of Fe(III)-

EDDS activating H_2O_2 and producing $HO^{\bullet}$, named Fenton-like process in this study. The work was performed in a large range of pH which was the key parameter influencing the efficiency of pollutant in the traditional Fenton process. The effects of Fe(III)-EDDS concentration, H_2O_2 concentration, oxygen concentration were also studied. The results showed that the 4-t-BP removal was slow in Fenton-like process. With the increasing Fe(III)-EDDS or H_2O_2 concentration, $R_{4\text{-t-BP}}$ firstly increased and then decreased. When the pH value increased from 2.0 to 9.0, $R_{4\text{-t-BP}}$ showed increasing trend in Fenton-like reaction. The 4-t-BP degradation rate accelerated when the dissolved oxygen concentration increased.

In the third part, the 4-t-BP degradation efficiency in UV/Fe(III)-EDDS/H_2O_2 (photo Fenton-like) process was investigated. A series of experiments were performed to investigate the oxidation efficiency of UV/Fe(III)-EDDS/H_2O_2 system. The effects of irradiation time, pH value, Fe(III)-EDDS concentration, H_2O_2 concentration and dissolved oxygen concentration on the degradation performance of 4-t-BP in this photo Fenton-like process were also investigated. The results showed that the 4-t-BP removal efficiency in photo Fenton-like reaction was much higher than that in Fenton-like reaction. With the increasing Fe(III)-EDDS concentration, $R_{4\text{-t-BP}}$ showed firstly increased and then decreased. With the increasing H_2O_2 concentration, $R_{4\text{-t-BP}}$ kept increasing and the optimal pH value was 7.5 in photo Fenton-like reaction. The target pollutant could be efficiently degraded at neutral pH or even alkaline condition. It overcame significant deficiency of the traditional Fenton reaction. This is the main advantage of this new iron complex. The 4-t-BP degradation rate also accelerated

when the dissolved oxygen concentration increased.

In the fourth part, 4-t-BP was degraded by $SO_4^{\bullet-}$ radical which were produced in UV/Fe(III)-EDDS/ $S_2O_8^{2-}$ system. The effect of Fe(III)-EDDS concentration, $S_2O_8^{2-}$ concentration and pH value on the degradation performance of 4-t-BP was investigated. It was observed that 4-t-BP was degraded efficiently in UV/Fe(III)-EDDS/$S_2O_8^{2-}$ system. According to the result of pH effect on both UV/Fe(III)-EDDS/$S_2O_8^{2-}$ and UV/Fe(III)/ $S_2O_8^{2-}$ systems, UV/ Fe(III)-EDDS/$S_2O_8^{2-}$ system was significantly better than UV/Fe(III)/$S_2O_8^{2-}$ system. With the increasing Fe(III)-EDDS concentration, $R_{4\text{-t-BP}}$ also showed firstly increased and then decreased in UV/Fe(III)-EDDS/$S_2O_8^{2-}$ system. When $S_2O_8^{2-}$ concentrations were lower than 1 mM, 4-t-BP degradation rate increased with the increasing $S_2O_8^{2-}$ concentration. Steady-state experiments and transient laser flash photolysis experiments were performed to determine the second order reaction rate constants. $k_{4\text{-t-BP, SO4}\bullet-}$, $k_{4\text{-t-BP, HO}\bullet}$, $k_{2\text{-Propanol, SO4}\bullet-}$ and $k_{\text{t-BuOH, SO4}\bullet-}$ were determined as 4.42×10^9 M^{-1} s^{-1}, 1.61×10^{10} M^{-1} s^{-1}, 6.68×10^7 M^{-1} s^{-1} and 7.88×10^5 M^{-1} s^{-1}, respectively. In the UV/Fe(III)-EDDS/ $S_2O_8^{2-}$ system, $SO_4^{\bullet-}$ is the major contribution to 4-t-BP degradation, much significant than the contribution of $HO^{\bullet}$.

Keywords：Photochemistry, Fe(III)-EDDS，Fenton-like，Hydroxyl radical，Persulfate, Sulfate radical, Endocrine disrupting chemicals, 4-t-BP

Acknowledgments

This project has been carried out in the cooperation between Fudan University and Blaise Pascal University. The writing of this thesis has been one of the most significant academic challenges I have ever had to face. Without the support, patience and guidance of the following people, this thesis would not have been completed. It is to them that I owe my sincere gratitude.

I would like to express the deepest gratitude to my Chinese supervisor Professor Wenbo Dong, who provided academic support and facilities for me to carry out researches in Fudan University. His mentorship is paramount in providing a well-rounded experience consistent my long-term career goals. He encouraged me to not only grow as a researcher but also as an independent thinker.

I am extremely grateful to Dr. Gilles Mailhot, my supervisor in Blaise Pascal University, who has always made himself available to clarify my doubts despite his many other academic and professional commitments. I consider it as a great opportunity to do my doctoral programme under his guidance and to learn from his research expertise. I also wish to express my gratitude to Dr. Marcello Brigante who provided me instruction for the laboratory experiments and his brilliant suggestions on solving various problems.

Many heartfelt thanks to all other members of the laboratory in France, Pr. Mohamed Sarakha, Mr. Guillaume Voyard, Pr. Pascal Wong Wah Chung, Dr. Monica

Passananti, Ms. Bienvenue Bafai, Ms. Angelica Bianco. My friends Ms. Marie Siampiringue, Ms. Eliana Silva, Ms. Shirin Monadjemi, Ms. Xiaobing Wang have always been a great support ever since I came to Clermont-Ferrand, and I owe them so much for their care and hospitality. Pr. Khalil Hanna who provided me a precious opportunity to do research in Ecole Nationale Supérieure de Chimie de Rennes, I appreciate his supportive guidance and encouragement.

I would like to thank the Department of Environment Science and Engineering at Fudan University, especially those members of my doctoral committee for their input, valuable discussions and accessibility. In particular, I would like to thank HongJing Li, who was kind enough to undertake the editing work and I acknowledge the meticulous work she has done. I received generous support from Mr. Peng Wang, who helped in assistance of laboratory experiments and literature search. I would like to express my sincere gratitude to him.

Thanks to the funding support from China Scholarship Council (CSC), National Natural Science Foundation of China (NSFC 21077027), Shanghai Tongji Gao Tingyao Environmental Science & Technology Development Foundation (STGEF), and the Graduate Innovative Fund of Fudan University (No. 13). This work was also supported by one project CMIRA founded by the Rhône-Alpes Region, the "Federation des Recherches en Environnement" through the CPER "Environnement" founded by the "Région Auvergne," the French government, FEDER from the European community, and the CNRS program EC2CO. Thanks for Ms. Jingmei Zhao who works in the Office of Educational Affairs of the Embassy of P.R. China in

France. I really appreciate this valuable opportunity to study in France.

Finally and most importantly, I would like to thank my family. My parents' support and encouragement were undeniably the bedrock upon which my life has been built. I appreciate their faith in me and allowing me to be as ambitious as I wanted. I would like to thank my fiance Longfei Wang, I couldn't tackle those challenges without his support.

Contents

Introduction

With the development of industry, the organic water pollution has become one of the most important fields in the environmental problems. In order to make the organic pollutant efficiently removed, the advanced oxidation processes (AOPs) are widely studied and applied in wastewater treatment. AOPs refer to a set of chemical treatment procedures designed to remove organic pollutants by oxidation through reactions with hydroxyl radicals ($HO^{\bullet}$) or other oxidative radicals. In the actual applications of wastewater treatment, this term usually refers more specifically to a subset of such chemical processes that employed ozone (O_3), hydrogen peroxide (H_2O_2) and/or UV light.

The Fenton reaction (Fe(II)/H_2O_2) and photoFenton reaction (UV/Fe(III)/H_2O_2) which can decompose most organics are important AOPs in wastewater treatment. However, they still have many shortcomings, specifically the strict acid pH range. In order to improve the efficiency of traditional Fenton/photoFenton reaction, the Fe(III)-EDDS complex was used for the organic pollutants degradation. The most obvious advantages of the Fe(III)-EDDS complex application are the low process costs, wide irradiation wavelengths, biodegradable and a pH range that is relatively wider than that of traditional Fenton and photo-Fenton processes (optimal pH around 3).

The AOPs based on activated persulfate ($S_2O_8^{2-}$) are widespread concerned due to

the advantages for the efficient degradation and the use of simple equipment. It has become a hot research issue all over the world. Indeed, the sulfate radical ($SO_4^{\bullet-}$) is also a strong oxidant. Because of its relative long life time and it may yield a greater mineralization than $HO^{\bullet}$, $SO_4^{\bullet-}$ has been used as a potential oxidative radical for remediation of contaminated water and soil. The key point of using $S_2O_8^{2-}$ for AOPs is the way to activate $S_2O_8^{2-}$. However, UV/Fe(III)-EDDS reaction can produce Fe(II) which can efficiently activate $S_2O_8^{2-}$ to generate $SO_4^{\bullet-}$.

4-tert-butylphenol (4-t-BP) is an alkylphenols (APs) and is one of the endocrine-disrupting chemicals (EDCs) with highly estrogenic effects. 4-t-BP has been largely used as a raw material for polymerization inhibitors and stabilizing agents in the chemical industry, and so it is widely detected in food, aquatic animals, human urine, and rivers. The serious threat to human health has already been made clear. It can cause reproductive disturbance in humans and wildlife. So it would be of great urgency to degrade 4-t-BP artificially in our living surroundings. For those reasons, we used 4-t-BP as a target pollutant in this work.

The purpose of this study was as follow: I.) Make a comprehensive understanding of the photochemical properties of Fe(III)-EDDS; II.) Make a further understanding of the role played in Fenton-like and photo Fenton-like system by Fe(III)-EDDS. Get a clear reaction mechanism, including parameters effect on the degradation of 4-t-BP; III.) Try to activate $S_2O_8^{2-}$ with Fe(III)-EDDS. 4-t-BP would be degraded by $SO_4^{\bullet-}$. And finally, compare the advantages and disadvantages between $SO_4^{\bullet-}$ and $HO^{\bullet}$ oxidation systems.

Firstly, the photo activity of Fe(III)-EDDS was investigated in this study. The effect of irradiation time, pH, Fe(III)-EDDS concentration, and O_2/N_2 on the photodegradation performance of 4-t-BP under UV light irradiation (300 nm < λ < 500 nm) was investigated. The second-order reaction rate constant between 4-t-BP and $HO^{\bullet}$ ($k_{4\text{-t-BP},\ HO\bullet}$) was also evaluated for the first time. Secondly, Fe(III)-EDDS was applied in Fenton-like and photo Fenton-like processes. The removal efficiency of 4-t-BP was followed in both processes. The effects of irradiation time, pH value, Fe(III)-EDDS, H_2O_2 and O_2 concentrations on the degradation performance of 4-t-BP were investigated. Thirdly, the 4-t-BP degradation by $SO_4^{\bullet-}$ oxidation was investigated in this study. The $SO_4^{\bullet-}$ was produced through the activation of $S_2O_8^{2-}$ in the presence of Fe(III)-EDDS. The effect of irradiation time, pH value, Fe(III)-EDDS concentration and $S_2O_8^{2-}$ concentration on the photodegradation performance of 4-t-BP was investigated. The second-order reaction rate constant of the reaction between 4-t-BP, 2-Propanol, tert-butanol and $SO_4^{\bullet-}$ were also evaluated for the first time by laser flash photolysis experiments.

Chapter 1

BIBLIOGRAPHY

Chapter 1 Bibliography

1.1 Advanced oxidation Processes (AOPs)

With the rapid development of modern industry of mankind, the natural environment is suffering a heavy burden. Many of emerging pollutants appear in the natural waters with the development of industry and it attracts the attention of researchers all over the world. The innovative wastewater treatment is needed for the elimination of such emerging contaminants.

Advanced oxidation processes (AOPs) are efficient technologies for the elimination of pollutants which spring up in the 1980s. The AOPs concept was established by Glaze et al.[1-23] who defined AOPs as processes involving the generation of highly reactive oxidizing species able to attack and degrade organic substances. These species, mainly $HO^{\bullet}$ (E^{o} = 2.80 V), have high oxidation capability and could induce a series of radical chain reactions to make that the organic pollutants degrade and are mineralized [4-5]. Free radicals in AOPs may be produced by non-photochemical and photochemical processes. Non-photochemical oxidation processes include ozone oxidation [6-78], traditional Fenton process [9-101112], chlorine dioxide oxidation [13-14], electrochemical oxidation [15-1617], wet air oxidation [18-19],

supercritical water oxidation [20-21] and ultrasonic oxidation [22-23]. Photochemical oxidation processes include UV/O_3 [24-25], UV/H_2O_2 [26], UV/TiO_2 [27-2829], photo Fenton process [30-3132]. However, in recent years, many studies have suggested that AOPs can also generate sulfate radical ($SO_4^{\bullet-}$) [33-3435] besides $HO^{\bullet}$.

The typical mechanisms of reaction between $HO^{\bullet}$ with organic pollutants are: i.) H abstraction from the organic molecule by $HO^{\bullet}$ and the subsequent formation of H_2O and the corresponding organic radical; ii.) addition of $HO^{\bullet}$ to the organic pollutants; iii.) electron transfer from the organic pollutants to $HO^{\bullet}$ [36].

The typical mechanism for $SO_4^{\bullet-}$ to attack pollutants is due to the lone pair of electrons. It has high oxidative capacity to oxide and mineralize the pollutants. The reaction pathway was similar with $HO^{\bullet}$.

AOPs are used in the treatment of organic pollutants, especially non-biodegradable compounds including organic dyes [37-38], antibiotics [39-4041], pesticides [42-43], landfill leachate [44] and so on. The advantages of AOPs are high degradation efficiency, non-selective and low cost. They have been used as the pretreatment technologies to improve the biodegradability of pollutants and also associate to the pollutants removal [45-4647].

1.2 Oxidation Process with iron species generating $HO^{\bullet}$

1.2.1 Fenton and photoFenton reactions

The chemical oxidation based on iron is an important part of advanced oxidation

technology. As we all know, iron is very common on the Earth as a chemical element. It exists in different media with different forms and also widely present in natural waters. The total iron concentration has been reported in rivers, lakes around the world (such as United Kingdom, the Atlantic, United States and Israel) [48-49] and also in Fog water, rain water [50-5152]. The dissolved iron concentration is ranged between 0.04-91 μmol L^{-1}. Therefore, the effective application of iron in AOPs will be an important development direction for the future wastewater treatment.

In 1894, chemist Mr. H.J.H. Fenton found that the solution mixed with Fe(II) and hydrogen peroxide (H_2O_2) (named Fenton reagent) had strong oxidation ability, which could oxidize many kinds of organic compounds (such as carboxylic acids, alcohols, and esters) and convert them to CO_2, H_2O and inorganic compounds efficiently [53]. But it would not attract attention of researchers until more than half century later. In the 1970s and 1980s, Fenton reagent found its position in the field of environmental chemistry. Fenton reaction was used in the degradation of refractory organic pollutants, such as polysaccharides [54], chlorophenol [55], chlorobenzene, formic acid, polychlorinated biphenyls [56], nitrophenol [57], dyes [58], atrazine [59] in wastewater and landfill leachate [60-61]. The chain reaction in Fenton process is shown in R1-1and R1-2 [62-63].

$$Fe^{2+} + H_2O_2 \rightarrow Fe^{3+} + HO^{\bullet} + OH^{-} \quad k = 76\ M^{-1}\ s^{-1} \text{ (R1-1)}$$

$$Fe^{3+} + H_2O_2 \rightarrow Fe^{2+} + HO_2^{\bullet} + H^{+} \quad k = 0.001\text{-}0.01\ M^{-1}\ s^{-1} \text{ (R1-2)}$$

The two radicals ($HO_2^{\bullet}$, $HO^{\bullet}$) are generated or consumed by the following reactions (R1-3 to R1-6) [64]:

$$Fe^{2+} + HO_2^{\bullet} \rightarrow Fe^{3+} + OH_2^- \quad k = 1.2\times10^6\ M^{-1}\ s^{-1} \text{ (R1-3)}$$

$$Fe^{3+} + HO_2^{\bullet} \rightarrow Fe^{2+} + O_2 + H^+ \quad k < 1.0\times10^3\ M^{-1}\ s^{-1} \text{ (R1-4)}$$

$$H_2O_2 + HO^{\bullet} \rightarrow HO_2^{\bullet} + H_2O \quad k = 2.6\times10^7\ M^{-1}\ s^{-1} \text{ (R1-5)}$$

$$Fe^{2+} + HO^{\bullet} \rightarrow Fe^{3+} + OH^- \quad k = 3.2\times10^8\ M^{-1}\ s^{-1} \text{ (R1-6)}$$

Moreover, iron is a photoreactive species and it will produce some oxidizing active radicals ($HO^{\bullet}$, $HO_2^{\bullet}$, $O_2^{\bullet-}$) through direct or indirect photochemical reaction. The oxidizing active radicals are the key factors for the degradation of pollutants. Under the conditions of pH = 2.5-5, the main form of dissolved ferric iron (Fe^{3+}) is iron hydroxy complex $Fe(OH)^{2+}$ and it can produce $HO^{\bullet}$ through its photolysis as shown in reaction R1-7. The quantum yield of $HO^{\bullet}$ production at 360 nm UV light was determined to be 0.075 [65] in this chemical reaction. The Fe(II) produced by photo reduction can be oxidized to Fe(III) by the oxygen in the solution. So the Fe(III)/Fe(II) redox cycle will produce oxidative radicals in the solution [66].

$$Fe(OH)^{2+} \xrightarrow{h\nu} Fe(II) + HO^{\bullet} \text{ (R1-7)}$$

In the 1990s, according to the mechanism of Fenton reaction and photolysis of Fe(III), researchers combined UV/Fe(III) and H_2O_2 to form a higher oxidation efficient technology, named photo-Fenton reaction [67]. It was applied in the removal of chlorophenols [68], nitrophenols [57], dye [69] and also in the degradation of more than ten kinds of pesticides and herbicides such as atrazine, azinphos-methyl, captan, glyphosate, metolachlor, picloram, simazine and so on [70]. Zepp et al. [71] reported the kinetic of $HO^{\bullet}$ generated from photo-Fenton reaction at pH 3-8. It confirmed the transient oxidants were generated when H_2O_2 reacted with Fe(II) which was produced from photo-reduction of Fe(III) (λ = 436 nm). Bauer and Fallmann [72] not only confirmed that the UV/Fe(II)/H_2O_2 system was the most efficient compare to TiO_2/UV, Fe(II)/H_2O_2/UV, Fe(II)/O_2/UV and Fe(II)/O_3/UV systems but also confirmed the economic feasibility for the photo-Fenton reaction through the actual wastewater treatment experiments.

However, Laat and Gallard showed that Fe(III) would be completely dissolved only in the pH < 3 [73]. When the pH was between 3 to 7, there was possibility for Fe(III) flocculation and the oxidation efficiency of Fenton reaction would be lower [74]. Pignatello [75] used Fenton and photo-Fenton reaction in the herbicides degradation and found that the optimum pH value was 2.8. The acid pH value was the limiting parameter of traditional Fenton/photo-Fenton technology which affected its application in wastewater treatment. In the early 21st century, researchers found the replacement of iron by iron complexes could expand the pH value to a wider range. This important discovery led the Fenton technology into a new era of rapid

development.

1.2.2 Fenton-like and photoFenton-like reactions with iron complex

The organic ligand was introduced in the traditional Fenton/photo-Fenton reaction to form iron complex to overcome the disadvantages of the previous reaction. In the early studies, polycarboxylic acid was used to form stable iron complex. Indeed, polycarboxylic acid, such as oxalic acid, citric acid, propionic acid were common constituents of rain, fog, surface water and soil solution [76-7778].

Lee et al. [79] added phosphotungstate ($PW_{12}O_{40}^{3-}$), a polyoxometalate, into Fe(III)/H_2O_2 system. $PW_{12}O_{40}^{3-}$ formed a soluble complex with iron that converted H_2O_2 into oxidants. It extended the working pH range of the Fe(III)/H_2O_2 system up to pH 8.5. Deng et al. [80] studied the degradation of dye in water using iron-oxalate complexes (Fe(III)-oxalate) with UV light. The results showed the optimum pH range was 4-5. Zhou et al. [81] compared the diethylstilbestrol degradation efficiency in both Fe(III)/UV and Fe(III)-oxalate/UV systems. The Fe(III)-oxalate/UV system showed higher degradation efficiency than Fe(III)/UV system. Hug et al. [82] studied the oxidation of trivalent arsenic As (III) by different oxidants in neutral pH conditions (pH = 6.5-8) under UVA irradiation. The results showed As (III) could not be removed by Fe(III) or H_2O_2 oxidation; when the citrate was added, As(III) was removed efficiently due to the formation of Fe(III)-citrate complex. Katsumata et al. [83] studied the herbicide alachlor degradation in photo Fenton-like system (UV/Fe(II)-citrate/H_2O_2). The degradation rate of alachlor was more than 85% when the pH range

was 2-5; When the pH rang was 6-8, the reaction rate was still able to maintain 65%-70% of degradation. The results in this research were very efficient compare to traditional photo-Fenton process. Silva et al. [84] studied the degradation of the herbicide tebuthiuron in UV/Fe(III)-citrate/H_2O_2 system. The results showed that its degradation rate was 100%-78% when the pH was changed from 2.5 to 7.5. Lipczynska-Kochany and Kochany [85] added humic acid salt in the traditional Fenton reagent to form Fenton-like system (Fe(II)-humate/H_2O_2). The degradation rate of toluene, o-xylene, m-xylene, p-xylene and methylene chloride were investigated both in acidic and neutral pH conditions. The results showed that the degradation rates were higher in acidic pH than in neutral pH in Fe(II)/H_2O_2 system; however, the degradation rates were higher in neutral pH than in acidic pH in Fe(II)-humate/H_2O_2 system.

In recent years, the research hot topic concerning iron-complex was iron-aminopolycarboxylic acids complexes. Aminopolycarboxylic acids (APCAs) are organic acids which contain a plurality of carboxyl groups and connected by nitrogen atom. APCAs can form stable, water-soluble complexes with Fe(III) or Fe(II). The most widely applied APCAs are Nitrilotriacetic acid (NTA) and Ethylene Diamine Tetraacetic acid (EDTA) [86]. Fe(III)-NTA and Fe(III)-EDTA complexes were confirmed to have good photochemical activity [87-88]. Howsawkeng et al. [89] and Ndjou'ou et al. [90] studied the degradation of perchlorethylene (PCE) with Fenton-like (Fe(III)-NTA/H_2O_2) reagents in soil under neutral conditions (pH = 7.6). The results showed high degradation rate of PCE in neutral pH value. Kim and Kong [91]

used alcohol and carbon tetrachloride as probes to study the oxidation efficient of Fe(III)-NTA/H_2O_2 reagent. The results showed that the degradation rate of the two probes increased with the increasing pH from 3 to 9; when the pH was higher than 12, the degradation was suppressed. Zhou et al. [92] studied the mechanism of 2, 4-dichlorophenol degradation in the Fe(II)-EDTA/ultrasound system. The results showed the high degradation efficient of 2,4-dichlorophenol due to the formation of H_2O_2 from dissolved oxygen in ultrasonic process generating the Fenton-like reagent (Fe(II)-EDTA/H_2O_2). It would produce a large number of $HO^{\bullet}$ to mineralize the contaminant. Based on the same mechanism in Liu et al. [93] paper, the Fe(II)-EDTA/microwave system was used in the degradation of 4-nitrophenol. It was oxidized to organic acids which were biodegradable.

Although iron-APCAs complexes are relatively stable and increase the solubility of iron in water, EDTA is known to be a pollutant which is not easily to be biodegraded. So, the applications of EDTA in wastewater treatment will cause secondary pollution. Therefore, looking for environmental friendly chelating agents become the research focus and hotspot.

1.2.3 Fe(III)-EDDS

A lot of chelating agents have been developed recently. Ethylene diamine disuccinic acid (EDDS) has been noticed by some researchers because of its special advantages. EDDS is a natural APCAs and an isomer of EDTA, which has similar strong metal complexing capacity as EDTA. Studies of Metsärinne [94] indicated that

EDDS could be more easily degraded than EDTA under irradiation of 315-400 nm UV light. All three stereoisomers of EDDS are [S,S]-EDDS, [R,R]-EDDS and [R,S/S,R]-EDDS and the chemical structures are shown in figure 1-1 [95]. [S,S]-EDDS is biodegradable while the other two stereoisomers are relatively difficult to be biodegraded [94-96]. So it is considered to be a safe and environmental friendly chelating agent to substitute EDTA as an eluent for heavy metals in soil and sludge [97-98].

Figure 1-1 Chemical structures of EDDS stereoisomers

In the last three years, Li et al. [99] reported the use of iron-Ethylene diamine disuccinic acid complexes (Fe(III)-[S,S]-EDDS, abbreviated as Fe(III)-EDDS) in the degradation of 17β-estradiol (E2). E2 was efficiently removed under UV irradiation in

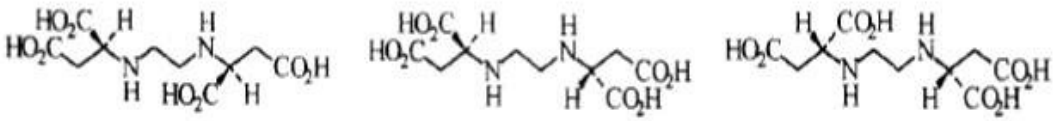

[S,S]-EDDS [S,R]-EDDS or [R,S]-EDDS [R,R]-EDDS

the presence of Fe(III)-EDDS in the pH range from 3 to 9. The quantum yield of HO• increased with the increasing pH value. The innovative results showed that the AOPs based on iron were no longer limited by the range of pH values since Fe(III)-EDDS was introduced into AOPs. Huang et al. [100] reported the degradation of bisphenol A (BPA) in Fenton-like system (Fe(III)-EDDS/H_2O_2). The results also showed the degradation rate of BPA increased with increasing pH values in the range of 3-9. The removal of BPA had improved significantly by the increasing dissolved oxygen

concentration. Huang et al. [101] studied the effect of EDDS on Fenton and photo-Fenton processes using goethite as an iron source. The highest degradation rate of BPA was obtained at pH = 6.2. Although these studies had shown significant advantages for the application of Fe(III)-EDDS in AOPs, the reaction mechanism was not clear yet and further researches are needed.

1.3 Oxidation Process with sulfate radical ($SO_4^{\bullet-}$)

1.3.1 Oxidant persulfate ($S_2O_8^{2-}$)

Persulfate is an oxidant with strong oxidizing ability and the standard redox potential of $S_2O_8^{2-}$ is E^o = 2.01 V. In 1878, French scientist Marcelin Berthelot [102] firstly produced persulfate by electrolysis of sulfate and started to use persulfate as dry-cleaning bleach. Subsequently, persulfate was used as an initiator for polymerizations of polytetrafluoroethylene, polyvinyl chloride, polystyrene and neoprene rubber. It also used as an inhibitor for the recombination of electrons and holes in photocatalytic reaction [103]. In recent years, persulfate is used as an attractive candidate to generate strong oxidizing sulfate radical ($SO_4^{\bullet-}$, E^o = 2.6-3.2 V). Because of its high solubility and better stability than H_2O_2, persulfate has been used as a potential source of $SO_4^{\bullet-}$ for remediation of contaminated water and soil.

1.3.2 Formation of $SO_4^{\bullet-}$

The generation of $SO_4^{\bullet-}$ is shown in R1-3 [102].The standard oxidation potential of $SO_4^{\bullet-}$ is higher than most common oxidants, the standard oxidation potentials of oxidants are shown in Table 1-1 [104]. The key point of using persulfate for advanced oxidation process is activating persulfate to generate $SO_4^{\bullet-}$. A free radical half-life of 4 s was reported. It was generated in the mixture of persulfate and ferrous ion concentration of 10^{-3} M and a temperature of 40 °C [105]. The persulfate can be achieved with physical and chemical modes. The activation ways include heating [106-107], UV light irradiation [108-109], transitional metal activation [110-111], microwave irradiation [112-113], alkali activation [114] and carbon activation [115]. The strong oxidizing $SO_4^{\bullet-}$ is generated by the breaking of -O-O-bond in $S_2O_8^{2-}$. $SO_4^{\bullet-}$ has a high oxidative capacity and it can oxidize many kinds of organic pollutants. The pollutants are oxidized to small organic molecules and finally mineralized to CO_2 and H_2O. The sulfate ions (SO_4^{2-}) are also formed during the reaction.

$$^{-}O_3S-O-O-SO_3^{-} \xrightarrow{activated} 2[^{\bullet}O-SO_3^{-}] \quad \text{(R1-3)}$$

Table 1-1 Standard potential of oxidants

oxidant	E^o (V)	Oxidant	E^o (V)
F_2	3.06	$HClO_4$	1.63
$HO^{\bullet}$	2.80	ClO_2	1.50

$SO_4^{\bullet-}$	2.6-3.2	Cl_2	1.36
O_2	2.07	$Cr_2O_7^{2-}$	1.33
H_2O_2	1.77	O_2	1.23
MnO_2	1.68	Br_2	1.10

A series of radical chain reactions can occur after the $SO_4^{\bullet-}$ generation and $HO^{\bullet}$ is also formed as shown in reaction R1-4 and R1-5 [116]. $SO_4^{\bullet-}$ and $HO^{\bullet}$ are coexisting and the ratio and the amount of each radical depend on the pH of the solution. Huang et al. [117] identified the type of radical after the bond breaking of persulfate in different pH by Electron Paramagnetic Resonance Technology (EPR). The results showed that there was mainly $SO_4^{\bullet-}$ in acidic and neutral conditions (pH = 2-7); $SO_4^{\bullet-}$ and $HO^{\bullet}$ were coexisting in the pH range 8-10 due to the reaction shown as R1-5; $HO^{\bullet}$ became the major oxidizing species in solution when the pH value was higher than 10. However, as the weak oxidative capacity of $HO^{\bullet}$ in alkaline conditions, $SO_4^{\bullet-}$ oxidation system has higher degradation efficiency of pollutants in acidic or neutral condition than in alkaline condition.

$$SO_4^{\bullet-} + H_2O \rightarrow SO_4^{2-} + HO^{\bullet} + H^+ \quad \text{(R1-4)}$$

$$SO_4^{\bullet-} + OH^- \rightarrow SO_4^{2-} + HO^{\bullet} \quad \text{(R1-5)}$$

1.3.3 Activated $S_2O_8^{2-}$ by iron to produce $SO_4^{\bullet-}$

The activation of persulfate that by transitional metal to produce sulfate radical is

simple and easily operated. It is low energy consumption and does not need harsh reaction conditions. The mechanism of $SO_4^{\bullet-}$ formation through transitional metal activation is shown in R1-6 and R1-7 [118]. Fe^{2+} is used most widely in the activation of persulfate, because Fe^{2+} is cheap, non-toxic and easily to find in natural surroundings.

$$S_2O_8^{2-} + M^{n+} \rightarrow M^{(n+1)+} + SO_4^{\bullet-} + SO_4^{2-} \quad \text{(R1-6)}$$

$$SO_4^{\bullet-} + M^{n+} \rightarrow M^{(n+1)+} + SO_4^{2-} \quad \text{(R1-7)}$$

Liang et al. [119] investigated the removal of groundwater contaminant such as trichloroethylene (TCE) by $SO_4^{\bullet-}$. Fe^{2+} was used as an activator under various molar ratios of $S_2O_8^{2-}/Fe^{2+}$/TCE in an aqueous system. It confirmed that Fe^{2+} played an important role in generating $SO_4^{\bullet-}$ and the rapid conversion of all Fe^{2+} to Fe^{3+} limited the ultimate oxidizing capability of the system. Ji et al. [120] investigated the Fe(II) activated decomposition of $S_2O_8^{2-}$, as a potential in situ chemical oxidation (ISCO) approach, for remediation of groundwater contaminated by antibiotics. In the system with Fe(II)/$S_2O_8^{2-}$ mediated ciprofloxacin (CIP) degradation was found to be more efficient than sulfamethoxazole (SMX) degradation. $HO^{\bullet}$ and $SO_4^{\bullet-}$ were determined to be responsible for the degradation of CIP and SMX in Fe(II)/$S_2O_8^{2-}$ system by molecular probes. Zhao et al. [121] studied the effect of temperature, pH, Fe(II) concentration, $S_2O_8^{2-}$ concentration on the degradation of 4-chlorophenol (4-CP). The results showed that the highest degradation rate of 4-CP was obtained at pH = 4 and

the degradation rate decreased with the increasing pH value. Zheng et al. [122] investigated the oxidation of As(III) in Fe(II)/$S_2O_8^{2-}$ system. The similar results were found. The highest As(III) oxidation rate was obtained at pH = 3 and the oxidation rate decreased with the increasing pH value. Zhang et al. [123] studied the kinetics of aniline degradation by persulfate with iron(II) activation at ambient temperature. With iron(II) as initiator, the oxidation reactions were found to follow a biphasic rate phenomenon: a rapid degradation in the first 30s followed by a slow but sustained oxidation process. After the initial fast oxidation, the reactions appeared to follow a pseudo-first-order model.

The above results showed that Fe(II)/$S_2O_8^{2-}$ system run well in acidic condition and the rapid degradation usually occurred at the beginning of the reaction (in the first 5 min or less than 5 min). The acidic pH was better for Fe(II)/$S_2O_8^{2-}$ system due to the easier oxidation of Fe(II) and precipitation of Fe(II) at high pH value. This is the similar limiting factor as traditional Fenton reaction. The reason for the rapid degradation occurred at the beginning of the reaction was the rapid conversion of all Fe(II) to Fe(III) and so generation of $SO_4^{\bullet-}$. Since the conversion of all Fe(II) to Fe(III) was finished, the oxidation would stop, because Fe(III) could not activate $S_2O_8^{2-}$ to radicals. Therefore, Fe(II)/$S_2O_8^{2-}$ system could not continuously degrade organic pollutants and it became the other disadvantage beside pH value. The researchers hoped that the introduction of iron complexes would overcome these shortcomings in Fe(II)/$S_2O_8^{2-}$ system.

1.3.4 Activated $S_2O_8^{2-}$ by iron complex to produce $SO_4^{\bullet-}$

In order to overcome the two main disadvantages of Fe(II)/$S_2O_8^{2-}$ system, researchers introduced citrate, EDTA and NTA into iron/persulfate system to form complexes. It was hoped that the oxidation efficiency would be improved and range of pH value would be broaden in the reaction.

Liang et al. [124] investigated oxidation of dissolved trichloroethylene (TCE) in aqueous and soil slurry systems by $SO_4^{\bullet-}$. The chelating agent (citric acid) was used in attempt to manipulate an appropriate quantity of Fe(II) in solution by providing an appropriate chelate/Fe(II) molar ratio. The results showed that the high levels of chelated Fe(II) concentration resulted in more persulfate decomposition and faster TCE degradation. The stop time of the oxidation reaction extend from 5 min to about 10 min. Zhang and Yang [125] studied the degradation of herbicide (diuron) in Fe(II)-citrate/$S_2O_8^{2-}$ system. The results showed that diuron was removed efficiently when the initial pH was 7.0 and the degradation reaction continued during 120 min. The reasons for the improvement by adding the chelating agent may be as follow: Firstly, the Fe(II)-citrate complex was formed and the dissolved Fe(II) was kept in the solution. So it appropriately delayed the formation of $SO_4^{\bullet-}$ and the reaction time could be lasted longer than Fe(II)/$S_2O_8^{2-}$ system; Secondly, the iron complex was stable in neutral or alkaline pH condition while Fe(II) only dissolved in acidic solution. So the pH range of reaction was expanded.

In addition, Liang et al. [126] also investigated the applicability of ethylene-

diamine-tetra-acetic acid (EDTA) chelated Fe^{3+} in activating persulfate for the degradation of TCE in aqueous phase under pH 3, 7 and 10. The results showed that the increasing pH lead to the increasing in pseudo-first-order-rate constants for TCE degradation and Cl^- generation. Accordingly, the experiments at pH 10 with different EDTA/Fe^{3+} molar ratios indicated that a 1/1 ratio resulted in a remarkably higher degradation rate of TCE. These findings indicated that the formation of the Fe(III)-complex could also activate persulfate and effectively broaden the range of pH value compared with Fe(II)/$S_2O_8^{2-}$ system. The permanent cycle between Fe(III) and Fe(II) could continuously generate $SO_4^{\bullet-}$. However, EDTA was difficult to be biodegrade and the utilization of EDTA would cause secondary pollution. Therefore, an environmentally friendly EDDS will substitute for EDTA in this study. Fe(III)-EDDS complex will be used to activate persulfate to produce $SO_4^{\bullet-}$. It is hoped the advanced oxidation technology will be developed in the presence of Fe(III)-EDDS.

1.4 Target pollutant: 4-tert-Butylphenol (4-t-BP)

4-tert-Butylphenol (4-t-BP), also known as p-tert-butylphenol, has a scientific name called 4- (1,1-dimethylethyl) phenol. The molecular formula of 4-t-BP is $C_{10}H_{14}O$ and the molecular weight is 150.22 g mol^{-1}. It is a white crystalline powder. It slightly dissolves in water but easily dissolves in methanol, acetone, benzene, ethanol, ether and other organic solvents. The solubility in water is 8.7 g L^{-1} (20 ℃). The

melting point is 96 - 101 ℃ and the boiling point is 236-238 ℃. The density is 0.908 g mL^{-1} at 25 ℃ [127]. Its chemical structure is shown in Figure 1-2.

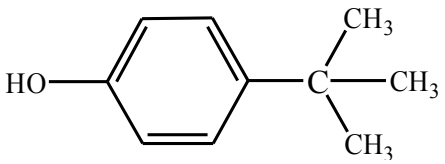

Figure 1-2 The structure of 4-t-BP

1.4.1 Sources and harms of 4-t-BP

4-t-BP is an important chemical raw material. Indeed, it used in wide range of application in chemical industry. The 4-t-BP is used in the manufacture of oil-soluble phenolic resin and in the manufacture of electrophoretic lacquer, varnish, enamel and other production in the paint industry. It is also used in the production of quick-drying, in the production of light and advanced ink in ink industry and widely used in the construction and transportation industries. In addition, 4-t-BP is used in manufacture of the polyvinyl chloride (PVC) stabilizer, of the ultraviolet absorber and of the surfactant [128]. During the process of 4-t-BP synthesis and its application, it is diffusing slowly into the surrounding as the form of particles, gases, droplets, dry deposition and wet deposition. So, 4-t-BP will be detected in the surface water through its introduction by rain, snow and surface runoff.

4-tert-butylphenol (4-t-BP) is an alkylphenols (APs) and is one of the endocrine

disrupting chemicals (EDCs) with highly estrogenic effects. EDCs are chemicals with potential negative effects on the reproductive and developmental systems of humans and wildlife [129]. In the past decade, research of EDCs has grown immensely since the publication of the book 'Our stolen future' [130]. EDCs are defined by US Environmental Protection Agency (US EPA) as an exogenous organism compound which can affect the synthesis, storage, secretion, transportation and elimination of hormone in the body [131]. The main types of EDCs are: alkylphenols (such as nonylphenol, octylphenol, butylphenol, bisphenol A, et al.), phthalates (such as, butyl benzyl phthalate, dibutyl phthalate, diethyl phthalate, dimethyl phthalate, di-n-octyl phthalate, et al.), exogenous human hormone (such as estrone, estradiol, ethinyl estradiol alcohol, estriol, diethylstilbestrol, et al.), heavy metals (such as mercury, cadmium, lead, et al.) and organic chlorine pesticides (such as hexachlorocyclohexane, dichloro diphenyl trichloroethane, et al.) [132]. Many countries in the world have already started the monitoring of EDCs and researching the control methods of them.

Since EDCs enter inside the human body or wildlife, it is difficult to be metabolized and it will accumulate in living organisms, change the body's hormonal balance and impact on the health of the life. Haavisto et al. [133] evaluated the effects that 4-tert-octylphenol (4-t-OP) and 4-tert-butylphenol (4-t-BP) had on the prenatal testicular testosterone surge at embryonic day (ED) 19.5 days in the rat. The results showed that 4-t-OP (10, 100, 500 mg L^{-1}) and BP (100 mg L^{-1}) significantly increased testosterone and progesterone levels by up to seven-fold and broke their proper

balance in the organism. Myllymäki et al. [134] evaluated the effects of diethylstilbestrol (DES), genistein (GEN) and two alkylphenols (4-t-BP and 4-t-OP) on the growth and survival of steroid hormone by isolated 14-day-old rat ovarian follicles. Both 4-t-BP and 4-t-OP decreased estradiol and testosterone secretion in a dose-dependent manner while no effect on aromatase activity was observed. Barse et al. [135] evaluated effects of 4-tert-butyl phenol on *Cyprinus carpio*, a species formed in sewage fed fisheries wastewater. There was significant decrease in alkaline phosphatase and aspartate aminotransferase activity. Alanine aminotranferase and acid phosphatase activity, vitellogenin production in muscle and hepatic- and reno-somatic indices were increased compared to control. According to the above researches, it is clearly showed that 4-t-BP has negative influence on organism.

1.4.2 Distribution of 4-t-BP in the environment

Currently, 4-t-BP enters into the environment usually through transportation by air and by the discharge of sewage. It has been widely discharged in the natural water and already been detected in many rivers and lakes all over the world. The distribution of 4-t-BP is showed in Table 1-2 and Table 1-3. However, until now, the researches on the concentration distribution of alkylphenols in waters were still very limited. Most of the studies focused on nonylphenol, octylphenol detection but the monitoring for butylphenol and bisphenol A were relatively less important.

Table 1-2 The current distribution of 4-t-BP in China

Waters	Concentration	Reference
Jiaozhou Bay	water: ＜LOD - 28.0 ng L^{-1} sediment: ＜LOD - 4.2 ng g^{-1}	M.Z. Fu, 2007[136]
Rivers around Jiaozhou Bay (Baisha River, Moshui River, Licun River, et al.)	water: 10.5 - 329.8 ng L^{-1} sediment: ＜LOD - 7.8 ng g^{-1}	M.Z. Fu, 2007[136]
Yangtze River in Nanjing	estuary in Jiangning: ＜LOD - 14 ng L^{-1} Meishan River: 3 - 11 ng L^{-1} shore zone in Pukou: 2 - 10 ng L^{-1} shore zone in Yanxi: 2 - 12 ng L^{-1} shore zone in Shangyuanmen: 1 - 11 ng L^{-1} estuary in Jiuxiang River: 1 - 13 ng L^{-1} estuary in Sanjiang River: 2 - 5 ng L^{-1}	G.P. Xue and C.Y. Yao, 2010[137]
Shore zone of Yellow Sea (Donggang, Yantai, Wendeng, Qingdao, Rizhao, Lianyungang, Haimen, Qidong, et al.)	benthic organisms: 5.19 - 195.59 ng g^{-1} sediment: ＜LOD - 24.45 ng g^{-1}	Z.W. Shao, 2011[138]

LOD = limit of detection

Table 1-3 The current distribution of 4-t-BP in foreign countries

Waters	Concentration	Reference
Japan	fish and shellfish: ＜1 ng g^{-1}	T. Tsuda, et al, 2000[139]
Turkey	sediment: 1.68 μg g^{-1}	C．Uguz, et al, 2003[140]
Japan	drinking water：＜LOD River 1: 0.01 ng mL^{-1} River 2: 0.05 ng mL^{-1} River 3: 0.03 ng mL^{-1}	K. Inoue, et al, 2002[141]
United States	indoor air: 3.4 - 290 ng m^{-3} dust: ＜LOD - 1.12 μg g^{-1}	R.A. Rudel, et al, 2003[142]
Singapore (Sea)	Sembawang Park: 0.03 μg L^{-1} Punggol: ＜LOD Pasir Ris: 0.03 μg L^{-1} Changi: 0.03 μg L^{-1} Jurong Pier: 1.06 μg L^{-1} Tuas Jetty: 0.95 μg L^{-1}	C. Basheer, et al, 2004[143]
United States (Sewage)	septic tank leachate: 0.16-3.2 μg L^{-1} untreated sewage: 0.042-0.1 μg L^{-1}	R.A. Rudel, et al, 1998[144]

	treated sewage: 0.02-0.032 μg L^{-1}	

LOD = limit of detection

According to the monitoring data obtained from China and abroad, it indicated that 4-t-BP is widely spread in various aquatic compartments and might be already accumulated in the organism. In 2006, Campbell et al. [145] reported that EDCs had strong estrogenic effects even in very low concentration such as ng L^{-1}. Thus, the health of human and various organisms are facing particularly to serious threat due to the presence of 4-t-BP.

1.4.3 Research on 4-t-BP

According to the study of the current research literature, most of 4-t-BP researches were concentrated in toxicity and monitoring methods [146-147]. The research on 4-t-BP degradation was relatively less significant. However, there were many researches on the degradation of other alkylphenols (such as nonylphenol and octylphenol). The removal technologies could be divided into physical adsorption, biodegradation and advanced oxidation degradation according to the removal mechanism.

Shibata, et al. [148] investigated the microbiological degradation of phenol and some of its alkyl-derivatives (p-cresol, 4-n-propylphenol, 4-i-propylphenol, 4-n-butylphenol, 4-sec-butylphenol, 4-t-butylphenol and 4-t-octylphenol). The experiments were performed under both aerobic and anaerobic conditions in seven

Japanese paddy soils. The results showed that the half-life of 4-t-BP in aerobic condition was approximately 8 days and there was no degradation of 4-t-BP after 224 days in anaerobic condition. Ogata, et al. [149] studied the removal of 4-t-BP by duckweeds in water. In this study, 4-t-BP was removed from water from four different environments in the presence of *Spirodela polyrrhiza*, giant duckweed, but 4-t-BP persisted in the natural waters in the absence of *S. polyrrhiza*. Also, 4-t-BP was not removed from autoclaved pond water with sterilized *S. polyrrhiza*. These results suggested that the 4-t-BP removal from the natural waters was caused by biodegradation stimulated by the presence of *S. polyrrhiza* rather than by uptake by the plants. Under the optimum condition, it took 15 h to achieve complete removal of 4-t-BP. Církva, et al. [150] investigated the influence of UV irradiation and combined Microwave-UV irradiation on 4-tert-butylphenol transformation in the presence and in the absence of sensitizers. The results showed that 4-t-BP irradiated by UV and MW-UV and formed dimers with -C-O-C- and -C-C- bonds. In non-polar solvents (hexane, heptane, toluene), 4-t-BP radiation led to the formation of products 1, 2 and 2TBP (Figure 1-3). Triplet-sensitized reaction with benzophenone in hexane gave moreover 2TBP and its ortho-ortho (3) and ortho-para (4) dimers. The simple mechanism was shown in Figure 1-3. Li et al. [151] studied the 4-t-BP degradation with a new technique, UV/H_2O_2/micro-aeration system. It could remove more effectively 4-t-BP in water than in the UV/H_2O_2 system. Indeed, the 4-t-BP (500 μg L^{-1}) could be totally degraded in 30 min with this new system. Sun et al. [152] investigated the degradation kinetics of 4-t-BP by chlorination in aqueous. The results showed that 4-t-

BP was rapidly oxidized by chlorine with different initial concentrations of HOCl and pH value. The optimum pH value for 4-t-BP degradation was 5 in this experiment condition. The corresponding half-life time of 4-t-BP was 12.1 min when chlorine concentration was 3 mg L^{-1}.

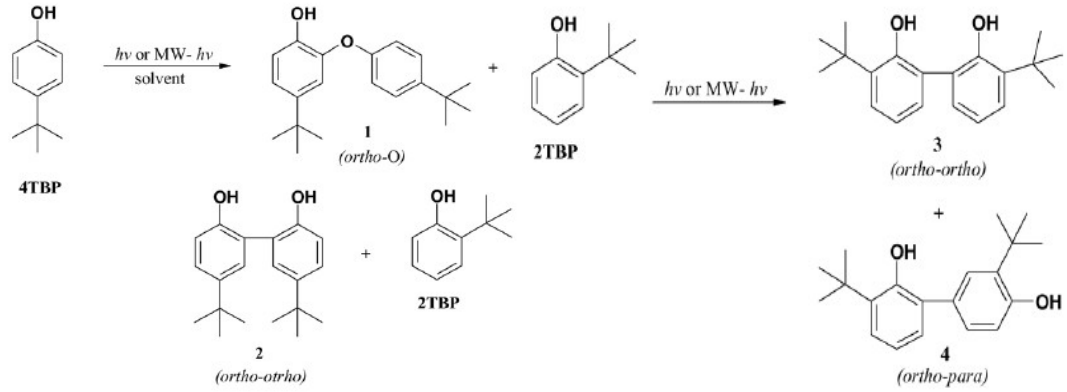

Figure 1-3 Mechanism of 4-t-BP photodegradation [150]

According to the above research results, the research on 4-t-BP degradation began in the early 21st century and was still in its infancy. It was mainly due to the fact that contaminant itself did not attracted peoples' attention yet. In addition, considering the mechanism of the 4-t-BP degradation, technologies like AOPs was much higher efficiency than the biological degradation technology. It also confirmed that 4-t-BP is slowly biodegradable and is a persistent organic pollutant. Once it enters into the environment, it will accumulate in living organisms and will be a potential threat to our daily life. In this study, the advanced oxidation technologies for 4-t-BP degradation will be further studied.

Chapter 2

MATERIALS AND METHODS

Chapter 2 Materials and methods

2.1 Reagents

All the chemicals used in the experiments were shown in Table 2-1. All reagents were used without further purification.

Table 2-1 Chemical reagents applied in the experiments

Reagent	Purity	Company
S, S'-Ethylenediamine-N,N'-disuccinic acid trisodium salt solution (EDDS-Na)	35% in water	Sigma-Aldrich
Ferric perchlorate ($Fe(ClO_4)_3 \cdot 9H_2O$)	≥ 97%	Fluka
4-tert-Butylphenol (4-t-BP)	99%	Sigma-Aldrich
Methanol (CH_3OH)	≥ 99.9%	Sigma-Aldrich
Hydrogen peroxide (H_2O_2)	30% in water	Fluka
Nitrobenzene (NB)	> 99.5%	Fluka
Sodium hydroxide (NaOH)	> 97%	Prolabo
Perchloric acid ($HClO_4$)	> 97%	Merck
2-Propanol	99.9%	Sigma-Aldrich
Sodium formate (HCOONa)	≥ 99.0%	Fluka
Tetrabutylammonium hydrogen sulfate (TBA-HS)	> 98%	Acros Organics
Acetic acid (CH_3COOH)	96%	Carlo Erba reagent
4-Hydroxyphenyl acetic acid (TAOH)	98%	Sigma-Aldrich
Ethylenediaminetetraacetic acid disodium salt (Na_2EDTA)	99%	Sigma-Aldrich
Peroxidase	----	Aldrich
Sodium dihydrogen phosphate (NaH_2PO_4)	99%	Aldrich
Disodium hydrogenorthophosphate (Na_2HPO_4)	> 99%	Aldrich
Potassium persulfate ($K_2S_2O_8$)	> 99%	Sigma-Aldrich
Ferrous ammonium sulfate hexahydrate $(NH_4)_2Fe(SO_4)_2 \cdot 6H_2O$	99%	Sigma-Aldrich
5,6-Diphenyl-3-(2-pyridyl)-1,2,4-triazine -4,4'-disulfonic acid disodium salt hydrate (Ferrozine)	97%	Sigma-Aldrich
Sodium acetate (CH_3COONa)	99%	Merck
tert-Butanol (t-BuOH)	99.5%	Aldrich
p-Nitroanisole (PNA)	97%	Aldrich
Pyridine	≥ 99.0%	Sigma-Aldrich

2.2 Preparation of solutions

All the solutions were prepared with Milli-Q ultrapure water.

(1) 4-t-BP stock solution (2 mM)

0.15 g 4-t-BP was diluted to 500 ml by adding an appropriate volume of Milli-Q water and then magnetic stirring was used for several hours to make 4-t-BP completely dissolved in water. It was stored avoid light. The concentrations of 4-t-BP used in all experiments in this study were 50 μM.

(2) Fe(III)-EDDS stock solution (5 mM)

50 mL of 10 mM EDDS solution and 50 mL of 10 mM $Fe(ClO_4)_3 \bullet 9H_2O$ were mixed together and formed Fe(III)-EDDS complex stock solution 100 ml. The stock solution can be stored and is stable for four days.

(3) H_2O_2 stock solution (100 mM)

1.02 ml H_2O_2 (30%， ρ = 1.11 g/cm^3) was diluted to 100 ml by adding an appropriate volume of Milli-Q water. It was stocked in the fridge.

(4) 2-Propanol stock solution (100 mM)

0.765 ml 2-Propanol was diluted to 100 ml by adding an appropriate volume of Milli-Q water and then stocked in the fridge.

(5) t-BuOH stock solution (100 mM)

0.949 ml t-BuOH was diluted to 100 ml by adding an appropriate volume of

Milli-Q water and then stocked in the fridge.

(6) $K_2S_2O_8$ stock solution (10 mM)

0.1352 g $K_2S_2O_8$ was diluted to 50 ml by adding an appropriate volume of Milli-Q water and then stocked in the fridge.

(7) Fe(II) stock solution (1.0 mM)

0.0980 g $(NH_4)_2Fe(SO_4)_2 \cdot 6H_2O$ was diluted to 250 ml by adding an appropriate volume of Milli-Q water. Fe(II) stock solution was newly prepared every time when it was needed. The pH was 2.5.

(8) Ferrozine stock solution (4 mM)

0.0985 g Ferrozine was diluted to 50 ml by adding an appropriate volume of Milli-Q water.

(9) Eluent A used in the detection of Fe(III)-EDDS

The eluent was the mixed solution of TBA-HS (2 mM) and HCOONa (15 mM) and the pH was adjusted to 4.0.

(10) Na_2EDTA stock solution (10 mM)

0.3722 g Na_2EDTA was diluted to 100 ml by adding an appropriate volume of Milli-Q water.

(11) Peroxidase stock solution

0.003 g peroxidase was dissolved and diluted to 50 ml by adding an appropriate volume of Milli-Q water.

(12) TAOH stock solution (1 mM)

0.0152 g TAOH was dissolved and diluted to 100 ml by adding an appropriate

volume of Milli-Q water.

(13) Buffers

pH = 7.0 NaH_2PO_4/Na_2HPO_4 buffer: 5.75 g NaH_2PO4 and 1.14 g Na_2HPO_4 were dissolved and diluted to 500 ml by adding an appropriate volume of Milli-Q water.

pH = 5.5 CH_3COOH/CH_3COONa buffer: 4.10 g CH_3COONa and 1.0 mL CH_3COOH were dissolved and diluted to 250 ml by adding an appropriate volume of Milli-Q water.

2.3 Irradiation experiments

2.3.1 Irradiation with home-made photoreactor

The irradiation experiments were performed in a homemade photoreactor which was shown in Figure 2-1. The quartz glass tube was placed in the center of the reactor and the inner diameter of the tube was 2.8 cm. The UV light could reach the solution through the quartz glass. The outer tube was connected with the thermostatic water circulation device to ensure the reaction temperature was kept at room temperature (20 ℃). Four fluorescent lamps (TLD 15W/05, Philips, Netherlands) were placed in the four different axes. The emission spectrum of the lamp was continuous from 300 nm to 500 nm with main UV light at 365 nm, 405 nm and 435 nm. A magnetic stirrer was placed at the bottom of the reactor and the solution could be continuously stirred during the irradiation. The solution for experiment was 50 ml and it was poured into

the quartz glass tube for irradiation.

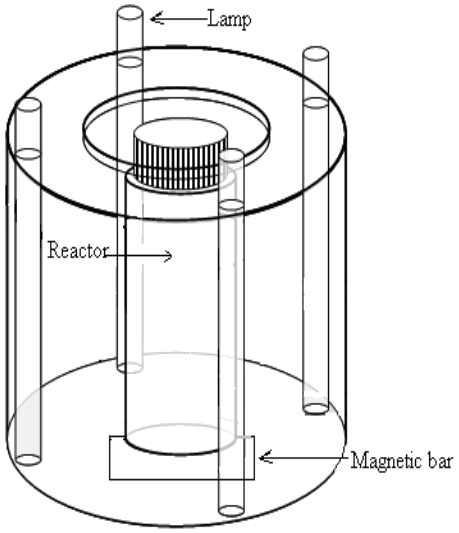

Figure 2-1 Home-made photoreactor with four tubes

The actual light intensity of the home-made phototreactor was measured. According to the literature [153], the method based on the photolysis of PNA in the presence of pyridine was taken to calculate the photon flux of the irradiation system. The reaction of PNA in the presence of pyridine was shown in reaction R2-1.The photolysis rate of PNA depended on the concentration of pyridine. The quantum yield for PNA degradation ($\Phi_{PNA/pyr}$) was calculated with the equation R2-2. The quantum yield was defined as molecules decomposed divided photons absorbed [154]. So the photons absorbed (I_a photon m^{-2} s^{-1}) in PNA degradation was calculated with equation R2-3 and ΔN_{PNA} (molecules m^{-2} s^{-1}) was the amount of decomposed PNA molecules. ΔN_{PNA} could be calculated with equation R2-4 (N_A was the Avogadro number; R_{PNA} was the degradation rate of PNA; V was the volume of the reaction solution, 50 ml; r was the radius of the photoreactor, 0.014 m; H was the height of the reaction solution, 0.1 m). Thus, I_a could be determined according to above calculation.

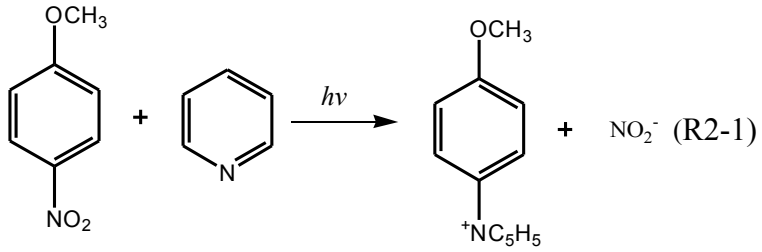

(R2-1)

$$\phi_{PNA/pyr} = 0.44[pyridine] + 0.00028 \quad \text{(R2-2)}$$

$$I_a = \frac{\Delta N_{PNA}}{\phi_{PNA/pyr}} \quad \text{(R2-3)}$$

$$\Delta N_{PNA} = \frac{N_A R_{PNA} V}{2\pi r H} \quad \text{(R2-4)}$$

According to Lambert - Beer law [155], the relationship between incident light intensity (I_o) and emitted light intensity (I_t) was shown in the equation R2-5. So the absorbed light intensity (I_a) could be calculated with equation R2-6 and the I_o at the particular wavelength could be calculated with equation R2-7. The incident light intensity for a particular wavelength band was the sum of I_o at each wavelength, shown in equation R2-8 (h was Planck's constant; c was velocity of light).

$$A = \lg \frac{I_o}{I_t} \quad \text{(R2-5)}$$

$$I_a = I_o - I_t = I_o - I_o 10^{-A} = I_o(1-10^{-A}) \quad \text{(R2-6)}$$

$$I_o = \frac{I_a}{1 - 10^{-A}} \qquad \text{(R2-7)}$$

$$I_{o(\lambda 1-\lambda 2)} = \sum_{i=\lambda 1}^{\lambda 2} \frac{I_a}{1 - 10^{-Ai}} (\text{photon m}^{-2}\ \text{s}^{-1}) = \sum_{i=\lambda 1}^{\lambda 2} \frac{I_a}{1 - 10^{-Ai}} \times \frac{hc}{\lambda i \times 10^{-6}} (\text{W m}^{-2}) \qquad \text{(R2-8)}$$

Irradiation of PNA solution (0.01 mM) in the presence of pyridine (0.1 mM) was performed for 240 min. The R_{PNA} was calculated as 1.57×10^{-10} M s^{-1} according to the decreased PNA concentration. ΔN_{PNA} was determined as 5.78×10^{14} molecules m^{-2} s^{-1}. So $\Phi_{PNA/pyr}$ and I_a were calculated as 3.24×10^{-4} and 1.79×10^{18} photon m^{-2} s^{-1}. The actual light intensity from 300-370 nm ($I_{o300-370nm}$) was determined as 567 W m^{-2}. The shape of the emission spectrum of the photoreactor was obtained by the optical fiber (Ocean Optics SD 2000) and then normalized energy by the results obtained in chemical actinometry though PNA degradation. The actual energy of the home-made phototreactor was shown in Figure 2-2.

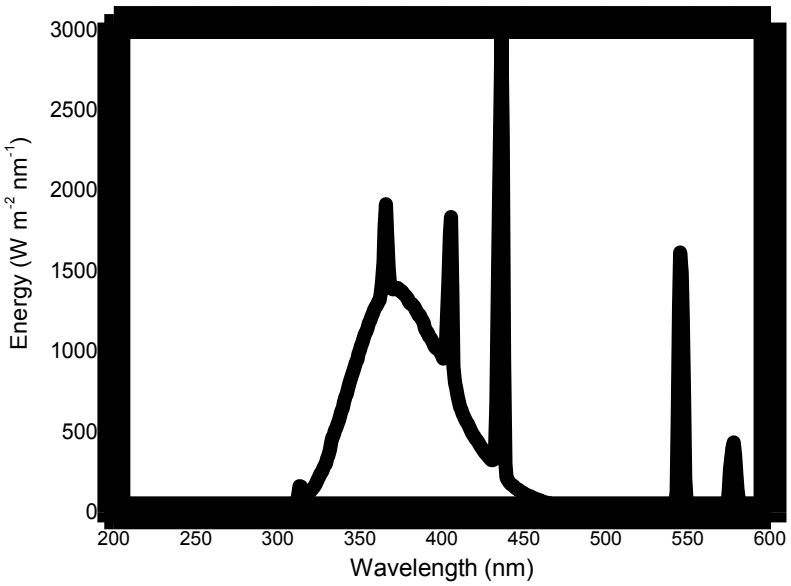

Figure 2-2 The actual spectrum of photoreactor

A. Photoreaction in the presence of Fe(III)-EDDS

The reaction solution was a mixture of by 4-t-BP and Fe(III)-EDDS solutions. The irradiation started since the solution was poured into the reactor. 0.5 ml solution was taken as a sample for the HPLC analysis at each fixed time. In this experiment,

the effects of pH, Fe(III)-EDDS concentration and dissolved oxygen concentration on the 4-t-BP degradation efficiency were investigated.

During the investigation on the effect of dissolved oxygen concentration, the solution was bubbled with oxygen or nitrogen for 30 min before the irradiation and during the irradiation.

B. Photoreaction in the presence of Fe(III)-EDDS and H_2O_2

The reaction solution was a mixture of 4-t-BP, Fe(III)-EDDS and H_2O_2 solutions. The experimental method was similar with photoreaction with Fe(III)-EDDS. In this experiment, the effects of pH, Fe(III)-EDDS concentration, H_2O_2 concentration and dissolved oxygen concentration on 4-t-BP degradation efficiency were investigated.

C. Reaction in the presence of Fe(III)-EDDS and H_2O_2

The reaction solution was a mixture of 4-t-BP, Fe(III)-EDDS and H_2O_2 solutions. However, it was poured into a brown reagent bottle and the reaction was performed without light. In this experiment, the effects of pH, Fe(III)-EDDS concentration, H_2O_2 concentration and dissolved oxygen concentration on 4-t-BP degradation efficiency were also investigated.

D. Photoreaction in the presence of Fe(III)-EDDS and $S_2O_8^{2-}$

The reaction solution was a mixture of 4-t-BP, Fe(III)-EDDS and $S_2O_8^{2-}$ solution. The experimental method was similar with photoreaction with Fe(III)-EDDS. In this

experiment, the effects of pH, Fe(III)-EDDS concentration, $S_2O_8^{2-}$ concentration and dissolved oxygen concentration on 4-t-BP degradation efficiency were investigated.

2.3.2 Irradiation with monochromator

For the determination of the second-order reaction rate constant between 4-t-BP and HO•, H_2O_2/4-t-BP solution was irradiated in monochromatic irradiation device (LOT-Oriel LTD. UK； light source: mercury lamp, 200 W). The wavelength of the monochromatic parallel beam was set at 313 nm. Because the photolysis of H_2O_2 would performed and HO• would be produced while the direct photolysis of 4-t-BP would not happen under the irradiation at this wavelength. So the 4-t-BP degradation was only due to the oxidation reaction with HO•. The sample was placed in the 1 cm quartz cell during the irradiation and was taken at a certain time interval for analysis of 4-t-BP concentration.

The 4-t-BP degradation rate ($R^d_{4\text{-t-BP}}$) was obtained after the irradiation experiment. Moreover, 2-Propanol was usually used as a quencher for HO• and the second-order reaction rate constant between 2-Propanol and HO• ($k_{2\text{-Propanol, HO}\bullet}$) was 1.9×10^9 M^{-1} s^{-1} [156]. So 2-Propanol and 4-t-BP were in competition with HO• during the irradiation. Different $R^d_{4\text{-t-BP}}$ was obtained when the different concentration of 2-Propanol was added. Finally, the second-order reaction rate constant between 4-t-BP and HO• ($k_{4\text{-t-BP, HO}\bullet}$) was calculated according to the $R^d_{4\text{-t-BP}}$ and 2-Propanol concentration (the particular mathematical calculation methods was shown in Chapter

3).

2.3.3 Laser flash photolysis experiment

The laser flash photolysis (LFP) experiments were performed to determine the second-order rate constants for the reactions between 4-t-BP and $SO_4^{\bullet-}$ ($k_{4\text{-t-BP, SO4}\bullet-}$), 2-Propanol and $SO_4^{\bullet-}$ ($k_{2\text{-Propanol, SO4}\bullet-}$), t-BuOH and $SO_4^{\bullet-}$ ($k_{\text{t-BuOH, SO4}\bullet-}$). The experiments were carried out using the fourth harmonic (λ_{exc} = 266 nm) of a Quanta Ray GCR 130-01 Nd:YAG laser system instrument, used in a right-angle geometry with respect to the monitoring light beam. The single pulse duration was 9 ns with an energy of ~40 mJ/pulse. The transient absorbance at the preselected wavelength was monitored by a detection system consisting of a pulsed xenon lamp (150 W), monochromator, and a photomultiplier (1P28). A spectrometer control unit was used for synchronizing the pulsed light source and programmable shutters with the laser output. The signal from the photomultiplier was digitized by a programmable digital oscilloscope (HP54522A). A 32 bits RISC-processor kinetic spectrometer workstation was used to analyze the digitized signal. The structure of the LFP device was shown in Figure 2-3.

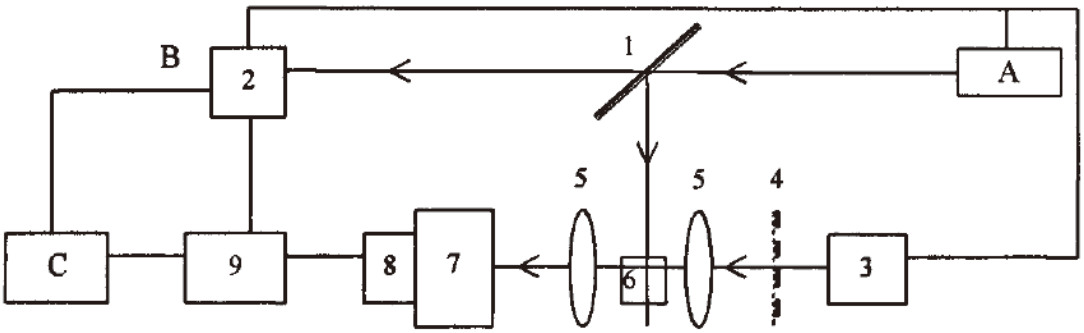

Figure 2-3 A sketch of the laser flash photolysis apparatus [157]

A. Laser generator; B. Transient absorption spectra device; C. Workstation

1. laser beam steering assembly; 2. spectrometor control unit; 3. xenon lamp; 4. cut-off (Chose according to the experiment); 5. lens; 6. sample cell; 7. monochromator; 8. photomultiplier; 9. digital oscilloscope.

An appropriate volume of chemicals stock solutions (4-t-BP, $S_2O_8^{2-}$, scavengers) was mixed just before each experiment to obtain the desired concentrations. Moreover a peristaltic pump was used to continuously replace the solution inside the cuvette in order to avoid sample degradation after LFP shot. All experiments were performed at ambient temperature (295 ± 2 K) and in aerated solution. The $SO_4^{\bullet-}$ decay was followed at 450 nm corresponding to the maximum absorption of the specie [158].

The $SO_4^{\bullet-}$ was produced through the photolysis of $K_2S_2O_8$ under the 266 nm laser irradiation. To determine the second-order rate constant for the quenching of $SO_4^{\bullet-}$, plots were made of the first-order decay constant of $SO_4^{\bullet-}$, determined from the regression lines of the logarithmic decays of $SO_4^{\bullet-}$ monitored at 450 nm, against the concentration of quencher (4-t-BP/2-Propanol/t-BuOH).

2.4 Analytical methods

2.4.1 High Performance Liquid Chromatographic method

The concentration of organic compounds in the aqueous solution were determined by high performance liquid chromatography (HPLC) equipped with a photodiode array detector (Waters 996, USA), two pumps (Waters 515, USA) and an autosampler (Waters 717 plus, USA).

A. Analysis of 4-t-BP

The column was a Nucleodur 100-5 C18 column (5 μm×4.6 mm×250 mm). The flow rate was 1 mL min^{-1}, and the mobile phase was a mixture of water and methanol (20/80, v/v). The injection volume was 50 μL and the temperature of column was 20℃. In this condition, the retention time of 4-t-BP (detected at 221 nm) was 6.5 min. The calibration curve of 4-t-BP was shown in Figure 2-4.

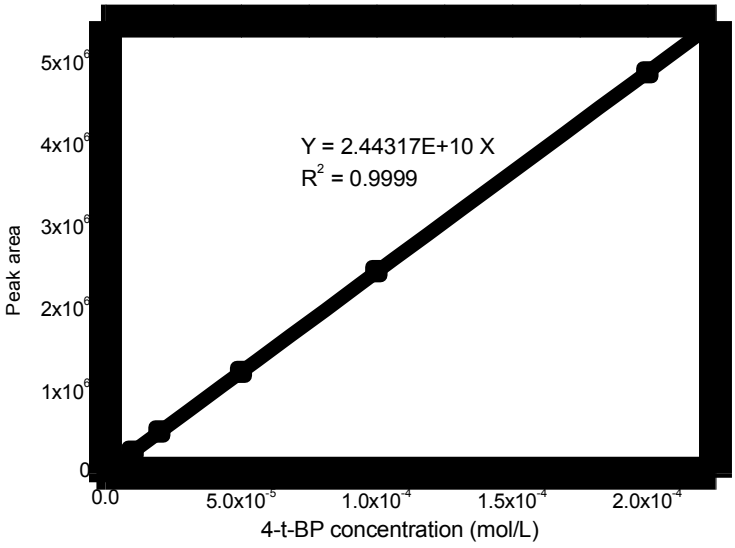

Figure 2-4 Calibration curve of 4-t-BP

B. Analysis of PNA

The column was a Zorbax RX-C8 column (5 μm×4.6 mm×250 mm). The flow rate was 1 mL min^{-1}, and the mobile phase was a mixture of water and methanol (40/60, v/v). The injection volume was 50 μL and the temperature of column was 20℃. In this condition, the retention time of PNA (detected at 317 nm) was 15.1 min. The calibration curve of 4-t-BP was shown in Figure 2-5.

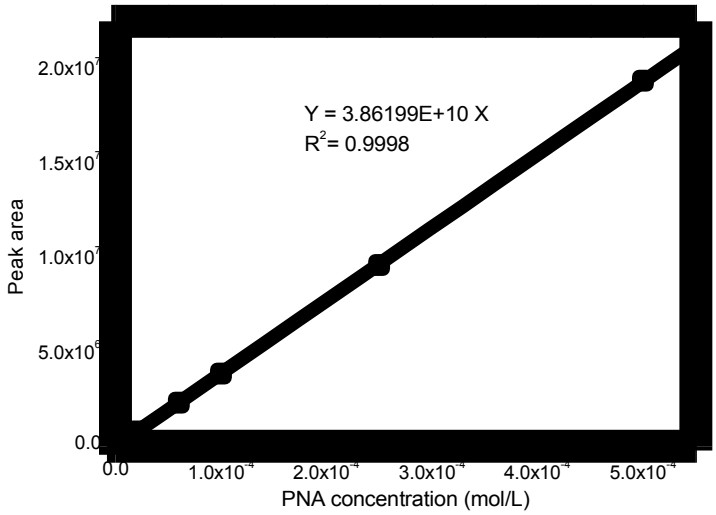

Figure 2-5 Calibration curve of PNA

C. Analysis of Fe(III)-EDDS

The column was a Agilent Eclipse XDB-C18 column (5 μm×4.6 mm×150 mm). The flow rate was 0.8 mL min^{-1}, and the mobile phase was a mixture of Eluent A (as described in section 2.2) and methanol (95/5, v/v). The injection volume was 50 μL and the temperature of the column was 20℃. In this condition, the retention time of Fe(III)-EDDS (detected at 240 nm) was 6.8 min. The calibration curve of Fe(III)-EDDS was shown in Figure 2-6.

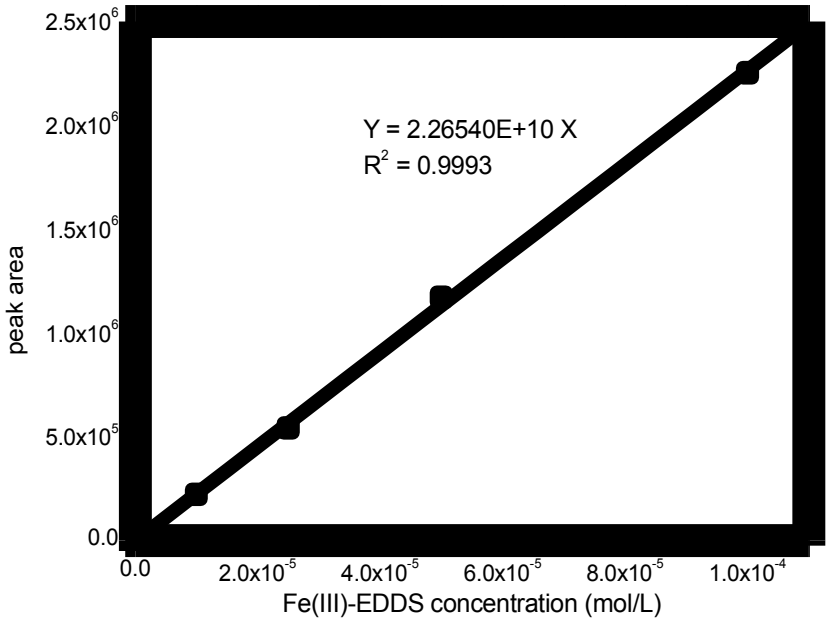

Figure 2-6 Calibration curve of Fe(III)-EDDS

2.4.2 Determination of H_2O_2 concentration

According to the literature [159-160], the TAOH reacted with H_2O_2 in the presence of peroxidase. The reaction was shown as R2-9. The TAOH which did not have fluorescence was transformed to p-hydroxyphenyl acetic acid dimer which had strong fluorescence and one H_2O_2 molecule was consumed in this reaction. The excitation wavelength of p-hydroxyphenyl acetic acid dimer was 320 nm and the emission wavelength of the fluorescence was 400 nm [161]. Therefore, the H_2O_2 concentration could be calculated by detecting the concentration of the p-hydroxyphenyl acetic acid dimer. In this study, the amount of Na_2EDTA was added to shield interference of iron ions. The calibration curve of H_2O_2 obtained by using this detection method was showed in Figure 2-7.

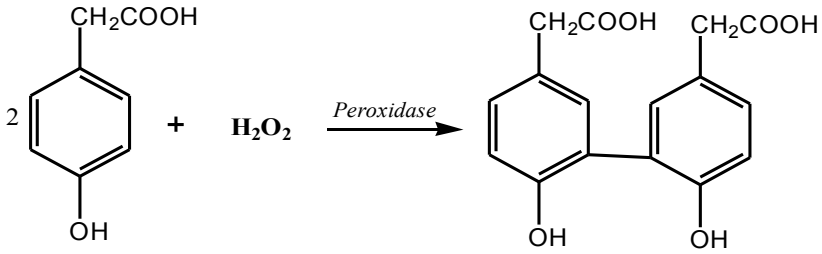
CH2COOH
2
+
H2O2
Peroxidase
CH2COOH
CH2COOH
OH
OH
OH

(R2-9)

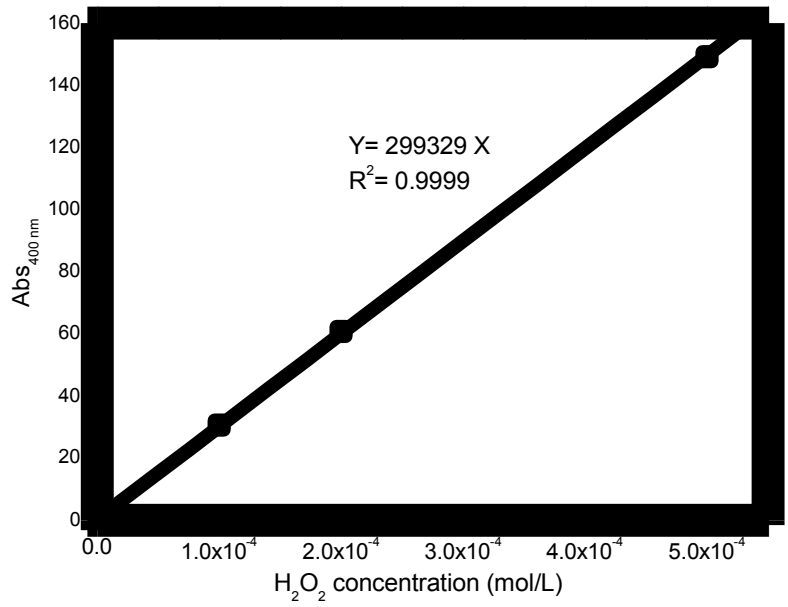
Y= 299329 X
R2= 0.9999
Abs400 nm
160
140
120
100
80
60
40
20
0
0.0
1.0x10-4
2.0x10-4
3.0x10-4
4.0x10-4
5.0x10-4
H2O2 concentration (mol/L)

Figure 2-7 Calibration curve of H_2O_2

2.4.3 Determination of dissolved ferrous iron

According to the literature [162], when the pH value of the solution was between 3 and 10, Fe(II) and Ferrozine could form a stable carmine complex which had the maximum absorption wavelength at 562 nm. In this study, the Fe(II) concentration was determined by complexometry with Ferrozine according to this mechanism. In previous studies, the molar absorption coefficient ($\varepsilon_{562\ nm}$) was reported as 2.65×10^4 M^{-1} cm^{-1} and 2.79×10^4 M^{-1} cm^{-1} [163].

Different concentrations of ferrous ammonium sulfate solutions were prepared and acetic acid/sodium acetate buffer was used to keep the pH of the solution at around 5.5. The calibration curve was obtained by this analysis method, shown in Figure 2-8. The $\varepsilon_{562\ nm}$ was calculated as 2.61×10^4 M^{-1} cm^{-1} which was close to the value in the literatures. It proved the feasibility of this analytical method. In this study, some samples with high Fe(II) concentration should be diluted before analysis.

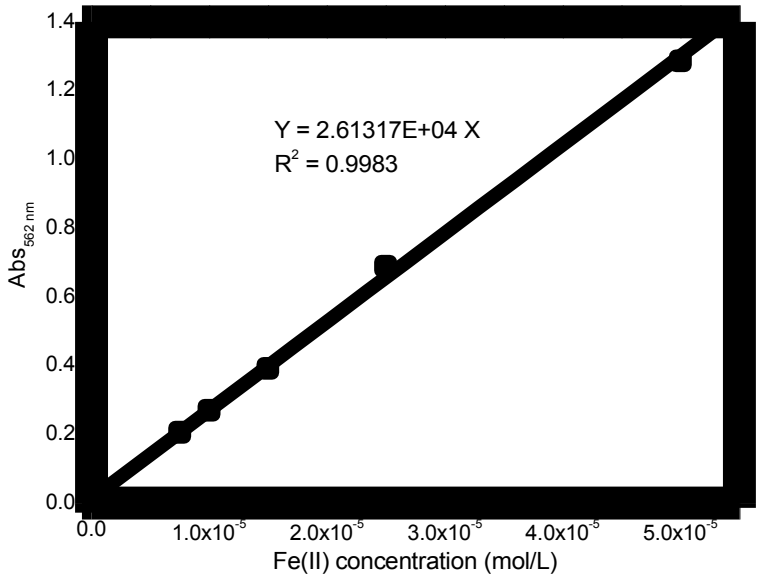
Y = 2.61317E+04 X
R2 = 0.9983
Abs562 nm
1.4
1.2
1.0
0.8
0.6
0.4
0.2
0.0
0.0
1.0x10-5
2.0x10-5
3.0x10-5
4.0x10-5
5.0x10-5
Fe(II) concentration (mol/L)

Figure 2-8 Calibration curve of Fe(II)

2.4.4 pH measurement

The pH value of the solution was adjusted with $HClO_4$ or NaOH. pH values of the solutions were measured using a Cyberscan 510 pH meter.

2.4.5 UV-vis Spectrophotometer

The UV-vis spectra of the solutions were recorded with a Cary 300 UV-visible spectrophotometer. The parameters of UV-visible spectrophotometer were shown in Table 2-2.

Table 2-2 The experimental parameters of UV-visible spectrophotometer

Parameters	UV-visible spectrophotometer
Model	Cary 300, Varian, USA
Detection wavelength range	200-800 nm
Precision of wavelength	1.0 nm
Scanning time	1.0 min

Chapter 3

PHYSICOCHEMICAL PROPERTIES OF Fe(III)-EDDS AND THE PHOTODEGRADATION OF 4-t-BP IN THE PRESENCE OF Fe(III)-EDDS

Chapter 3 Physicochemical properties of Fe(III)-EDDS and the photodegradation of 4-t-BP in the presence of Fe(III)-EDDS

It is well known that iron is one of the most widespread natural elements. Many

researchers hoped that the natural resources could be furthest utilized. So the studies had already performed on the photochemical properties of iron complexes (including: Fe(III)-citrate, Fe(III)-oxalate, Fe(III)-NTA, Fe(III)-EDTA) and their application on the degradation of contaminants.

However, so far, the research on the physicochemical properties of new iron complex Fe(III)-EDDS is not complete. This chapter will study the mechanism of the photodegradation of 4-t-BP in the presence of Fe(III)-EDDS and the effects of pH value, Fe(III)-EDDS concentration and dissolved oxygen on the 4-t-BP degradation efficiency will be investigated. It will provide a theoretical basis for the Fe(III)-EDDS application in advanced oxidation technology.

3.1 Characteristics of Fe(III)-EDDS and 4-t-BP

3.1.1 Characteristics of Fe(III)-EDDS

The UV-visible spectrum of Fe(III)-EDDS solution was shown in Figure 3-1. No absorption was observed at $\lambda > 400$ nm.

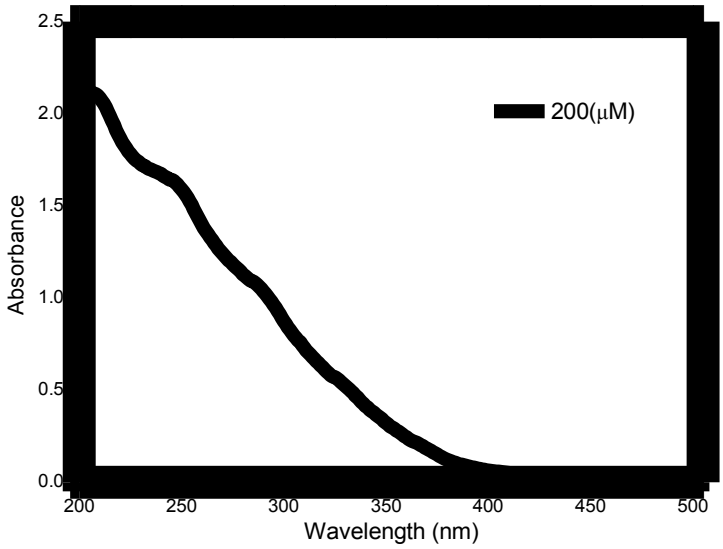

Figure 3-1 UV-vis absorption spectra of Fe(III)-EDDS

Fe(III)-EDDS was a complex formed by Fe(III) and EDDS in specific proportion. Job's Method [164] was used to determine the proportion between Fe(III) and EDDS in this study. Job's method was built in 1928 by chemist P. Job [165] and was used to determine the stoichiometry of a binding event. This method was widely used in analytical chemistry, instrumental analysis, advanced chemical equilibrium texts and research articles [166-167].

In solutions where two species were present (A and B), one A molecule might bind to the one B molecule. In some cases, more than one A would bind with a single B. So the Job's Method was used to determine the amount of A binding to B. In this method, the total molar concentrations of the two binding partners (A and B) were held constant, but their mole fractions were varied. An observable that was proportional to complex formation (such as absorption signal) was plotted against the mole fractions of these two species. The maximum on the plot corresponded to the stoichiometry of the two species. The result of Job's Method was shown in Figure 3-2.

According to the results, the stoichiometry of Fe(III)-EDDS formation was Fe(III): EDDS = 1:1. Meanwhile, the experimental result showed that Fe(III)-EDDS solution could keep stable for at least 7 days.

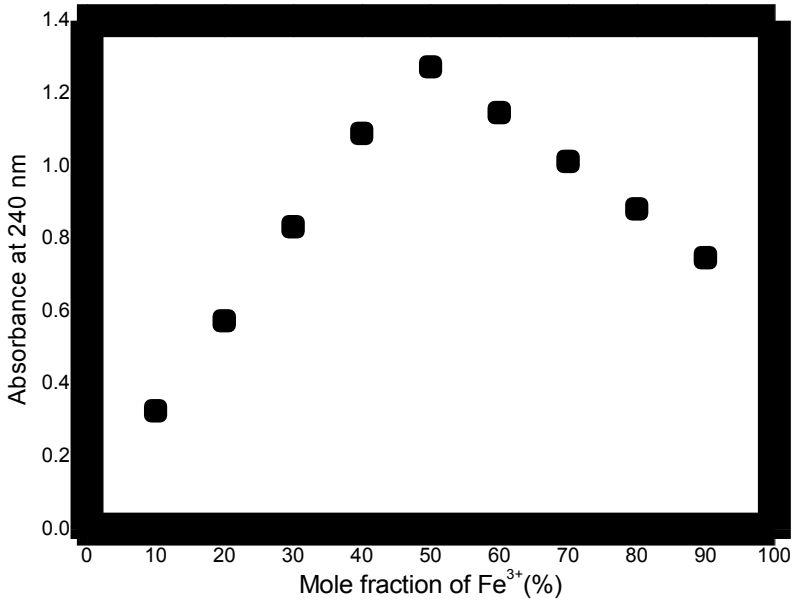

Figure 3-2 Effect of molar ratio on the binding of Fe(III) and EDDS

3.1.2 Characteristics of 4-t-BP

The UV-visible spectra of 4-t-BP solution (100 μM) at different pH were shown in Figure 3-3. The results showed that 4-t-BP remained the molecular form when the pH was lower than 8.8; the 4-t-BP molecule began to ionize in alkaline conditions when the pH was higher than 8.8.

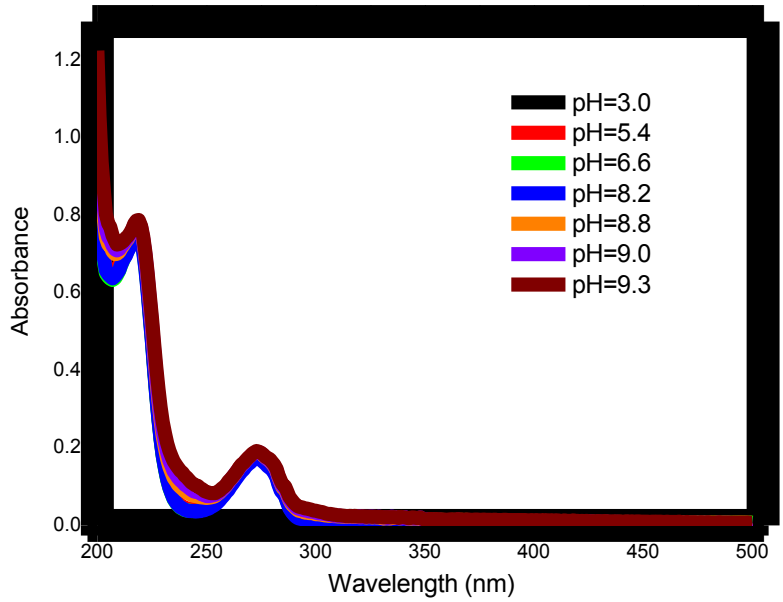

Figure 3-3 UV-vis absorption spectra of 4-t-BP (100 μM) at different pH

The UV-visible spectra of 4-t-BP solution with different concentration were shown in Figure 3-4. The results showed that no absorption was observed at $\lambda > 300$ nm; Two absorption peaks were at 221 nm and 274 nm; the molar absorption coefficients at 221 nm and 274 nm were calculated as $\varepsilon_{221nm} = 7185\ M^{-1}\ cm^{-1}$ and ε_{274nm}

= 1592 M^{-1} cm^{-1}.

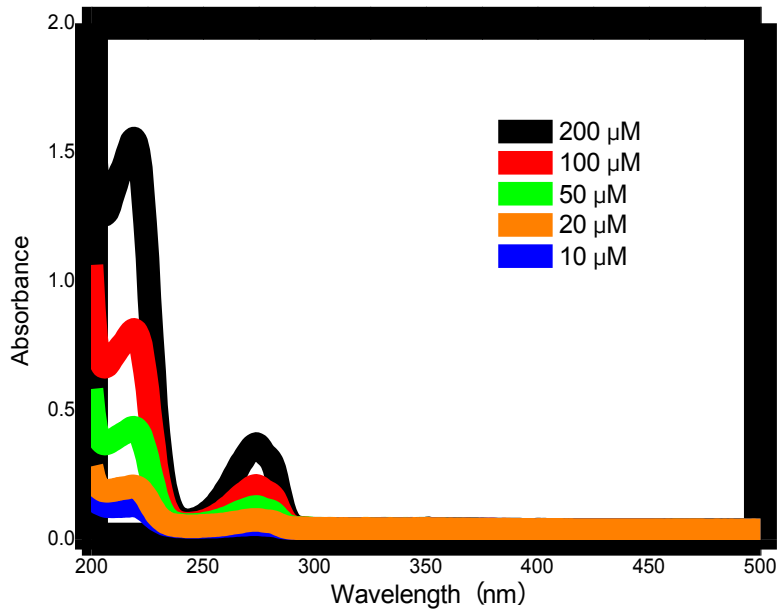
2.0
1.5
1.0
0.5
0.0
Absorbance
200
250
300
350
400
450
500
Wavelength (nm)
200 μM
100 μM
50 μM
20 μM
10 μM

Figure 3-4 UV-vis absorption spectra of 4-t-BP at different concentration

3.2 Photochemical reactivity of Fe(III)−EDDS

The degradation efficiency of 4-t-BP was obtained to present the photochemical reactivity of Fe(III)-EDDS. The 4-t-BP concentration was followed during the irradiation in the presence of Fe(III)-EDDS. The results were shown in Figure 3-5. 4-t-BP was not photodegraded without Fe(III)-EDDS because 4-t-BP did not absorb the UV light whose wavelength was higher than 300 nm. 4-t-BP also did not react with Fe(III)-EDDS without UV irradiation. However, in the presence of UV light and Fe(III)-EDDS, approximately 17% of the 4-t-BP was transformed after 10 min of irradiation but only 5% of it was removed in the following 50 min. The Fe(III)-EDDS concentration was followed at the same time. The result showed that 95% of Fe(III)-EDDS was consumed in the first 10 min of the reaction. Therefore, the degradation of 4-t-BP was due to the photolysis of Fe(III)-EDDS.

The photoreduction reaction and a series of radical chain reactions were occurred in the presence of Fe(III)-EDDS during the UV irradiation. Fe(II) and HO• were generated as the final products of these reactions, shown as R3-1. HO• attacked 4 -t-BP and 4-t-BP was degraded.

$$Fe(III)\text{-}EDDS \xrightarrow{h\nu} Fe(II) + EDDS^{\bullet} \cdots \rightarrow Fe(II) + HO^{\bullet} \quad \text{(R3-1)}$$

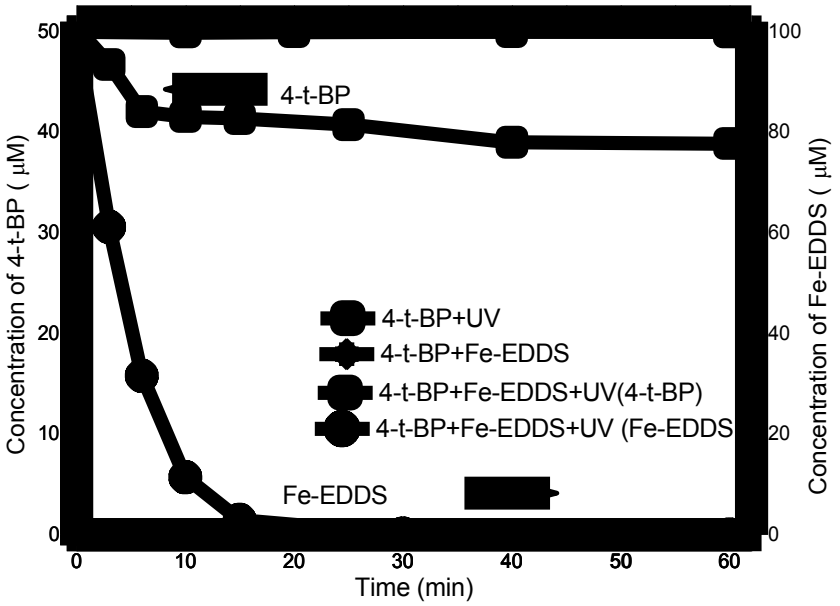

Figure 3-5 4-t-BP degradation in the presence of different systems with or without light and with or without Fe(III)-EDDS

Chemical kinetics, also known as reaction kinetics, was the study on the rates of chemical processes and how different experimental conditions (such as pH value, concentration, temperature and catalyst) influenced the chemical reaction rate [168]. The rate laws usually included zero-order reactions (the reaction rate was independent

of concentration), first-order reaction and second-order reaction. Most of the chemical reactions obeyed the first-order kinetic model which meant the reaction rate was proportional to the concentration of reactant. The formula was shown as R3-2.

$$v = -\frac{dC}{dt} = kC \quad \text{(R3-2)}$$

The initial time and reactant concentration were set as t = 0 and C_o. The final time and reactant concentration were set as is t and C_t. The integral of R3-2 could form the formula R3-3. The k was the first-order reaction rate constant and the unit was s^{-1}.

$$InC_t - InC_0 = -kt \quad \Rightarrow In\frac{C_t}{C_0} = -kt \quad \text{(R3-3)}$$

In the degradation of 4-t-BP, the reaction process took place efficiently in the first 10 min. So the data obtained in 10 min were plotted according to the first-order kinetic model and the result was shown in Figure 3-6. The result showed that 4-t-BP photodegradation in the presence of Fe(III)-EDDS obeyed the first-order reaction kinetic model and $k = 3.6679\times10^{-4}$ s^{-1}. The degradation rate of 4-t-BP was calculated with the equation $R^d_{4\text{-t-BP}} = kC_0 = 1.83\times10^{-8}$ M s^{-1}. $R^d_{4\text{-t-BP}}$ was used to indicate the 4-t-BP degradation efficiency in our following study.

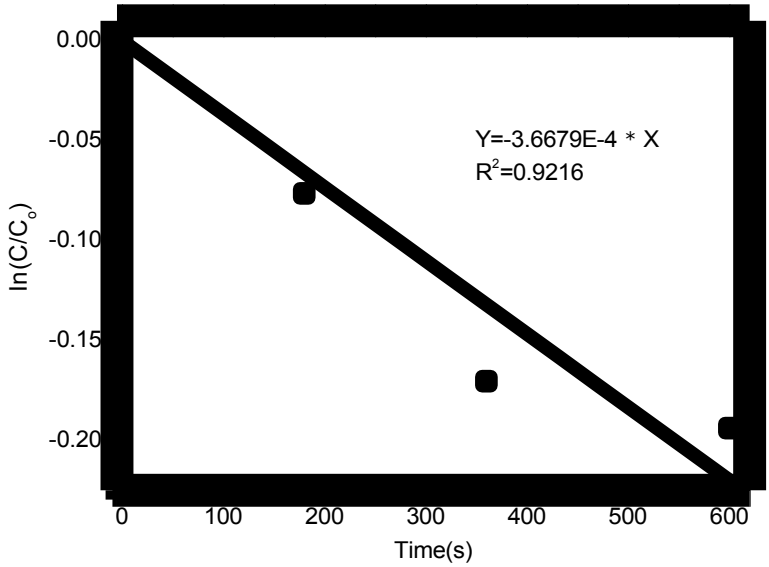

Figure 3-6 The first-order kinetic model of 4-t-BP degradation in UV/Fe(III)-EDDS system

3.3 Effect of pH

3.3.1 pH effect on form of Fe(III)-EDDS

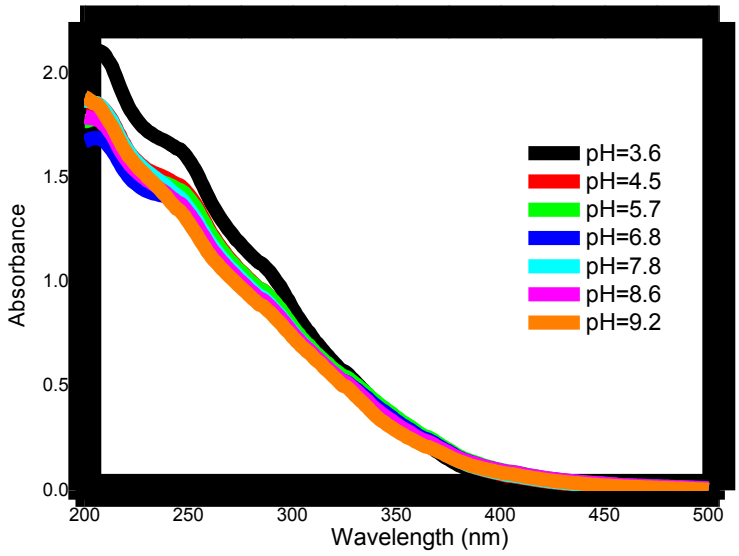

The UV-visible

spectra of Fe(III)-EDDS solution (200 μM) at different pH were shown in Figure 3-7. According to the results, the form of Fe(III)-EDDS was obviously affected by pH value. Even small changes in pH value could cause the changes in its form.

Figure 3-7 UV-vis absorption spectra of Fe(III)-EDDS (200 μM) at different pH

According to the chemical structure showed in Figure 1-1, EDDS was a weak tetra-acid (expressed H_4L). Its ionization equilibriums were shown as R(3-4) to R(3-7) [169]. H_4L, H_3L^-, H_2L^{2-}, HL^{3-} and L^{4-} were the main existence form of EDDS at pH <2.4, 2.4-3.9, 3.9-6.8, 6.8-9.8 and > 9.8, respectively.

$$H_4L \rightarrow H^+ + H_3L^- \quad pK_1 = 2.4 \quad \text{(R3-4)}$$

$$H_3L^- \rightarrow H^+ + H_2L^{2-} \quad pK_2 = 3.9 \quad \text{(R3-5)}$$

$$H_2L^{2-} \rightarrow H^+ + HL^{3-} \quad pK_3 = 6.8 \quad \text{(R3-6)}$$

$$HL^{3-} \rightarrow H^{+} + L^{4-} \quad pK_4 = 9.8 \quad \text{(R3-7)}$$

Fe(III) bound with EDDS and then formed Fe(III)-EDDS. Fe(III)-EDDS also exhibited four different main forms (FeL^-、$Fe(OH)L^{2-}$、$Fe(OH)_2L^{3-}$ and $Fe(OH)_4^-$) at different pH [170].Theoretical calculations with software Gaussian09 were performed and the distribution of four different forms at different pH values was shown in Figure 3-8. The results from theoretical calculation showed that FeL^- was the main (only) species when the pH value was lower than 6.0. With the increase of pH value, $Fe(OH)L^{2-}$、$Fe(OH)_2L^{3-}$ and $Fe(OH)_4^-$ were formed gradually, while the proportion of FeL^- was decreased. Meanwhile, with the increase of pH, $Fe(OH)_3$ was gradually formed, so the total amount of soluble Fe(III) showed a gradual decline.

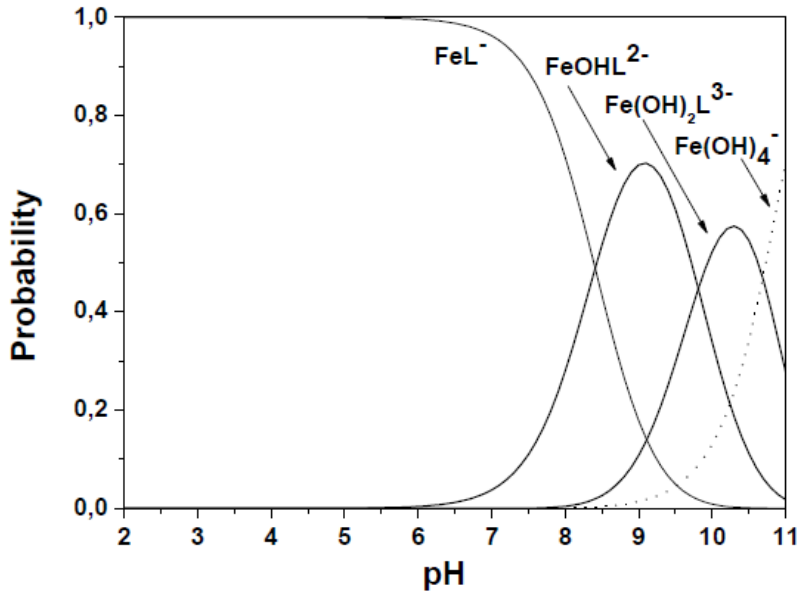

Figure 3-8 Proposed theoretical model distribution of the predominant species for the Fe(III)-EDDS complex as a function of pH

3.3.2 pH effect on 4-t-BP degradation

To better understand the effect of pH value during the photodegradation of 4-t-BP in the presence of Fe(III)-EDDS, experiments at different pHs between 2.6 and 9.3 were conducted. In this series of experiments, Fe(III)-EDDS concentration was 100 μM. The results reported in Figure 3-9 showed the rapidly increasing degradation rate of 4-t-BP ($R_{4\text{-t-BP}}$) between pH 2.6 and 4.5, and the slowly increase of $R_{4\text{-t-BP}}$ between pH 4.5 and 8.0, whereas $R_{4\text{-t-BP}}$ started to decrease at pH higher than 8.0. $R_{4\text{-t-BP}}$ was calculated from the data obtained at the beginning 10 min of irradiation to ensure the pH was unchanged. Li et al. [99] reported similar results at pH between 3.1 and 8.0.

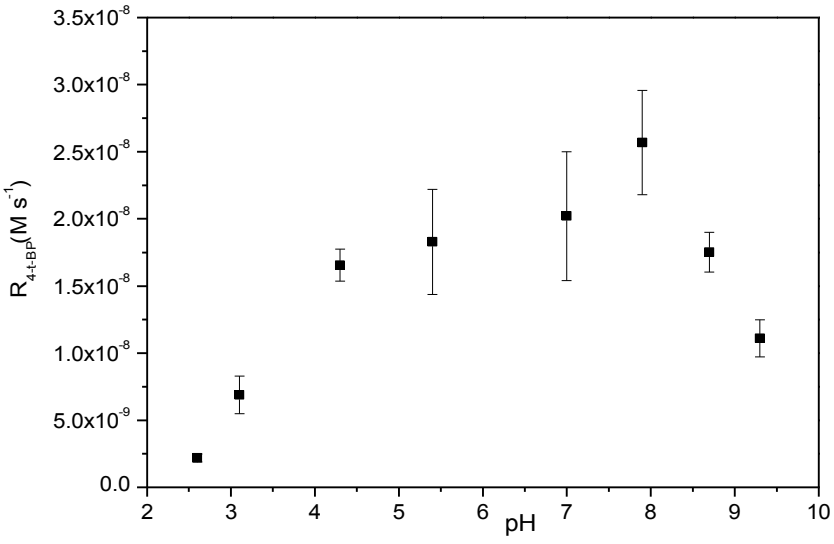

Figure 3-9 Effect of pH value on the degradation rate of 4-t-BP

As it is mentioned in the paper of Huang et al. [100], the observed effect of pH could be due to the formation of $HO_2^{\bullet}/O_2^{\bullet-}$ radicals and/or to the presence of different

forms of the complex Fe(III)-EDDS as a function of pH. The $HO_2^{\bullet}/O_2^{\bullet-}$ radicals were formed in UV/Fe(III)-EDDS system by reaction R3-8, R3-9 and R3-10 [156, [171]]. The $HO^{\bullet}$ was produced from $HO_2^{\bullet}/O_2^{\bullet-}$ and Fe(II) by the reaction R3-11[171] and R3-12[[172]] in this system. However, for the first part of the effect of pH, until pH 6.0, the effect of Fe(III)-EDDS speciation could be excluded. Indeed, as we evaluated by theoretical calculation the second form of the complex appear from pH 6.0 (Figure 3-8). On the contrary, the decrease of the degradation rate of 4-t-BP from pH 8.0, correspond to the presence of the second form $Fe(OH)L^{2-}$ at 50% and 50% of the starting form FeL^{-} present in acidic pH. For the first time, we proved that the hydroxylated form $Fe(OH)L^{2-}$ of such complex was less efficient photochemicaly in terms of photoredox process (R3-8).

$$Fe(III)\text{-}EDDS + h\nu \rightarrow Fe(II) + EDDS^{\bullet+} \qquad \text{(R3-8)}$$

$$EDDS^{\bullet+} + O_2 \rightarrow product + O_2^{\bullet-} \qquad \text{(R3-9)}$$

$$HO_2^{\bullet} \leftrightarrow O_2^{\bullet-} + H^+ \quad pK_a=4.88 \qquad \text{(R3-10)}$$

$$O_2^{\bullet-} + HO_2^{\bullet} + H_2O \rightarrow H_2O_2 + O_2 + OH^- \quad k=9.7\times10^7\ M^{-1}\ s^{-1} \qquad \text{(R3-11)}$$

$$Fe^{2+} + H_2O_2 \rightarrow Fe^{3+} + HO^{\bullet} + OH^- \quad k=76\ M^{-1}\ s^{-1} \qquad \text{(R3-12)}$$

The observed increase of the degradation rate of 4-t-BP until pH 8.0 was due to

the iron cycle and the relative concentration between Fe(III) and Fe(II) species. These relative concentrations were strongly impacted (reactions R3-13 to R3-16 [173-174175]) by the presence of $HO_2^{\bullet}/O_2^{\bullet-}$ radicals photogenerated from the complex Fe(III)-EDDS (reactions R3-8, R3-9 and R3-10). Obviously, $O_2^{\bullet-}$ formed in alkaline condition was in favour of the presence of Fe(II) species. As a contrary, the presence of $HO_2^{\bullet}$ favoured the formation of Fe(III) species.

$$Fe^{3+} + O_2^{\bullet-} \rightarrow Fe^{2+} + O_2 \quad k=5.0\times10^7\ M^{-1}\ s^{-1} \qquad \text{(R3-13)}$$

$$Fe^{2+} + O_2^{\bullet-} + 2H_2O \rightarrow Fe^{3+} + H_2O_2 + 2OH^- \quad k=1.0\times10^7\ M^{-1}\ s^{-1} \qquad \text{(R3-14)}$$

$$Fe^{3+} + HO_2^{\bullet} \rightarrow Fe^{2+} + O_2 + H^+ \quad k<1.0\times10^3\ M^{-1}\ s^{-1} \qquad \text{(R3-15)}$$

$$Fe^{2+} + HO_2^{\bullet} + H_2O \rightarrow Fe^{3+} + H_2O_2 + OH^- \quad k=1.2\times10^6\ M^{-1}\ s^{-1} \qquad \text{(R3-16)}$$

To generate the maximum concentration of $HO^{\bullet}$, a photochemically efficient Fe(III) species was needed and also the formation of Fe(II) species which were essential for the Fenton process producing of $HO^{\bullet}$ (reaction R3-12). Moreover, in the iron cycle the oxidation of Fe(II) into Fe(III) was strongly pH dependent in terms of efficiency and also in terms of Fe(III) species formed. The slow increasing of the 4-t-BP degradation rate observed after pH 4.5 was due to the formation of different forms of iron species and of insoluble iron oxides which present a lowest photoactivity.

3.4 Effect of Fe(III)-EDDS concentration

4-t-BP disappearance was followed at different initial concentrations of Fe(III)-EDDS ranging from 50 to 600 μM at pH 4.5. The results were shown in Figure 3-10. The rate of 4-t-BP degradation increased with increased concentrations of Fe(III)-EDDS in the range of 50 to 400 μM, but much higher concentration of Fe(III)-EDDS (such as 500 and 600 μM) inhibited 4-t-BP degradation. Li et al. [99] reported the similar degradation rate variation under various Fe(III)-EDDS complex concentrations.

These results gave clear evidence that photolysis of Fe(III)-EDDS could induce the degradation of 4-t-BP due to the reaction between 4-t-BP and $HO^{\bullet}$ which was formed during the photolysis of Fe(III)-EDDS. But $HO^{\bullet}$ could also react with Fe(III)-EDDS. When the concentration of Fe(III)-EDDS was high, Fe(III)-EDDS played the role as a competitor for $HO^{\bullet}$. In fact, considering that the second order rate constant between Fe(III)-EDDS and $HO^{\bullet}$ has been estimated around 2×10^{8} M^{-1} s^{-1} [176], it could be calculated that about 98% of photogenerated $HO^{\bullet}$ reacted with 4-t-BP at lower concentration of Fe(III)-EDDS (50 μM). On the other hand, 23% of $HO^{\bullet}$ were reacting with iron complex at 600 μM of Fe(III)-EDDS. Therefore, the appropriate concentration of Fe(III)-EDDS should be chosen for 4-t-BP degradation.

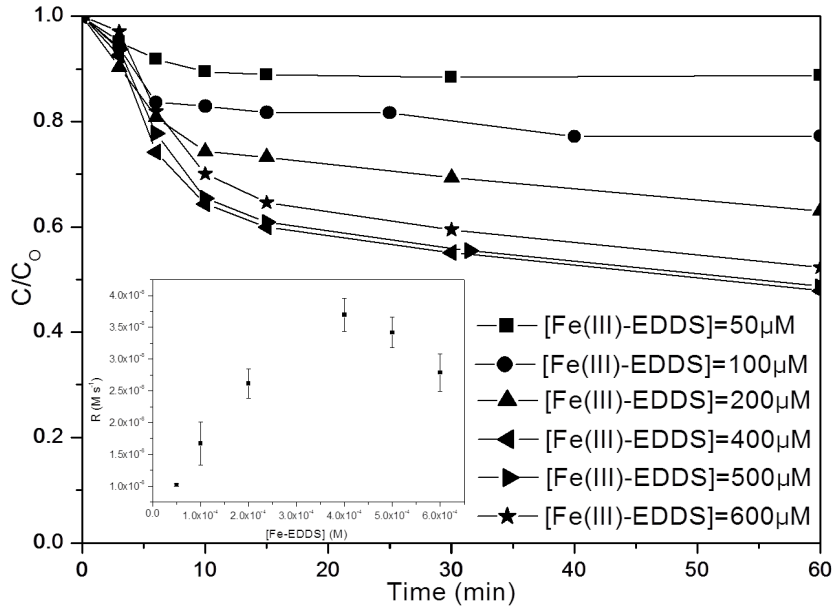

Figure 3-10 Effect of Fe(III)-EDDS concentration on the degradation of 4-t-BP (Insert: The 4-t-BP degradation rate as a function of Fe(III)-EDDS concentration)

3.5 Effect of oxygen

The effect of oxygen on 4-t-BP photodegradation in the presence of Fe(III)-EDDS was shown in Figure 3-11. The faster decay of 4-t-BP was noticed at higher oxygen concentration (bubbling oxygen), while at the lower oxygen concentration (bubbling nitrogen) the 4-t-BP removal was retarded. Another control experiment was taken to confirm the mechanism of the photochemical process of Fe(III)-EDDS complex. 5 mM of 2-Propanol was added in the solution which was bubbled with nitrogen. The result showed that 4-t-BP was not degraded due to the quenching of $HO^{\bullet}$ by 2-Propanol and so confirmed the formation of this radical in the photochemical process from Fe(III)-EDDS complex, even in the absence of oxygen.

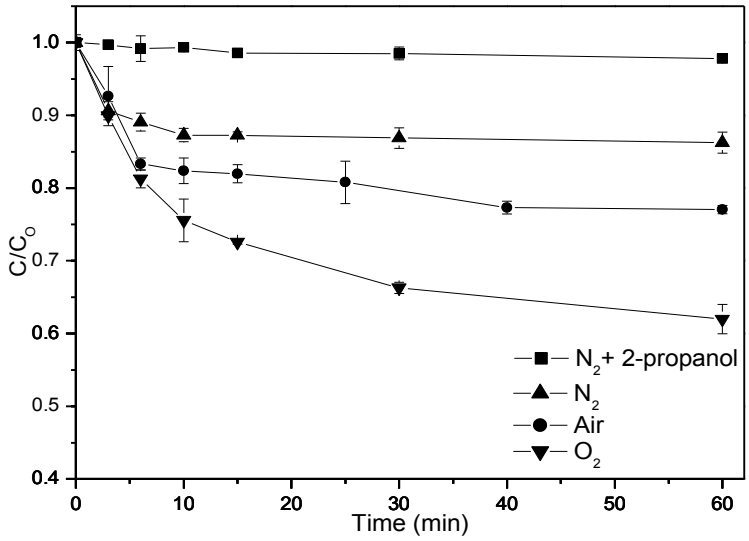

Figure 3-11 Effect of oxygen on the degradation rate of 4-t-BP

According to the reactions listed in section 3.3.2, dissolved oxygen (DO) was an important factor for HO• formation. So with the higher concentration of DO, greater amount of HO• was generated and more 4-t-BP molecules were degraded. The control experiment by adding 2-Propanol gave the further evidence of the 4-t-BP degradation which was caused by HO•.

3.6 Determination of the second-order rate constant between HO• and 4-t-BP

The rate constant of the reaction between HO• and 4-t-BP was measured by competition kinetics with 2-propanol, a compound of known reaction rate constant with HO•. The degradation efficiencies of 4-t-BP in the presence of different

concentrations of 2-propanol were shown in Figure 3-12. H_2O_2 (1.0 mM) photolysis was used as source of HO•, which would induce the following main reactions (R3-17 to R3-20) in the system containing both 2-propanol and 4-t-BP.

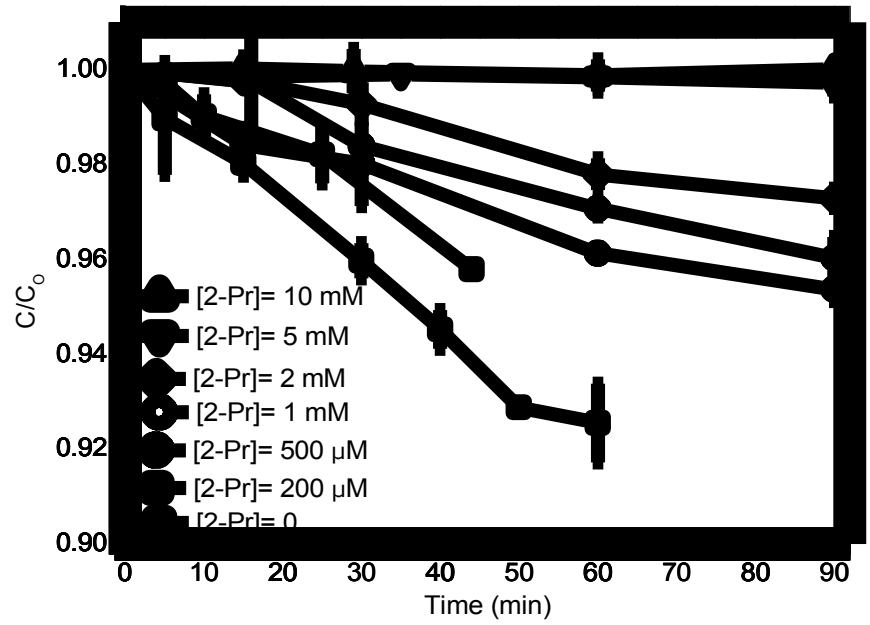

Figure 3-12 Effect of 2-Propanol concentration on the degradation of 4-t-BP

$$H_2O_2 + h\nu \rightarrow 2\,HO^{\bullet} \qquad R^{f}_{\bullet OH}(M\,s^{-1}) \qquad \text{(R3-17)}$$

$HO^{\bullet} + 4\text{-t-BP} \rightarrow$ products $\quad k_{4\text{-t-BP},\bullet OH}$ (R3-20)

$H_2O_2 + HO^{\bullet} \rightarrow H_2O + HO_2^{\bullet}$ $\quad k_{H2O2,\bullet OH} = 2.7\times10^7\ M^{-1}\ s^{-1}$ [177] (R3-21)

2-propanol $+ HO^{\bullet} \rightarrow$ products $\quad k_{2\text{-propanol},\bullet OH} = 1.9\times10^9\ M^{-1}\ s^{-1}$[177] (R3-22)

The application of the steady-state approximation to the concentration of $HO^{\bullet}$ yielded to the following equation (Eq. 3-1) to describe the degradation rate of 4-t-BP ($y = R^d_{4\text{-t-BP}}$) as a function of 2-propanol concentration ($x = [2pr]$).

$$R^d_{4\text{-t-BP}} = \frac{R^f_{\bullet OH} k_{4\text{-t-BP},\bullet OH}[4\text{-t-BP}]}{k_{4\text{-t-BP},\bullet OH}[4\text{-t-BP}] + k_{H_2O_2,\bullet OH}[H_2O_2] + k_{2\_pr,\bullet OH}[2pr]} \quad \text{(Eq. 3-1)}$$

The $R^d_{4\text{-t-BP}}$ obtained at different 2-Propanol concentration was plotted in Figure 3-13 and they were fitted with a rational equation type: $y = \frac{A}{1 + Bx}$ with

$$A = \frac{R^f_{\bullet OH} k_{4\text{-t-BP},\bullet OH}[4\text{-t-BP}]}{k_{4\text{-t-BP},\bullet OH}[4\text{-t-BP}] + k_{H_2O_2,OH}[H_2O_2]} \text{ and } B = \frac{k_{2pr,\bullet OH}}{k_{4\text{-t-BP},\bullet OH}[4\text{-t-BP}] + k_{H_2O_2,\bullet OH}[H_2O_2]}.$$

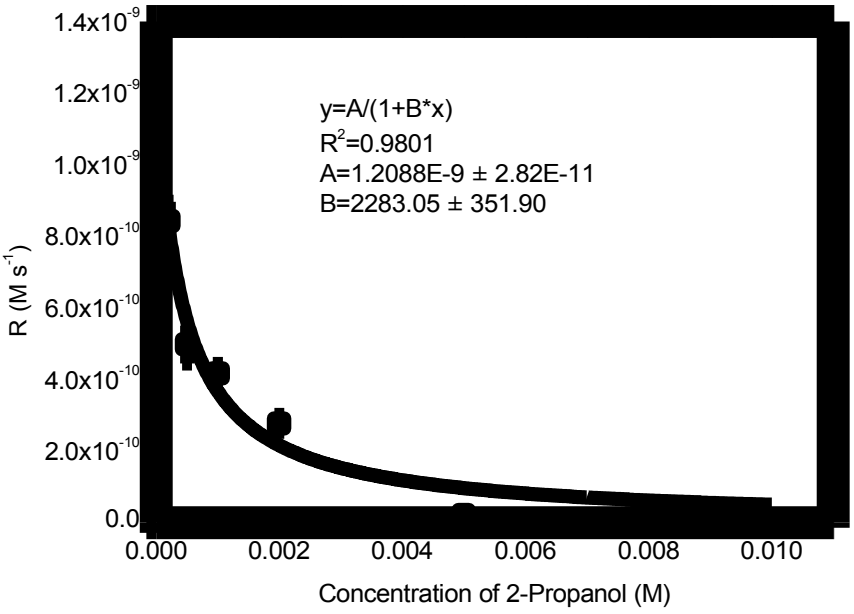
y=A/(1+B*x)
R2=0.9801
A=1.2088E-9 ± 2.82E-11
B=2283.05 ± 351.90
R (M s-1)
1.4x10-9
1.2x10-9
1.0x10-9
8.0x10-10
6.0x10-10
4.0x10-10
2.0x10-10
0.0
0.000
0.002
0.004
0.006
0.008
0.010
Concentration of 2-Propanol (M)

Figure 3-13 Degradation rate of 4-t-BP in the presence of different 2-propanol concentration

The formation rate of $HO^{\bullet}$ ($R^{f}_{\bullet OH}$) and the second-order rate constant of the reaction between $HO^{\bullet}$ and 4-t-BP ($k_{4\text{-t-BP}, \bullet OH}$) were estimated to be $(1.24 \pm 0.07)\times10^{-9}$ M s^{-1} and $(1.61 \pm 0.26)\times10^{10}$ M^{-1} s^{-1}, respectively. According to the literature [178-179], the second-order rate constants of the reaction between $HO^{\bullet}$ and *o*-cresol/*p*-cresol were 1.1×10^{10} M^{-1} s^{-1} and 1.2×10^{10} M^{-1} s^{-1} respectively. Both of them had similar chemical structure with 4-t-BP and so the result obtained for $k_{4\text{-t-BP}, HO\bullet}$ seems reasonable.

3.7 Conclusion

Theoretical and experimental approaches were used to investigate the stability and photoreactivity of Fe(III)-EDDS complex in this chapter. This study was performed in a large range of pH which was the main parameter influencing the efficiency of the photochemical process and also the effects of Fe(III)-EDDS and oxygen concentrations were studied.

From this part of work, we could conclude that before pH 8 the main process responsible for the observed trend was attributed to the iron cycle reactivity between Fe(III)/Fe(II). The relative concentration between Fe(III) and Fe(II) was mainly due to their reactivity with the radicals $HO_2^{\bullet}/O_2^{\bullet-}$ which were photogenerated from the Fe(III)-EDDS complex, and to their oxido-reduction and solubility in aqueous solution. Moreover, the main new result was coming from theoretical calculation for

the distribution of the predominant species of the complex Fe(III)-EDDS as a function of pH. We demonstrated that the most photoactive form is the nonhydroxylated present mainly at pH lower than 8.0.

Chapter 4

FENTON-LIKE OXIDATION OF 4-t-BP IN THE PRESENCE OF Fe(III)-EDDS

Chapter 4 Fenton-like oxidation of 4-t-BP in the presence of Fe(III)-EDDS

According to the results presented in chapter 1, there were iron complexes which could activate H_2O_2 without UV irradiation to produce HO•. The Fenton-like reaction was higher efficiency than traditional Fenton reaction and also had a wider pH range of application.

In this chapter, Fe(III)-EDDS would be introduced into the Fenton-like reaction

for the degradation of 4-t-BP. The effects of irradiation time, pH, Fe(III)-EDDS, H_2O_2 and dissolved oxygen concentrations on the degradation performance of 4-t-BP were investigated.

4.1 Degradation kinetics of 4-t-BP

The time evolution of 4-t-BP concentration in Fenton-like process was shown in Figure 4-1. When the concentration of both H_2O_2 and Fe(III)-EDDS were low (100 μM), the initial degradation rate of 4-t-BP ($R_{4\text{-t-BP}}$) was almost negligible. With higher concentration of both H_2O_2 and Fe(III)-EDDS increased to 500 μM, $R_{4\text{-t-BP}}$ was calculated as $1.39 \pm 0.09 \times 10^{-9}$ M s^{-1}. The control experiment of 4-t-BP with high H_2O_2 concentration (1 mM) alone revealed that there was no degradation of 4-t-BP.

According to the results obtained in the experiments, it was clear that H_2O_2 could not react with 4-t-BP and the participation of Fe(III)-EDDS achieved the degradation of 4-t-BP. A slow reactivity of the complex with H_2O_2 led to the generation of Fe(II) and superoxide/hydroperoxide radical (R4-1). Fe(II) would activate H_2O_2 to produce $HO^{\bullet}$ according to the mechanism of traditional Fenton process (R1-1). The concentration of Fe(II) was followed during the reaction (Figure 4-2). The result showed that only less than 10% of Fe(III)-EDDS (initial concentration was 500 μM) was transformed into Fe(II) at the end of experiment. The formation speed and amount of Fe(II) were both very slow. This resulted in the low formation efficiency of $HO^{\bullet}$ and low degradation rate of 4-t-BP.

$$\text{Fe(III)-EDDS} + H_2O_2 \rightarrow Fe^{2+} + \text{EDDS}^{\bullet+} + HO_2^{\bullet}/O_2^{\bullet-} + H^+ \qquad \text{(R4-1)}$$

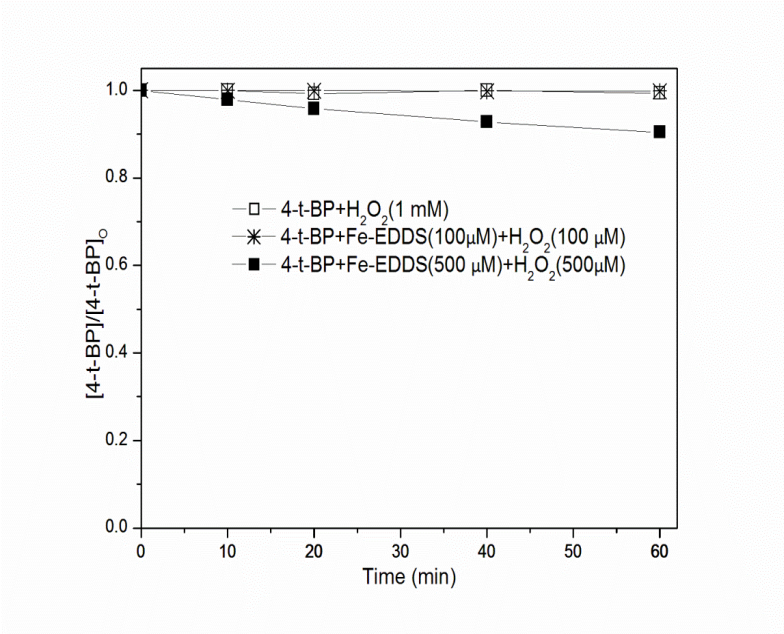

Figure 4-1 Degradation of 4-t-BP in Fenton-like process

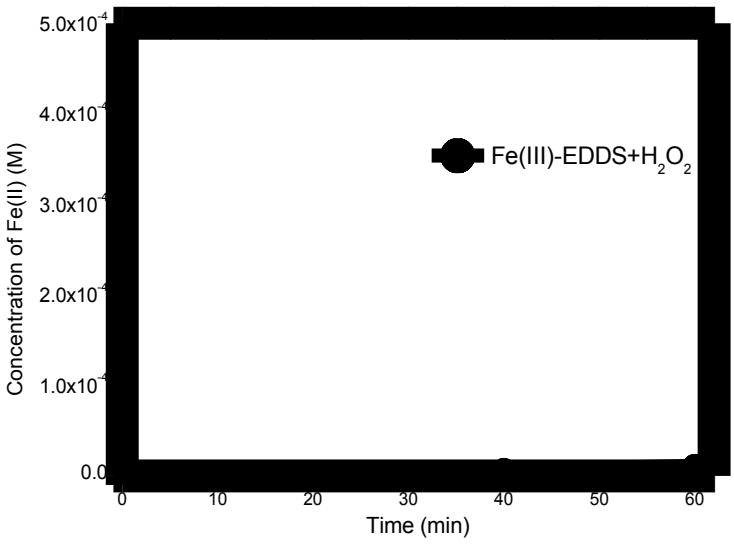

Figure 4-2 The formation of Fe(II) in Fe(III)-EDDS/H_2O_2 reaction

4.2 Effect of Fe(III)-EDDS concentration

The degradation of 4-t-BP using different Fe(III)-EDDS concentrations was performed with the following initial concentrations: hydrogen peroxide 500 μM and Fe(III)-EDDS from 100 μM up to 3 mM. As shown in Figure 4-3, the highest degradation efficiency of 4-t-BP was performed when the Fe(III)-EDDS concentration was 1 mM in Fenton-like process.

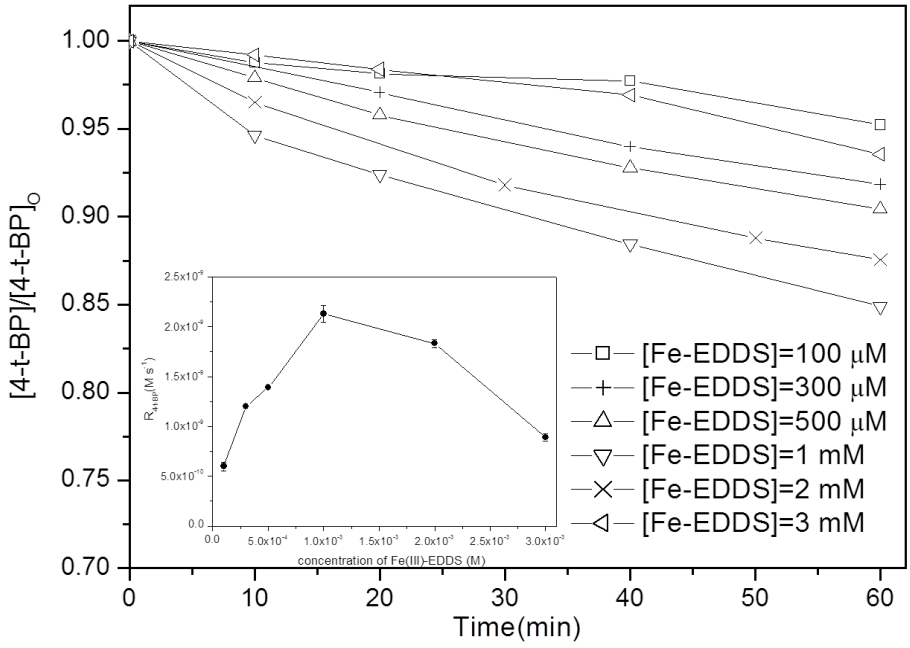

Figure 4-3 Effect of Fe(III)-EDDS concentration on the degradation of 4-t-BP (Insert: The 4-t-BP degradation rate as a function of Fe(III)-EDDS concentration)

These results gave clear evidence that the 4-t-BP degradation was due to the reaction between 4-t-BP and HO• which was mainly generated during the reaction

between Fe^{2+} and H_2O_2 (Fenton reaction). The negative effect of highest Fe(III)-EDDS concentrations in experimental series was highlighted by the $HO^{\bullet}$ steady-state concentration ($[HO^{\bullet}]_{ss}$) reported in Table 4-1. The $[HO^{\bullet}]_{ss}$ was obtained from the Eq. 4-1.

$$\frac{d[4-t-BP]}{dt} = R_{4-t-BP} = k_{HO^{\bullet},4-t-BP}[HO^{\bullet}]_{ss}[4-t-BP] \qquad \text{(Eq. 4-1)}$$

$k_{HO^{\bullet},4-t-BP}$ and [4-t-BP] were the second order rate constant between $HO^{\bullet}$ and 4-t-BP and initial concentration of 4-t-BP, respectively. R_{4-t-BP} was the degradation rate of 4-t-BP obtained in experimental work. According to the results in Table 4-1, $[HO^{\bullet}]_{ss}$ increased up to 1 mM of Fe(III)-EDDS and then decreased. After the maximum the decrease of $R_{4\text{-t-BP}}$ was due to the competitive role of Fe(III)-EDDS observed at high concentrations.

Table 4-1Hydroxyl radical steady-state concentration as a function of Fe(III)-EDDS concentration in Fenton-like experiment

[Fe(III)-EDDS] (M)	$[HO^{\bullet}]_{ss}$ (M)
1×10^{-4}	7.44×10^{-16}
3×10^{-4}	1.49×10^{-15}
5×10^{-4}	1.73×10^{-15}
1×10^{-3}	2.94×10^{-15}
2×10^{-3}	2.28×10^{-15}

3×10^{-3}	1.10×10^{-15}

4.3 Effect of H_2O_2 concentration

To elucidate the effect of H_2O_2 concentrations on the 4-t-BP degradation, a series of experiments were conducted using Fe(III)-EDDS 1 mM and different concentrations of H_2O_2 (from 100 μM to 2 mM). As shown in Figure 4-3, 4-t-BP removal in terms of initial degradation rate ($R_{4\text{-t-BP}}$) increased from 100 to 700 μM of H_2O_2 and slowly decreased for higher H_2O_2 concentrations in Fenton-like process. Huang et al. [100] reported a similar degradation rate variation under various H_2O_2 concentrations.

This was mainly due to the high concentration of H_2O_2 which reacted with the $HO^{\bullet}$ (R4-2) [177] as a quencher of $HO^{\bullet}$. Therefore, 4-t-BP degradation was suppressed when the H_2O_2 concentration was higher than 700 μM.

$$HO^{\bullet} + H_2O_2 \rightarrow HO_2^{\bullet} + H_2O \quad k_{HO^{\bullet},H_2O_2} = 2.7\times10^{7}\,M^{-1}s^{-1} \qquad \text{(R4-2)}$$

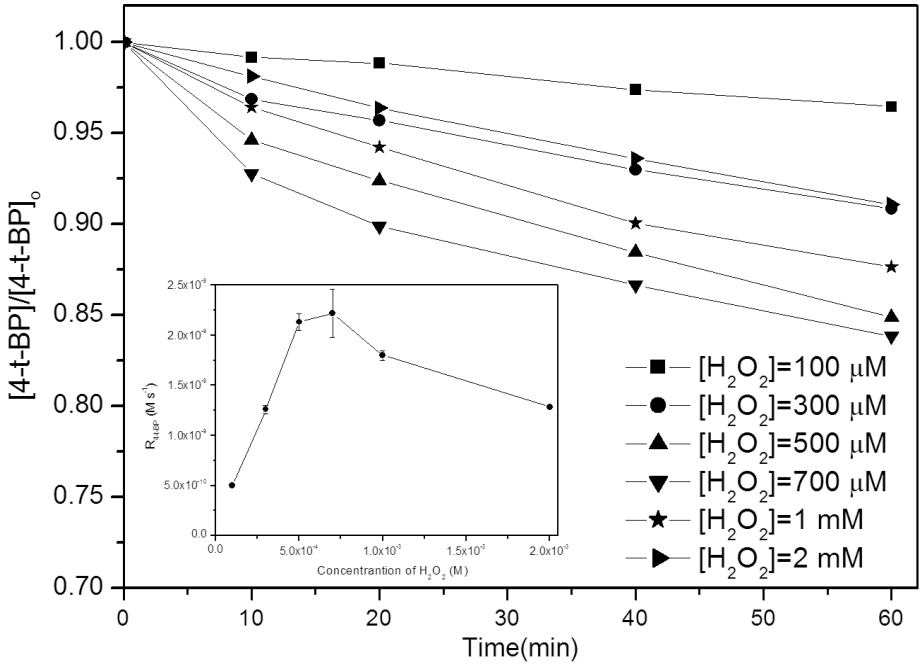

Figure 4-3 Effect of H_2O_2 concentration on the degradation of 4-t-BP

(Insert: The 4-t-BP degradation rate as a function of H_2O_2 concentration)

4.4 Effect of pH

To better understand the applicable pH value during the Fenton-like process, experiments at pH between 2.7 to 8.9 were conducted. The initial concentration of both Fe(III)-EDDS and H_2O_2 were 500 μM. The results reported in Figure 4-4 showed a slow increase of $R_{4\text{-t-BP}}$ at pH less than 6.0 and much more rapid increase of $R_{4\text{-t-BP}}$ between pH 6.0 and 9.0 in Fenton-like process. Huang et al. [100] reported similar results at pH between 3.1 and 8.7 in homogenous Fenton-like process for the BPA degradation.

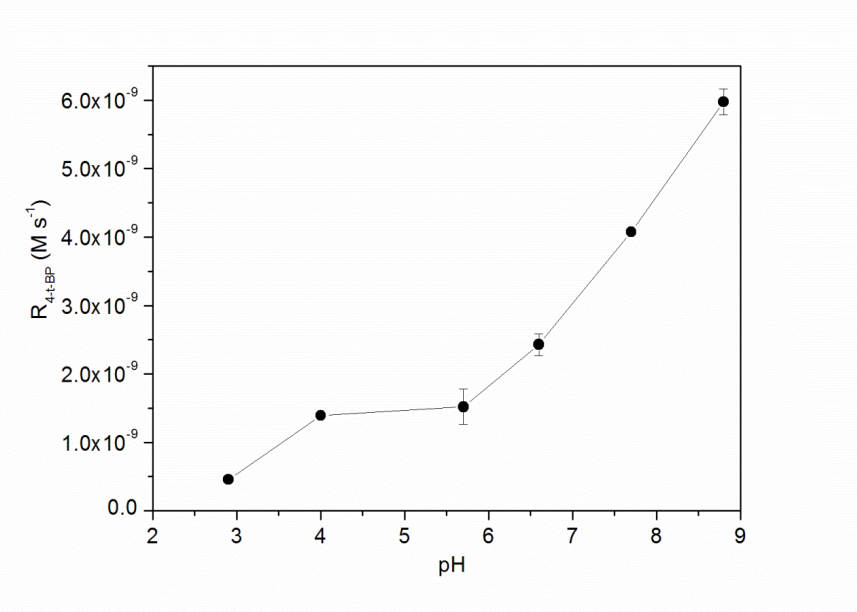

Figure 4-4 Effect of pH value on the degradation rate of 4-t-BP

In previous works, our group had studied the mechanism of the pH-dependent performance on the pollutants degradation [100]. Firstly, the increase of 4-t-BP degradation at higher pH could be explained by the effect of hydroperoxyl radical ($HO_2^{\bullet}$)/superoxide radical anion ($O_2^{\bullet-}$) on the Fe(III)/Fe(II) cycle. At pH < 4.8, the main form present in solution is $HO_2^{\bullet}$ which favored the formation of Fe(III) compared with the formation of Fe(II) (R3-15 and R3-16). In the presence of $O_2^{\bullet-}$ at higher pH, the equilibrium was displaced to the formation of Fe(II) (R3-13 and R3-14). The $R_{4\text{-t-BP}}$ would be significantly affected because of the Fe(III)/Fe(II) cycle and also the formation of Fe(II) was the most important step for the efficiency of Fenton process. Summarizing the experiment results and the mechanisms in this study, Fenton-like process was mainly affected by $HO_2^{\bullet}/O_2^{\bullet-}$ formation in different pH.

4.5 Effect of oxygen

The effect of dissolved oxygen on 4-t-BP degradation in Fenton-like process was shown in Figure 4-5. The initial concentration of Fe(III)-EDDS and H_2O_2 were 1 mM and 500 μM, respectively. The faster decay of 4-t-BP was noticed at higher oxygen concentration (bubbling oxygen), while in the lower oxygen concentration (bubbling nitrogen) the 4-t-BP removal was retarded in Fenton-like process. The Fe(III)-EDDS concentration was also followed during the reaction in order to confirm the mechanism of the effect of oxygen. The result was showed in Figure 4-6 and it showed that the decomposition of Fe(III)-EDDS was not affected by oxygen.

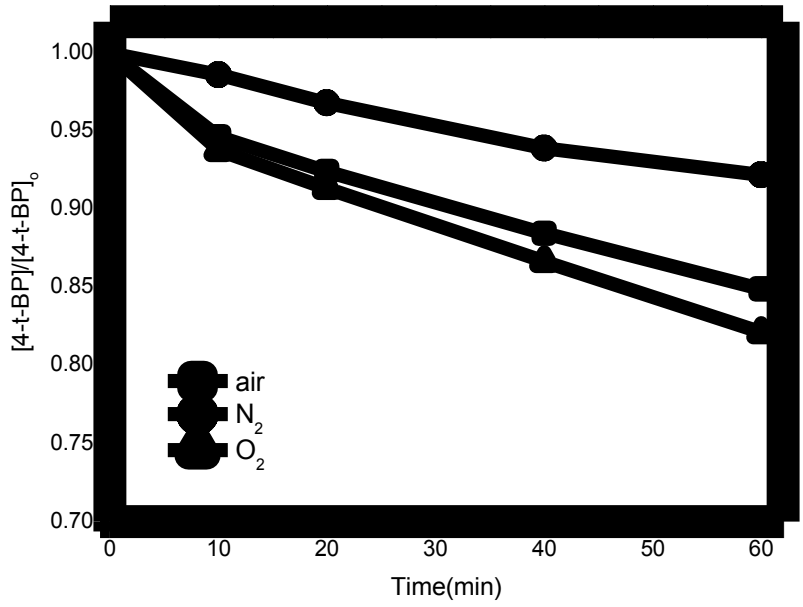

Figure 4-5 Effect of dissolved O_2 concentration on the degradation of 4-t-BP

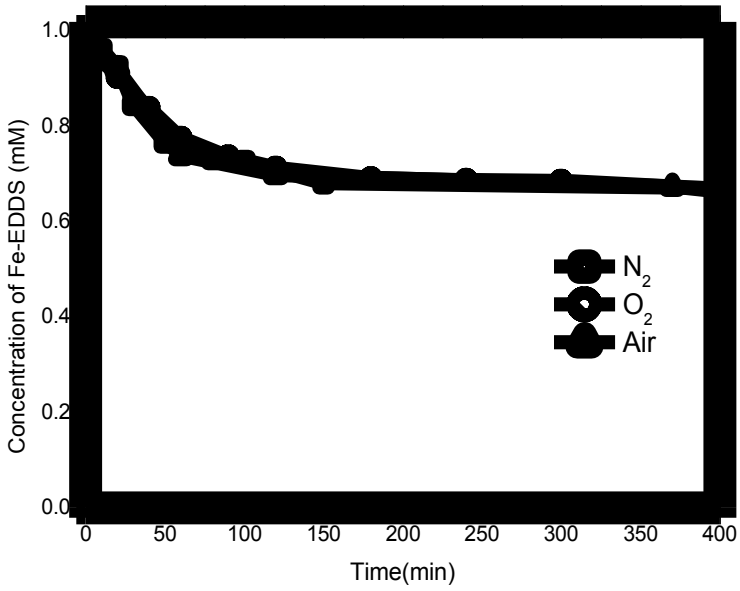

Figure 4-6 Effect of dissolved O_2 concentration on the decomposition of Fe(III)-EDDS

As it is mentioned in section 4.1, the first step in Fenton-like process in this study was the decomposition of Fe(III)-EDDS to produce Fe(II). The results showed in Figure 4-6 clearly proved that the formation of Fe(II) was not affected by oxygen.

The effect of oxygen in Fenton-like process could be mainly attributed to the reaction between O_2 and the 4-t-BP radical (4-t-BP$^{\bullet}$) which formed subsequently by the HO$^{\bullet}$ hydrogen abstraction of the phenoxyl hydrogen group of 4-t-BP (R4-3). It would be more easily to form 4-t-BP radical cation (4-t-BP$^{\bullet+}$) in the presence of oxygen (R4-4) and 4-t-BP$^{\bullet+}$ would be more easily to degrade (R4-5) [180].

$$HO^{\bullet} + 4\text{-}t\text{-}BP \rightarrow 4\text{-}t\text{-}BP^{\bullet} + H_2O \qquad \text{(R4-3)}$$

$$4\text{-}t\text{-}BP^{\bullet} + O_2 \rightarrow 4\text{-}t\text{-}BP^{\bullet+} + O_2^{\bullet-} \qquad \text{(R4-4)}$$

$$4\text{-}t\text{-}BP^{\bullet+} \rightarrow \rightarrow \text{products} \qquad \text{(R4-5)}$$

4.6 Conclusion

In this chapter, a series of experiments were performed to investigate the mechanism of Fe(III)-EDDS activating H_2O_2 and producing $HO^{\bullet}$. This reaction was named Fenton-like process in this study. The study was performed in a large range of pH which was the key parameter influencing the efficiency of the traditional Fenton process and also the effects of Fe(III)-EDDS concentration, H_2O_2 concentration, oxygen concentration were studied.

From this part of work, we could conclude that the Fenton-like process could be used in a lager pH rang, even in alkaline conditions. It was attributed to the stability of Fe(III)-EDDS in alkaline conditions and the oxido-reduction between radicals $HO_2^{\bullet}/O_2^{\bullet-}$ and Fe(III)/Fe(II). Moreover, the optimum concentrations of Fe(III)-EDDS and H_2O_2 were obtained. Because the high concentrations of both Fe(III)-EDDS and H_2O_2 would inhibit the degradation of 4-t-BP with the quench of $HO^{\bullet}$. The dissolved O_2 concentration could accelerate the formation of 4-t-$BP^{\bullet+}$ and then increased the 4-t-BP degradation rate. In general, Fenton-like process in this study was better than traditional Fenton process in the pH application range but the oxidation efficiency of 4-t-BP was not high enough.

Chapter 5

PHOTO FENTON-LIKE OXIDATION OF 4-t-BP IN THE PRESENCE OF Fe(III)-EDDS

Chapter 5 Photo Fenton-like oxidation of 4-t-BP in the presence of Fe(III)-EDDS

According to the results obtained in chapter 3, Fe(II) and oxidative radicals ($HO^{\bullet}$, $HO_2^{\bullet}$, $O_2^{\bullet-}$) were generated from the Fe(III)-EDDS photolysis. The literatures showed the mechanism of traditional Fenton reaction, which was Fe(II) activated H_2O_2 and quickly produced $HO^{\bullet}$ to efficiently degrade organic pollutants. Therefore, it was clear that UV/Fe(III)-EDDS/H_2O_2 could produce $HO^{\bullet}$ according to the above mechanism.

In this chapter, the oxidation efficiency of UV/Fe(III)-EDDS/H_2O_2 system was investigated. The effects of irradiation time, pH, Fe(III)-EDDS, H_2O_2 and dissolved oxygen concentrations on the degradation performance of 4-t-BP in this photo Fenton-like process were also investigated.

5.1 Degradation kinetics of 4-t-BP

The degradation efficiency of 4-t-BP UV/Fe(III)-EDDS/H_2O_2 system was obtained. The 4-t-BP concentration was followed during the irradiation in the presence of Fe(III)-EDDS (100 μM) and H_2O_2 (100 μM). The results were shown in

Figure 5-1. 4-t-BP was degraded very fast in the beginning 10 min. The initial degradation rate of 4-t-BP ($R_{4\text{-t-BP}}$) in photo Fenton-like process was calculated as $(1.48 \pm 0.17) \times 10^{-7}$ M s^{-1}. The control experiment with 4-t-BP alone revealed that there was no photolysis of 4-t-BP under the irradiation used in our experimental conditions ($300 < \lambda < 500$ nm).

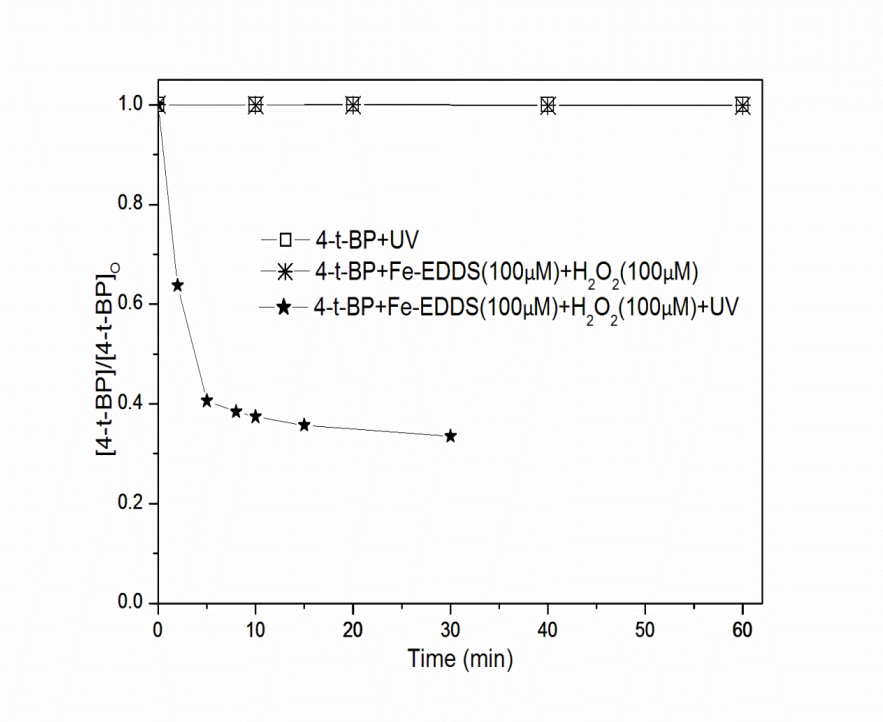

Figure 5-1 Degradation of 4-t-BP in photo Fenton-like process

According to the mechanism of traditional Fenton process (R1-1), Fe(II) was a key factor of HO• formation in the presence of H_2O_2. In photo Fenton-like experiments, Fe(II) could be generated via reaction (R3-8) in the UV radiation of Fe(III)-EDDS. The HO• would be produced rapidly from the reaction between Fe(II) and H_2O_2. The concentration of Fe(II) formed during the reaction was followed, as shown in Figure 5-2. Fe(II) concentration reached a plateau at around 10 min of

irradiations while a significant lower formation rate of HO• was estimated. The plateau observed during photo Fenton-like reaction could be attributed to the completely photolysis of Fe(III)-EDDS. Moreover, according to the H_2O_2 monitoring in the photo Fenton-like process (Figure 5-3), 95% H_2O_2 were consumed after 5 min irradiation and so after 5 min 4-t-BP degradation reached a plateau value as reported in Figure 5-1.

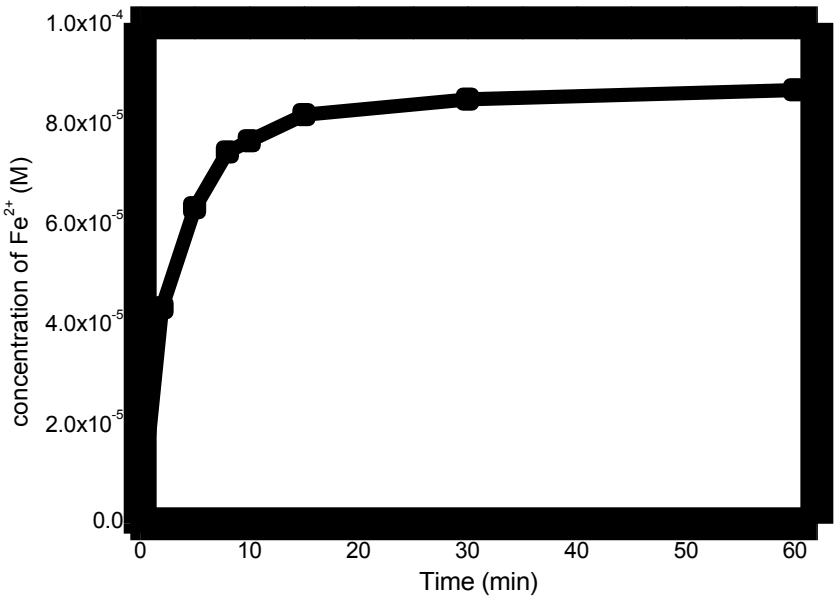

Figure 5-2 The formation of Fe(II) in UV/Fe(III)-EDDS/H_2O_2 reaction

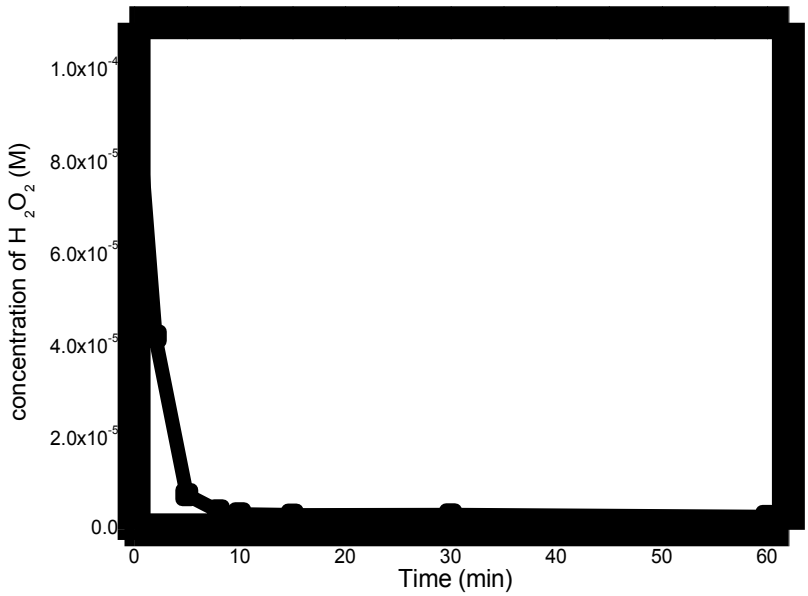

Figure 5-3 The consumption of H_2O_2 in photo Fenton-like process

5.2 Effect of Fe(III)-EDDS concentration

The degradation of 4-t-BP using different Fe(III)-EDDS concentrations was performed using following initial concentration: H_2O_2 100 μM and Fe(III)-EDDS between 20 μM and 1 mM. As shown in Figure 5-4, the highest degradation efficiency of 4-t-BP was performed when the Fe(III)-EDDS concentration was 300 μM in photo Fenton-like process.

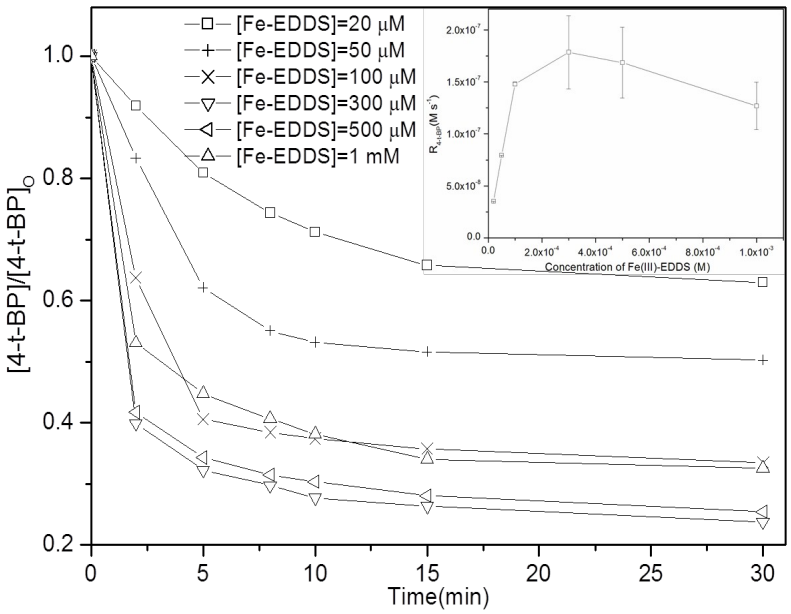

Figure 5-4 Effect of Fe(III)-EDDS concentration on the degradation of 4-t-BP (Insert: The 4-t-BP degradation rate as a function of Fe(III)-EDDS concentration)

The mechanism of this trend was similar with Fenton-like process, due to the reaction between HO• and Fe(III)-EDDS. The HO• steady-state concentration was also calculated, shown in Table 5-1. $[HO^{\bullet}]_{ss}$ increased up to 300 μM in presence of light. After this maximum 4-t-BP degradation rate, decreases due to the competitive role observed at high Fe(III)-EDDS concentrations.

Table 5-1Hydroxyl radical steady-state concentration as a function of Fe(III)-EDDS concentration in photo Fenton-like experiment

[Fe(III)-EDDS] (M)	$[HO^{\bullet}]_{ss}$ (M)
2×10^{-5}	4.38×10^{-14}
5×10^{-5}	9.88×10^{-14}

1×10^{-4}	1.84×10^{-13}
3×10^{-4}	2.22×10^{-13}
5×10^{-4}	2.09×10^{-13}
1×10^{-3}	1.58×10^{-13}

5.3 Effect of H_2O_2 concentration

A series of experiments were conducted using different concentrations of H_2O_2 (from 100 μM to 2 mM). The Fe(III)-EDDS concentration was fixed at 100 μM. As shown in Figure 5-5, the trend in photo Fenton-like process was different with Fenton-like process. $R_{4\text{-t-BP}}$ increased rapidly from 100 μM to 1 mM of H_2O_2 and kept slowly growing in higher H_2O_2 concentrations reaching a plateau at around 2 mM of H_2O_2.

In addition to reaction between Fe(II) and H_2O_2, the irradiation of H_2O_2 would also produce hydroxyl radical. A control experiment was performed showing that about 10% of 4-t-BP concentration was degraded in 30 min using 2 mM of H_2O_2 under the UV irradiation (Figure 5-6). Such photo reactivity could represent a non-negligible contribution in accelerating the degradation of pollutant and minimizing the negative effect of high H_2O_2 toward generated $HO^{\bullet}$ (R4-2).

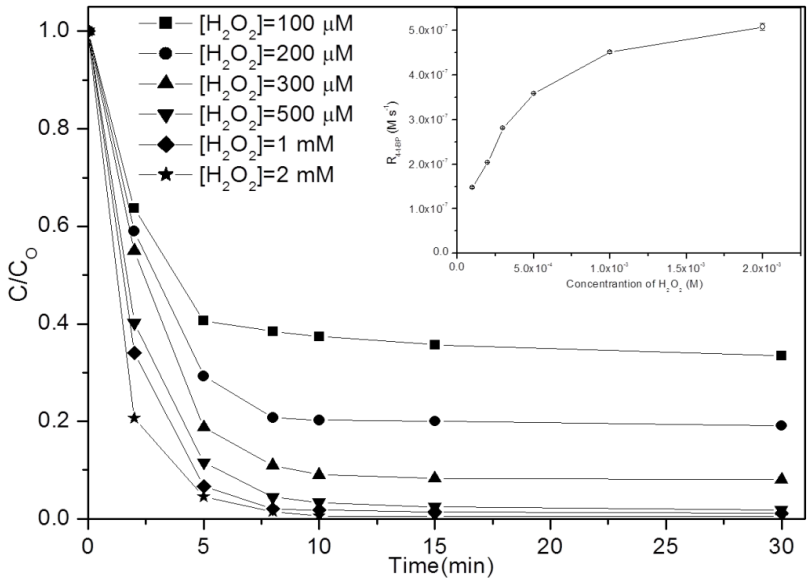

Figure 5-5 Effect of H_2O_2 concentration on the degradation of 4-t-BP

(Insert: The 4-t-BP degradation rate as a function of H_2O_2 concentration)

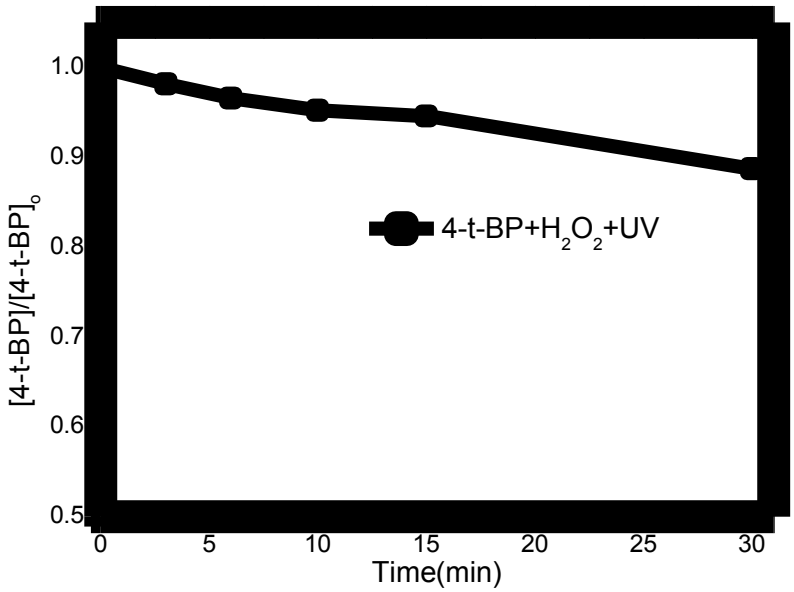

Figure 5-6 The degradation of 4-t-BP in UV/H_2O_2 control experiment

5.4 Effect of pH

To better understand the applicable pH value during the photo Fenton-like process, experiments at pHs between 2.7 to 8.9 were conducted. The results reported in Figure 5-7 showed that the $R_{4\text{-t-BP}}$ increased between pH 2.7 and 7.5, whereas a decreased degradation rate was noticed at pH higher than 7.5.

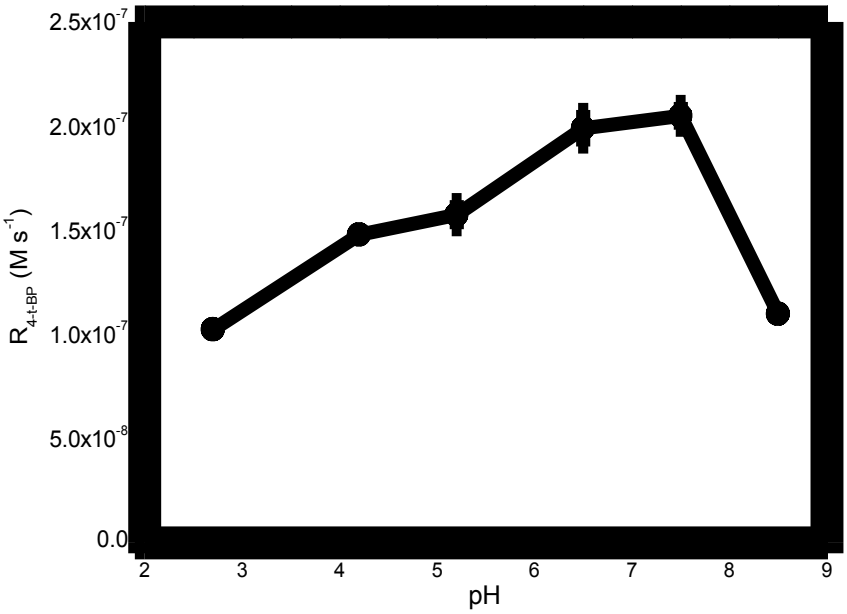

Figure 5-7 Effect of pH value on the degradation rate of 4-t-BP

The $R_{4\text{-t-BP}}$ obtained in photo Fenton-like process showed a perfect correlation with the result obtained on the photo chemical activity of Fe(III)-EDDS (shown as Figure 3-9). Beside the effect by radicals as Fenton-like process, the photo Fenton-like process was mainly affected by the pH-depended photochemical activity of Fe(III)-EDDS. As reported in chapter 3, Fe(III)-EDDS had different form in different pH range. The hydroxylated form $Fe(OH)L^{2-}$ of such complex was less efficient in

photochemical activity. The most efficient form FeL^- transformed to $Fe(OH)L^{2-}$ after pH 7 and the dissolved Fe(III) was decreased at this moment. So the 4-t-BP degradation efficiency was inhabited.

5.5 Effect of oxygen

The effect of oxygen on 4-t-BP degradation in photo Fenton-like process was investigated and the results were shown in Figure 5-8. The increased degradation rate of 4-t-BP was noticed at higher oxygen concentration. The Fe(III)-EDDS concentration was also followed during the reaction (Figure 5-9). The result showed that the decomposition of Fe(III)-EDDS was not affected by oxygen concentration in this process, the same as Fenton-like process.

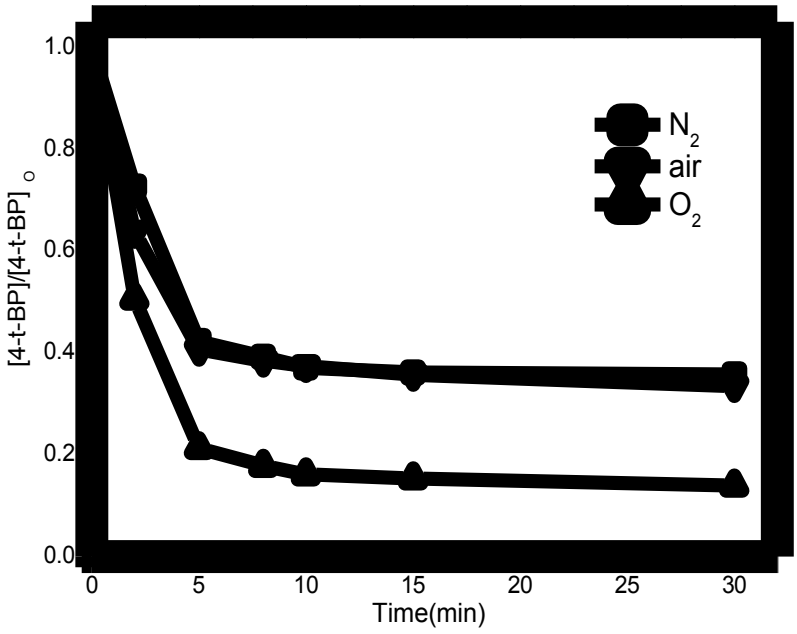

Figure 5-8 Effect of dissolved O_2 concentration on the degradation of 4-t-BP

The first step in photo Fenton-like processes in this study was the decomposition of Fe(III)-EDDS to produce Fe(II). The results showed in Figure 5-9 clearly proved that the formation of Fe(II) was not affected by oxygen.

As the similar mechanism in Fenton-like process (shown in section 4.5), O_2 could promote the formation of 4-t-BP$^{\bullet+}$ which transferred from 4-t-BP$^{\bullet}$ and accelerated the degradation of 4-t-BP. Beside this important reason, the effect of oxygen in photo Fenton-like process was also due to the reactivity of molecular oxygen on the EDDS radical (R3-9) to form $O_2^{\bullet-}/HO_2^{\bullet}$ [181] which played an important role on the Fe(II)/Fe(III) cycle.

Finally, molecular oxygen could also play a key role enhancing the Fe(II) oxidation into Fe(III). Under such condition an opposite effect could be discerned on the 4-t-BP degradation: in photo Fenton-like process the oxygen enhances the Fe(III) formation via Fe(II) oxidation doping the HO$^{\bullet}$ formation from the Fe(III) photolysis [182-183]。

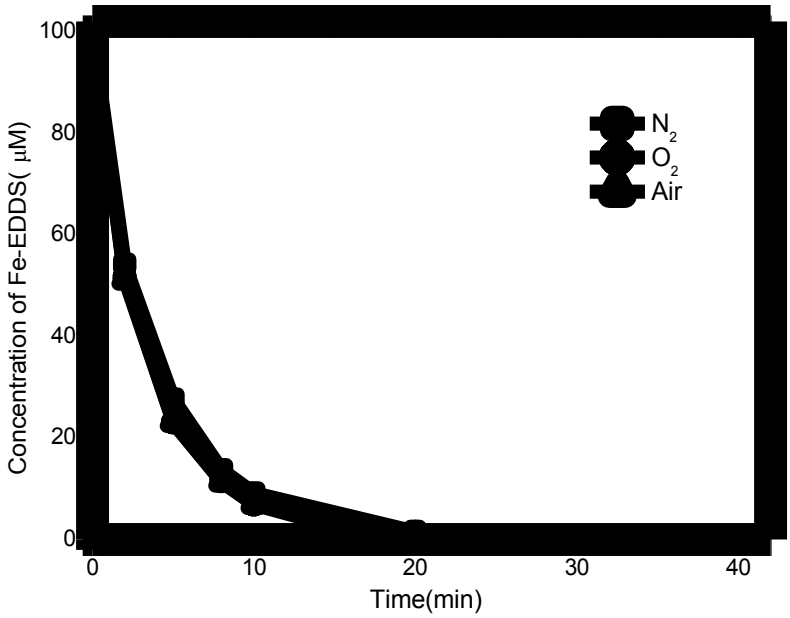

Figure 5-9 Effect of dissolved O_2 concentration on the decomposition of Fe(III)-EDDS

5.6 Conclusion

In this chapter, a series of experiments were performed to investigate the mechanism of the photo Fenton-like process in the presence of Fe(III)-EDDS. The study was performed in a large range of pH which was the key parameter influencing the efficiency of the traditional Fenton process and also the effects of Fe(III)-EDDS concentration, H_2O_2 concentration, oxygen concentration were studied.

From this part of work, we could conclude that the photo Fenton-like process performed much higher efficiency than Fenton-like process and the key step had been attributed to the faster generation of Fe(II) under UV irradiation. $R_{4\text{-t-BP}}$ increased with the increasing concentration of Fe(III)-EDDS and was inhibited when the Fe(III)-EDDS concentration was too high. $R_{4\text{-t-BP}}$ kept increasing when H_2O_2 concentrations increased from 100 μM to 2 mM in photo Fenton-like process. The optimal $R_{4\text{-t-BP}}$

obtained at pH 7.5. The degradation of 4-t-BP was obviously accelerated with high O_2 concentration in photo-Fenton process compared with Fenton-like process.

Chapter 6

PHOTODEGRADATION OF 4-t-BP BY $SO_4^{\bullet-}$ PRODUCED VIA $S_2O_8^{2-}$ ACTIVATION IN THE PRESENCE

OF Fe(III)-EDDS

Chapter 6 Photodegradation of 4-t-BP by $SO_4^{\bullet-}$ produced via $S_2O_8^{2-}$ activation in the presence of Fe(III)-EDDS

According to the results obtained in chapter 5, UV/Fe(III)-EDDS/H_2O_2 system could produce oxidative radicals ($HO^{\bullet}$, $HO_2^{\bullet}$, $O_2^{\bullet-}$) and degraded 4-t-BP efficiently. The literatures in chapter 1 showed one of the pathway of $SO_4^{\bullet-}$ formation was the activation of $S_2O_8^{2-}$ by transition metal. In particular, Fe(II) was used as the transition metal to activate $S_2O_8^{2-}$ and the mechanism of Fe(II) activation was similar to the traditional Fenton reaction [184]. The reaction between Fe(II) and $S_2O_8^{2-}$ was expressed by R6-1 [185]. However, it had several defects, especially pH limitation and iron precipitation as the traditional Fenton system.

$$S_2O_8^{2-} + Fe^{2+} \rightarrow Fe^{3+} + SO_4^{2-} + SO_4^{\bullet-} \quad (k = 27\ M^{-1}\ s^{-1}) \qquad (R6\text{-}1)$$

In this chapter, Fe(III)-EDDS was used to activate $S_2O_8^{2-}$ under UV irradiation. The effect of irradiation time, pH, Fe(III)-EDDS concentration and $S_2O_8^{2-}$ concentration on the photodegradation performance of 4-t-BP under UV light irradiation (300 nm < λ < 500 nm) was investigated. The second-order reaction rate constant of the reaction between 4-t-BP and $SO_4^{\bullet-}$ was also evaluated for the first time by laser flash photolysis.

6.1 Degradation kinetics of 4-t-BP

Figure 6-1 displayed the measured spectral irradiance of the four tubes used during these experiments, as well as a UV-vis spectrum of $S_2O_8^{2-}$ in water solution (taken with a Cary 300 scan UV-visible spectrophotometer) to show the spectral overlap. Emission spectrum reaching solution was measured with an Ocean Optics SD 2000 CCD spectrophotometer (calibrated using a DH-2000-CAL Deuterium Tungsten Halogen reference lamp) and normalized to the actinometry results using para-nitroanisole (PNA)/pyridine actinometer [153].

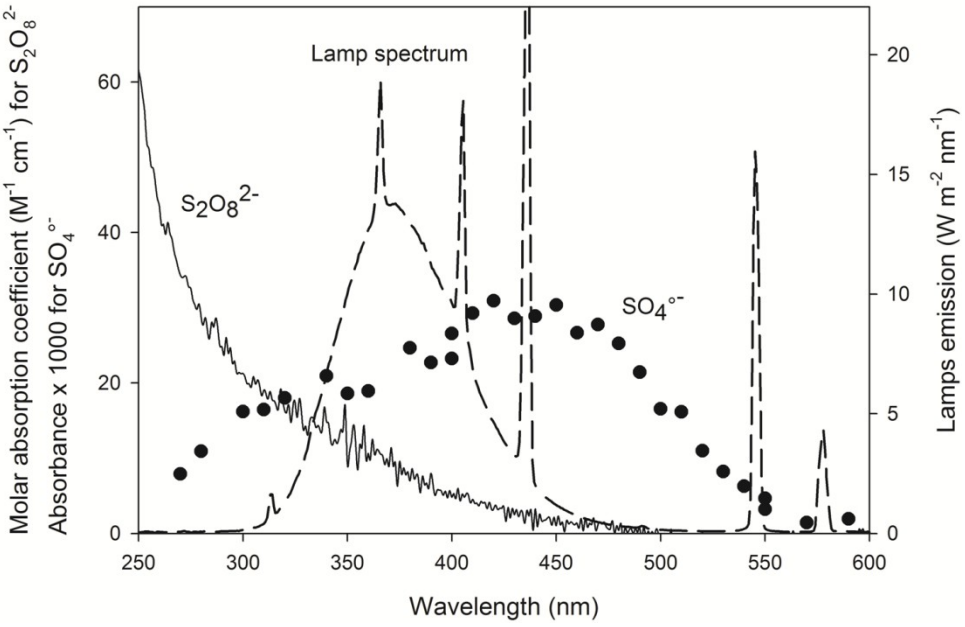

Figure 6-1 Molar absorption spectrum of $S_2O_8^{2-}$ solution (solid line), absorption spectrum of $SO_4^{\bullet-}$ transient acquired after 0.5 μs excitation at 266 nm of $S_2O_8^{2-}$ 10 mM solution (filled circle) and emission spectrum of the irradiation system reaching the solution (dashed line)

The 4-t-BP concentration was follow during the reaction in the UV/ Fe(III)-EDDS/$S_2O_8^{2-}$ system and UV/Fe(III)/$S_2O_8^{2-}$ system. The control experiments without UV irradiation or without iron were also performed. The $S_2O_8^{2-}$ concentration was 500 μM and Fe(III)/Fe(III)-EDDS concentration was 100 μM. As the results showed in Figure 6-2, there was no degradation of 4-t-BP without UV irradiation and about 7% degradation of 4-t-BP without iron in control groups. However, there was about 80% degradation of 4-t-BP after 40 min irradiation in both UV/Fe(III) -EDDS/$S_2O_8^{2-}$ and UV/Fe(III)/$S_2O_8^{2-}$ system. The apparent first-order rate constant (k_1) of both processes were calculated and the results were shown in Table 6-1. As shown in Table 6-1, the k_1 obtained in UV/Fe(III)-EDDS/$S_2O_8^{2-}$ process was three times higher than that

obtained in UV/Fe(III)/$S_2O_8^{2-}$.

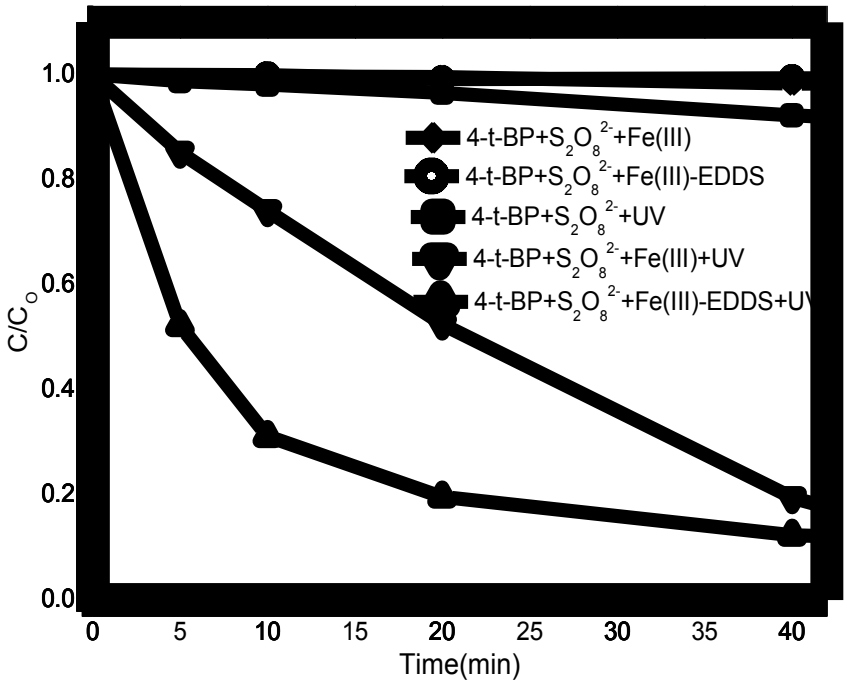

Figure 6-2 Degradation of 4-t-BP in $S_2O_8^{2-}$ related reactions

Table 6-1 The k_1 of 4-t-BP degradation in different reaction condition

System	k_1 (s^{-1})	R^2
UV/Fe(III)/$S_2O_8^{2-}$	$5.30\times10^{-4} \pm 8.32\times10^{-6}$	0.9984
UV/Fe(III)-EDDS/$S_2O_8^{2-}$	$1.51\times10^{-3} \pm 1.57\times10^{-4}$	0.9364

According to the literatures in section 1.3, $S_2O_8^{2-}$ could be activated by UV light and decomposed to $SO_4^{\bullet-}$ (R6-2). But the UV activation was not the main reaction in our experiment due to the small percentage (7%) of 4-t-BP degradation in control group. In both UV/Fe(III)-EDDS/$S_2O_8^{2-}$ and UV/Fe(III)/$S_2O_8^{2-}$ system, the first step was the formation of Fe(II) through the photolysis of Fe(III)-EDDS/Fe(III) (R1-2 and

R3-1). Fe(II) activation of $S_2O_8^{2-}$ (R6-1) was the main source of $SO_4^{\bullet-}$ in this experiments and the 4-t-BP degradation rate was much higher. However, beside the production of $SO_4^{\bullet-}$, Fe(II) was also the scavenger of $SO_4^{\bullet-}$ (R6-3) [180]. So Liang et al. [124] reported the molar ratio between Fe(II) and $S_2O_8^{2-}$ should be controlled lowly, otherwise Fe(II) would turn to the $SO_4^{\bullet-}$ quencher. This is the reason for the low concentrations of Fe(III)-EDDS and Fe(III) which we used in the study.

$$S_2O_8^{2-} + h\nu \rightarrow 2SO_4^{\bullet-} \qquad \text{(R6-2)}$$

$$Fe(II) + SO_4^{\bullet-} \rightarrow Fe(III) + + SO_4^{2-} \quad \text{(R6-3)}$$

6.2 Effect of pH

The pH value of aqueous solution plays a significant role in the degradation of organic compounds. Experiments of 4-t-BP degradation in both UV/Fe(III)-EDDS/ $S_2O_8^{2-}$ and UV/Fe(III)/$S_2O_8^{2-}$ systems were carried out at pHs between 2.2 to 8.8. The initial degradation rates of 4-t-BP ($R_{4\text{-t-BP}}$) with different pH values were obtained and are shown in Figure 6-3. The $S_2O_8^{2-}$ concentration was 500 μM and Fe(III)/ Fe(III)-EDDS concentration was 100 μM. With the increasing of pH, the efficiency of 4-t-BP degradation decreased in both reaction processes, indicating that the acidic pH was more favorable to the 4-t-BP degradation than neutral and alkaline pHs. However, the efficiency of 4-t-BP degradation decreased much more rapidly in UV/Fe(III)/ $S_2O_8^{2-}$

system since the pH was higher than 3. The $R_{4\text{-t-BP}}$ decreased to nearly 0 when the pH was higher than 5 in UV/Fe(III)/$S_2O_8^{2-}$ system. However, there was still relatively high degradation rate in UV/Fe(III)-EDDS/ $S_2O_8^{2-}$ at pH 5.3.

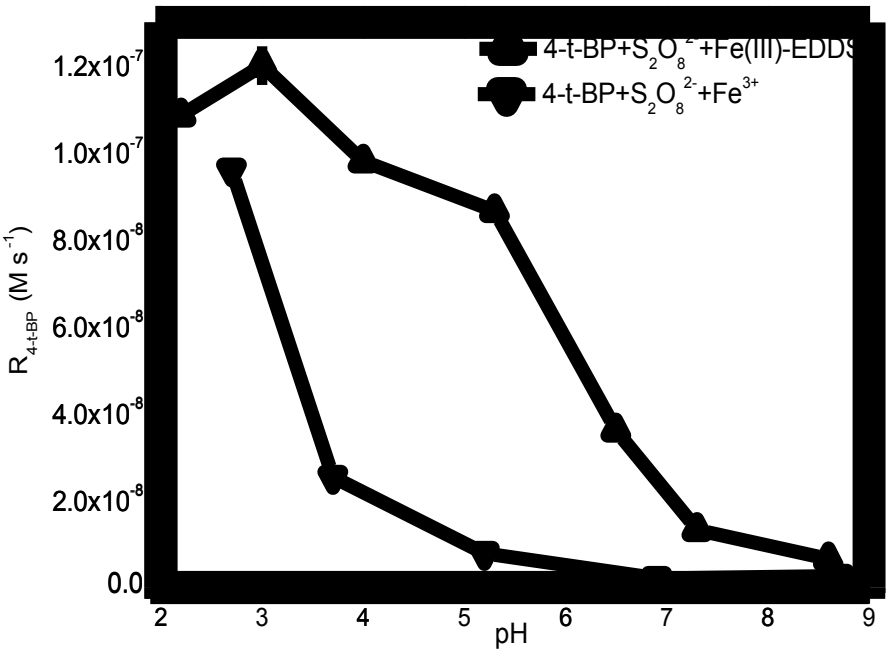

Figure 6-3 Effect of pH value on the initial degradation rates of 4-t-BP

The rapidly decreased $R_{4\text{-t-BP}}$ in the neutral and alkaline media might result from the precipitation of ferric ions in UV/Fe(III)/$S_2O_8^{2-}$ system. The precipitation of ferric ions occurs when pH> 4.0 [186]. But for Fe(III)-EDDS complex, it is much more stable than ferric ions in the neutral and alkaline media [187]. So the decreasing of $R_{4\text{-t-BP}}$ was relatively slow in UV/Fe(III)-EDDS/$S_2O_8^{2-}$ process. In our previous study, the quantum yield of Fe(II) formation ($\Phi^{f,Fe(II)}_{290\text{-}400nm}$) under the irradiation of Fe(III)-EDDS was estimated at pH 4.0, 6.0 and 8.6. Obtained values for $\Phi^{f,Fe(II)}_{290\text{-}400nm}$ are 0.09, 0.11

and 0.10 at pH 4.0, 6.0 and 8.6 respectively. However, the amount of soluble Fe(II) could decrease due to the formation of $FeOH^+$ complexes when the pH value is higher than 4.0 [188]. It would hinder the further reaction between Fe(II) and $S_2O_8^{2-}$.

In summary, according to the results in this section UV/Fe(III)-EDDS/$S_2O_8^{2-}$ system was superior to UV/Fe(III)/$S_2O_8^{2-}$ system on the performance of 4-t-BP degradation. Subsequently, the UV/Fe(III)-EDDS/$S_2O_8^{2-}$ process would be further investigated.

6.3 Effect of Fe(III)-EDDS concentration

The photolysis of Fe(III)-EDDS formed Fe(II) which was one of the main species that could catalyze $S_2O_8^{2-}$ to produce $SO_4^{\bullet-}$ [34]. The existence of Fe(III)-EDDS could influence the efficiency of the pollutant degradation significantly. Figure 6-4 showed the effect of Fe(III)-EDDS concentration on the degradation of 4-t-BP. The initial $S_2O_8^{2-}$ concentration was 100 μM. When the Fe(III)-EDDS concentration varied from 100 μM to 1 mM, the $R_{4\text{-t-BP}}$ increased from 1.25×10^{-8} M s^{-1} to 3.86×10^{-8} M s^{-1}. However, with a further increasing of Fe(III)-EDDS concentration up to 1.5 mM, the $R_{4\text{-t-BP}}$ was reduced to 2.07×10^{-8} M s^{-1}.

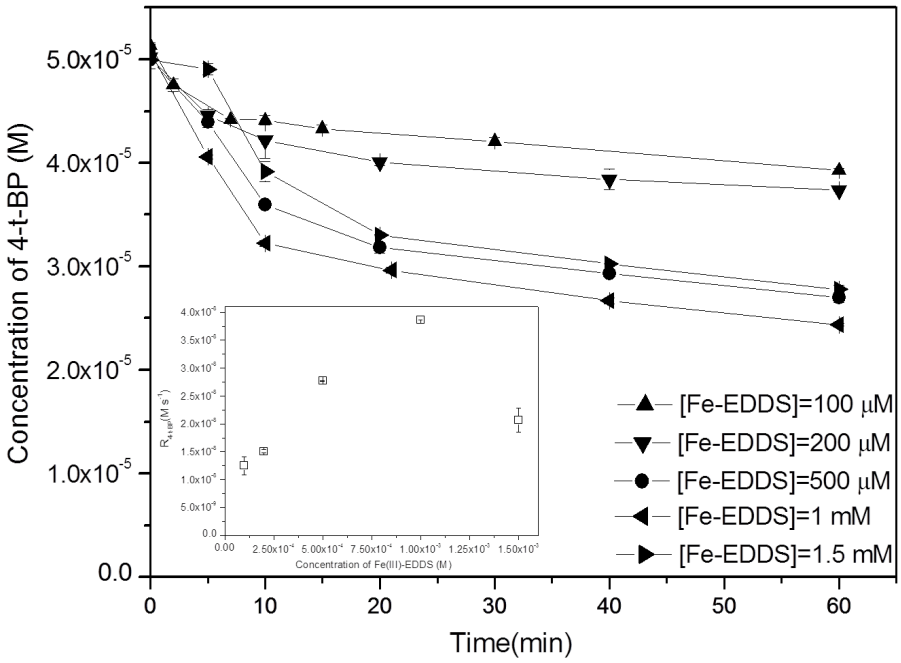

Figure 6-4 Effect of Fe(III)-EDDS concentration on the degradation of 4-t-BP (Insert: The 4-t-BP degradation rate as a function of Fe(III)-EDDS concentration)

The higher efficiency of 4-t-BP degradation at the higher Fe(III)-EDDS concentration resulted from the more production of $SO_4^{\bullet-}$ during the reaction. However, the photogenerated Fe(II) could also act as a $SO_4^{\bullet-}$ scavenger at its high concentration as expressed by R6-3 (k = 3.0×10^8 M^{-1} s^{-1}) [189-190]. Liang et al. [191] studied the reaction between one $S_2O_8^{2-}$ and Fe(II). It reported one $S_2O_8^{2-}$ and one Fe(II) to form $SO_4^{\bullet-}$ (R6-1), which then rapidly reacted with a second Fe(II) (R6-3). When the reactions had gone to completion, no sulfate free radical was available for further attack of target organic contaminants. On the other hand, high concentration of Fe(III)-EDDS could also quench $HO^{\bullet}$ which was another important radical produced in this reaction.

6.4 Effect of $S_2O_8^{2-}$ concentration

Persulfate played an important role as a source of $SO_4^{\bullet-}$ generation. The effect of $S_2O_8^{2-}$ dosage on 4-t-BP degradation was examined by varying concentration of $S_2O_8^{2-}$ from 100 μM to 1 mM. As shown in Figure 6-5, the 4-t-BP degradation efficiency increased with the increasing $S_2O_8^{2-}$ concentration. The $R_{4\text{-t-BP}}$ was also calculated and the results were shown in Figure 6-6. According to the National Secondary Drinking Water Regulations by United States Environmental Protection Agency (US EPA), the maximum contaminant level (MCL) of SO_4^{2-} is 250 mg/L (2.6 mM) [116]. So the photodegradation of 4-t-BP in $S_2O_8^{2-}$/Fe(III)-EDDS system was performed with a relatively low $S_2O_8^{2-}$ concentration.

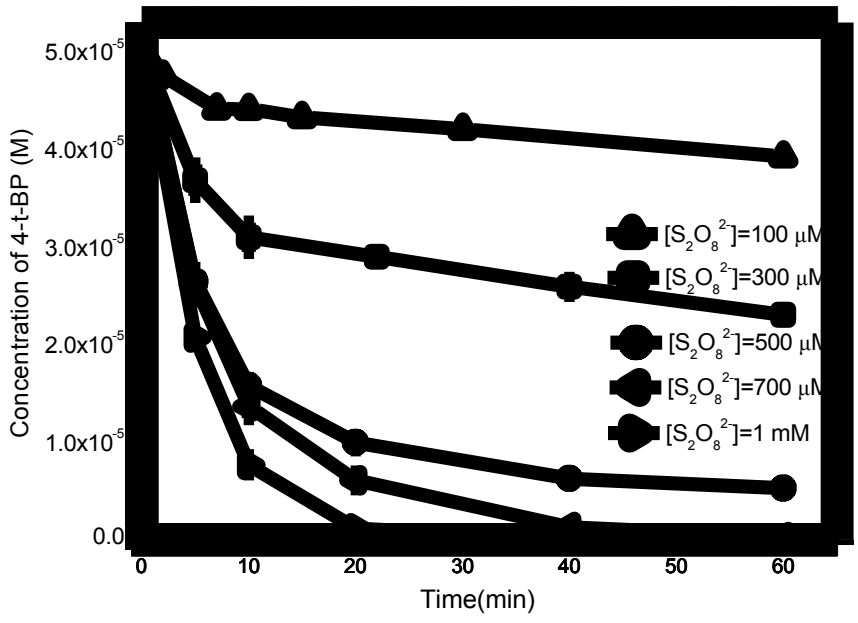

Figure 6-5 Effect of $S_2O_8^{2-}$ concentration on the degradation of 4-t-BP

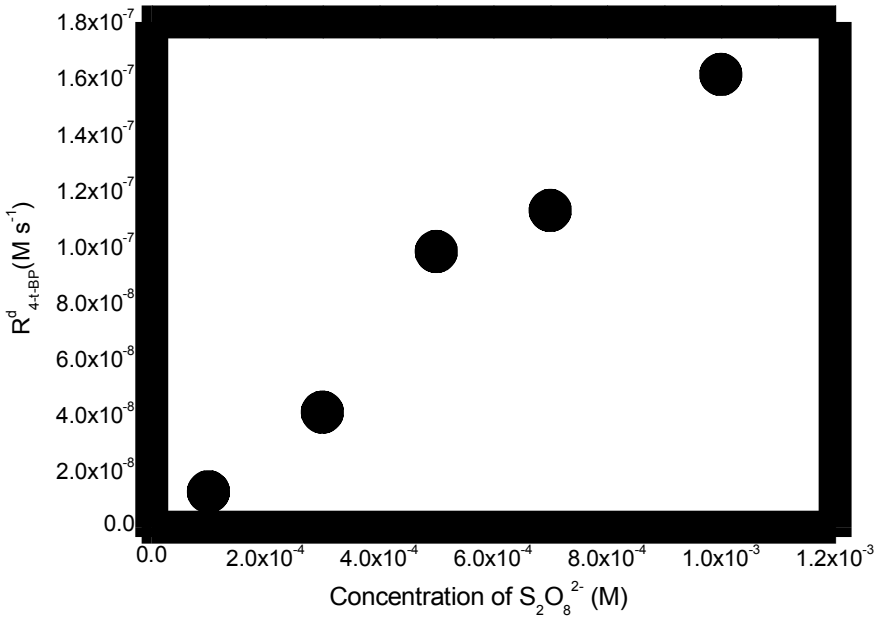

Figure 6-6 The 4-t-BP degradation rate as a function of Fe(III)-EDDS concentration

The increased $R_{4\text{-t-BP}}$ in the high $S_2O_8^{2-}$ concentration resulted from the increasing amount of $SO_4^{\bullet-}$. However, as the $S_2O_8^{2-}$ concentration kept increasing, it would inhabit the degradation of 4-t-BP due to the self-quenching of $SO_4^{\bullet-}$ (R6-4) and the reaction between $S_2O_8^{2-}$ and $SO_4^{\bullet-}$ (R6-5) [189].

$$SO_4^{\bullet-} + SO_4^{\bullet-} \rightarrow S_2O_8^{2-} \qquad \text{(R6-4)}$$

$$SO_4^{\bullet-} + S_2O_8^{2-} \rightarrow SO_4^{2-} + S_2O_8^{-} \qquad \text{(R6-5)}$$

6.5 Determination of the second-order rate constant

4-t-BP was considered to be a quencher as 2-propanol and t-BuOH in the

experiments performed in laser flash photolysis. To determine the second-order rate constant for the quenching of $SO_4^{\bullet-}$, plots were made of the first-order decay constant of $SO_4^{\bullet-}$, determined from the regression lines of the logarithmic decays of $SO_4^{\bullet-}$ monitored at 450 nm, against the concentration of quencher.

6.5.1 $k_{4\text{-t-BP, SO4}^{\bullet-}}$

Figure 6-7 showed the transient absorption spectra obtained after 266 nm laser excitation of $S_2O_8^{2-}$ (10 mM) in water in absence of 4-t-BP. Maximum absorption of $SO_4^{\bullet-}$ was 450 nm [192] as previously indicated and transient decays with a pseudo-first order constant $k'_{SO_4^{\bullet-}}$ of $3.3\times10^4 \pm 5.31\times10^3$ s^{-1} in water.

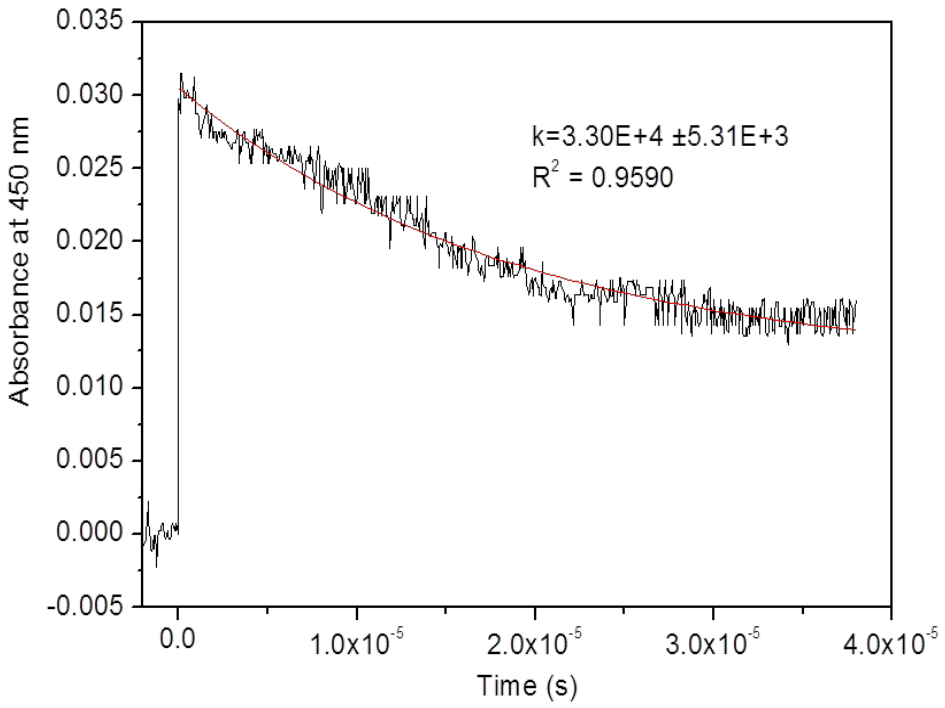

Figure 6-7 The decay curve of $SO_4^{\bullet-}$ as a function of time

After addition of 4-t-BP the transient decays rate increased, indicating a reaction between $SO_4^{\bullet-}$ and 4-t-BP. When the $S_2O_8^{2-}$/4-t-BP solution was irradiated by laser, there were there reactions as follow (R6-6 to R6-8):

$$SO_4^{\bullet-} + SO_4^{\bullet-} \rightarrow S_2O_8^{2-} \quad k_{SO4\bullet-,\,SO4\bullet-} = 5.0\times10^8\ M^{-1}\ s^{-1}\ [193] \quad \text{(R6-6)}$$

$$SO_4^{\bullet-} + 4\text{-}t\text{-}BP \rightarrow product \quad k_{4\text{-t-BP},\,SO4\bullet-} \quad \text{(R6-7)}$$

$$SO_4^{\bullet-} + S_2O_8^{2-} \rightarrow SO_4^{2-} + S_2O_8^{\bullet-} \quad k_{S2O82-,\,SO4\bullet-} = 1.2\times10^6\ M^{-1}\ s^{-1}\ [194] \quad \text{(R6-8)}$$

The $SO_4^{\bullet-}$ concentration could be calculated by Eq.6-1.

$$-\frac{d[SO_4^{\bullet-}]}{dt} = k_{SO4\bullet-,SO4\bullet-}[SO_4^{\bullet-}]^2 + k[4tBP][SO_4^{\bullet-}] + k_{S2O82-,SO4\bullet-}[S_2O_8^{2-}][SO_4^{\bullet-}] \quad \text{(Eq.6-1)}$$

The molar extinction coefficient of $SO_4^{\bullet-}$ (ε_{450}) was 1000 $M^{-1}cm^{-1}$ [192] and the initial $SO_4^{\bullet-}$ concentration could be calculated as 0.031 mM. But the 4-t-BP concentration (0.1-0.6 mM) was much higher than $SO_4^{\bullet-}$ concentration and the Eq. 6-1 could be simplified to Eq. 6-2.

$$-\frac{d[SO_4^{\bullet-}]}{dt} = k_{SO4\bullet-,SO4\bullet-}[SO_4^{\bullet-}]^2 + k'[SO_4^{\bullet-}] + k_{S2O82-,SO4\bullet-}[S_2O_8^{2-}][SO_4^{\bullet-}] \quad \text{(Eq.6-2)}$$

The pseudo-first order constants of $SO_4^{\bullet-}$ transient decay in different 4-t-BP concentrations were shown in Table 6-2.

Table 6-2 The *k'* of $SO_4^{\bullet-}$ decay in different reaction condition

[4-t-BP] (mM)	*k'* (s^{-1})
0	$3.30\times10^4\pm5.31\times10^3$
0.1	$4.31\times10^5\pm1.80\times10^4$
0.2	$9.77\times10^5\pm4.02\times10^4$
0.3	$1.53\times10^6\pm6.60\times10^4$
0.4	$1.72\times10^6\pm7.26\times10^4$
0.6	$2.68\times10^6\pm1.23\times10^5$

The second-order rate constant between 4-t-BP and $SO_4^{\bullet-}$ ($k_{4\text{-t-BP, SO4}\bullet-}$) was obtained from the linear fitting between *k'* and 4-t-BP concentration. As the results shown in Figure 6-8, the $k_{4\text{-t-BP, SO4}\bullet-}$ was calculated as 4.53×10^9 M^{-1} s^{-1}.

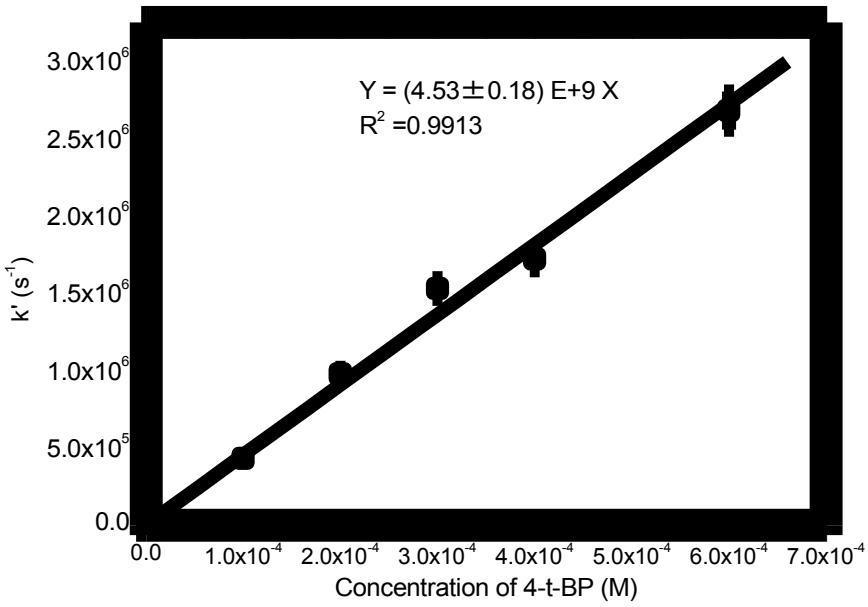

Figure 6-8 The fitting of second order reaction rate constant between 4-t-BP and $SO_4^{\bullet-}$

Moreover the new transition specie absorbing between 350 and 430 with a maximum at 410 had been attributed to the phenoxy radical anion (4-t-BP$^{\bullet-}$) generated after H-abstraction from phenolic group of 4-t-BP. This transient was also observed, with a lower absorption, upon direct excitation at 266 nm of 4-t-BP in pure water.

6.5.2 $k_{\text{2-Propanol, SO4}^{\bullet-}}$

Figure 6-9 showed the transient absorption spectra obtained after 266 nm laser excitation of $S_2O_8^{2-}$ (10 mM) in water in absence and present of 2-Propanol. As the similar calculation method used in section 6.5.1, the pseudo-first order constants with different 2-Propanol concentration were obtained and shown in Table 6-3.

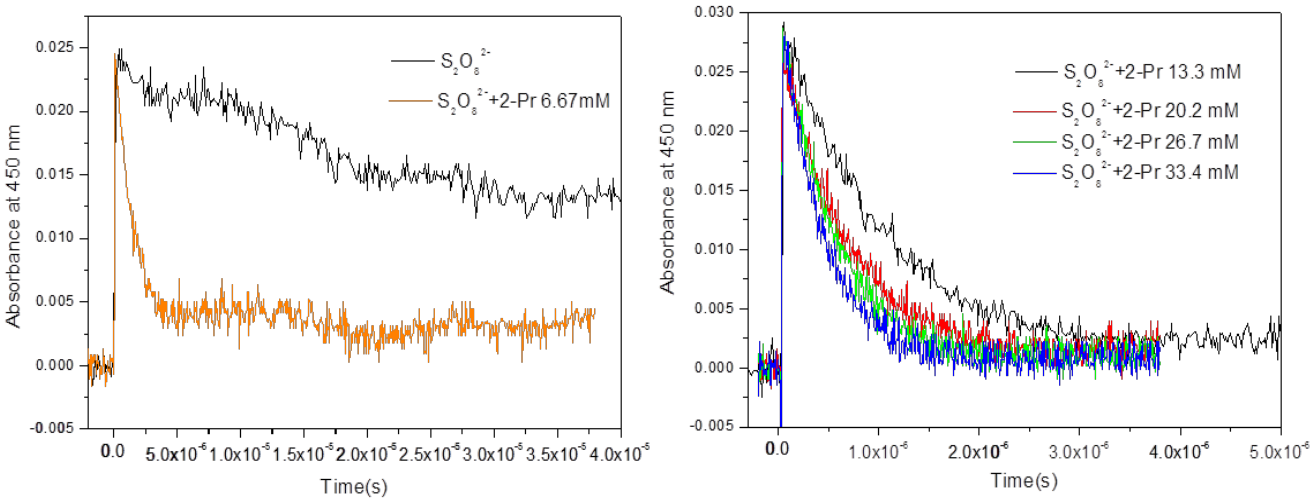

Figure 6-9 The decay curve of $SO_4^{\bullet-}$ with different 2-propanol concentration

Table 6-3 The *k* of $SO_4^{\bullet-}$ decay in different reaction condition

[2-Propanol] (mM)	k (s^{-1})
0	$6.10\times10^{4}\pm4.80\times10^{3}$
6.67	$7.30\times10^{5}\pm4.50\times10^{4}$
13.3	$1.08\times10^{6}\pm3.60\times10^{4}$
20.2	$1.56\times10^{6}\pm4.20\times10^{4}$
26.7	$1.93\times10^{6}\pm5.40\times10^{4}$
33.4	$2.40\times10^{6}\pm7.50\times10^{4}$

The second-order rate constant between 2-propanol and $SO_4^{\bullet-}$ ($k_{2\text{-propanol, SO4}\bullet-}$) was obtained from the linear fitting between *k'* and 2-propanol concentration. As the results shown in Figure 6-10, the $k_{2\text{-propanol, SO4}\bullet-}$ was calculated as 7.42×10^7 M^{-1} s^{-1}. The pH was 4.5 without adjustment. As reported in literatures [195-196197], $k_{2\text{-propanol, SO4}\bullet-}$ was determined as $(1.2\text{-}8.5) \times 10^7$ M^{-1} s^{-1}. The $k_{2\text{-propanol, SO4}\bullet-}$ obtained in this research was similar with the literatures. It also proved the calculation method was reasonable.

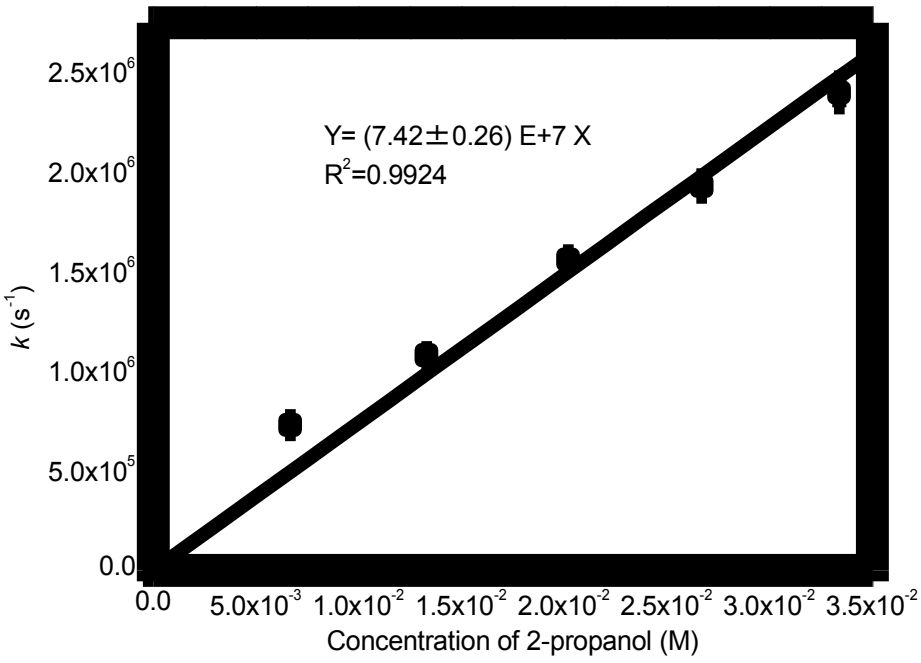

Figure 6-10 The fitting of second order reaction rate constant between 2-Propanol and $SO4^{\bullet-}$

A series of experiments were also conducted in different pH (pH 2.5 and 6.3) to investigate the effect of pH on the second order reaction rate constant. Table 6-4 showed the $k_{2\text{-propanol, SO4}^{\bullet-}}$ obtained in different pH. The results showed that the pH value did not have significant effect on the second order reaction rate constant of the reaction between 2-Propanol and $SO4^{\bullet-}$.

Table 6-4 $k_{2\text{-propanol, SO4}^{\bullet-}}$ obtained in different pH value

pH	$k_{2\text{-propanol, SO4}^{\bullet-}}$ (M^{-1} s^{-1})
2.5	$7.82\times10^{7}\pm4.29\times10^{6}$
4.5	$7.42\times10^{7}\pm2.55\times10^{6}$
6.3	$7.83\times10^{6}\pm4.30\times10^{6}$

6.5.3 $k_{\text{t-BuOH, SO4}^{\bullet-}}$

Figure 6-11 showed the transient absorption spectra obtained after 266 nm laser excitation of $S_2O_8^{2-}$ (10 mM) in water in absence and present of tert-Butanol (t-BuOH). The pseudo-first order constants with different t-BuOH concentration were obtained and shown in Table 6-4.

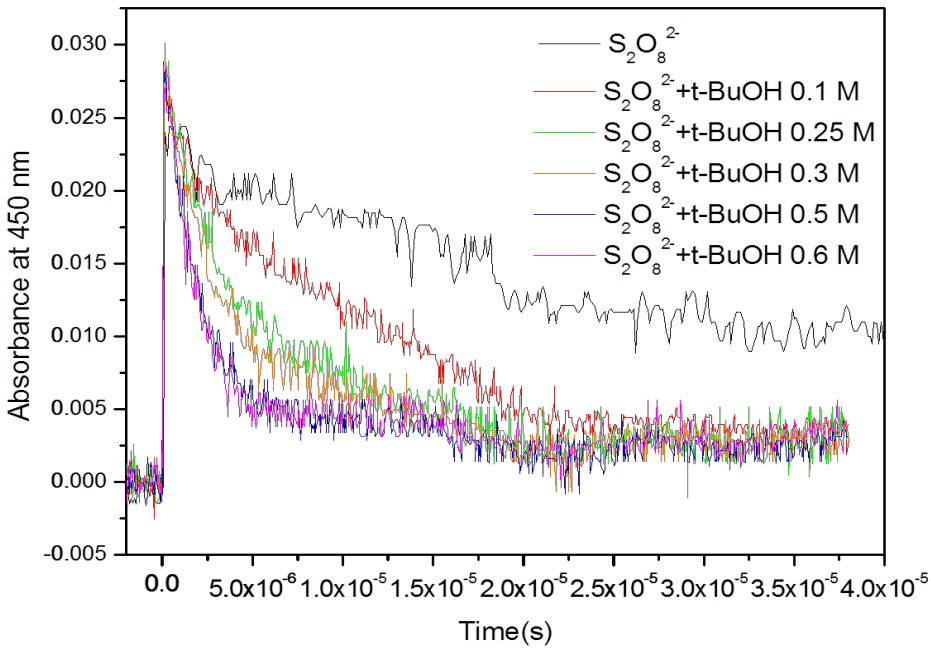

Figure 6-11 The decay curve of $SO_4^{\bullet-}$ with different t-BuOH concentration

Table 6-4 The *k* of $SO_4^{\bullet-}$ decay in different reaction condition

[t-BuOH] (M)	k (s^{-1})
0	$5.50\times10^4\pm3.60\times10^3$
0.1	$8.99\times10^4\pm4.05\times10^3$
0.25	$1.87\times10^5\pm1.17\times10^4$
0.3	$2.30\times10^5\pm1.47\times10^4$
0.5	$4.10\times10^5\pm1.92\times10^4$
0.6	$5.20\times10^5\pm2.40\times10^4$

The second-order rate constant between t-BuOH and $SO_4^{\bullet-}$ ($k_{\text{t-BuOH, SO4}\bullet-}$) was obtained from the linear fitting between *k'* and t-BuOH concentration. As the results shown in Figure 6-12, the $k_{\text{t-BuOH, SO4}\bullet-}$ was calculated as 8.31×10^5 M^{-1} s^{-1}. The pH was

4.5 without adjustment. As reported in literatures [118,[198]-[199]], $k_{t\text{-}BuOH,\ SO4^{\bullet-}}$ was determined as (4.0-9.1)×10^5 M^{-1} s^{-1}. The $k_{t\text{-}BuOH,\ SO4^{\bullet-}}$ obtained in this research was similar with the literatures.

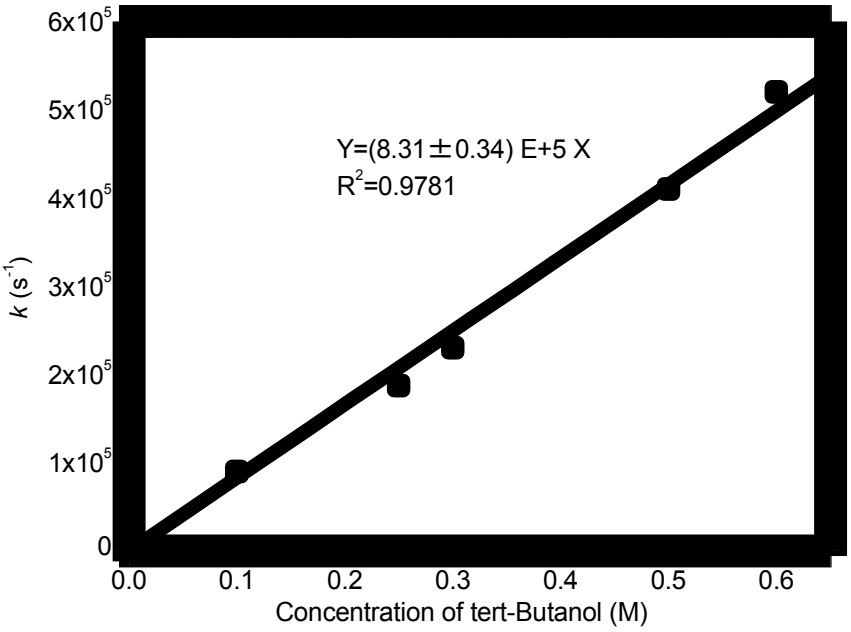

Figure 6-12 The fitting of second order reaction rate constant between t-BuOH and $SO4^{\bullet-}$

A series of experiments were also conducted in different pH (pH 2.5 and 6.5) to investigate the effect of pH on the second order reaction rate constant. Table 6-5 showed the $k_{t\text{-}BuOH,\ SO4^{\bullet-}}$ obtained in different pH. The results showed that the pH value did not have significant effect on the second order reaction rate constant of the reaction between t-BuOH and $SO4^{\bullet-}$.

Table 6-5 $k_{t\text{-}BuOH,\ SO4^{\bullet-}}$ obtained in different pH value

pH	$k_{t\text{-}BuOH,\ SO4^{\bullet-}}$ ($M^{-1}\ s^{-1}$)
2.5	$8.93\times10^5\pm2.32\times10^4$
4.5	$8.31\times10^5\pm3.35\times10^4$
6.5	$8.48\times10^5\pm1.51\times10^4$

6.6 Sulfate radical identification

In this study, $S_2O_8^{2-}$ was chemically activated by Fe^{2+} to form $SO4^{\bullet-}$, and $SO4^{\bullet-}$ could react with water to yield $HO^{\bullet}$, which could be expressed by R6-9 and R6-10 [200-201].

$$SO_4^{\bullet-} + H_2O \rightarrow SO_4^{2-} + HO^{\bullet} + H^+ \quad \text{(R6-9)}$$

$$SO_4^{\bullet-} + OH^- \rightarrow SO_4^{2-} + HO^{\bullet} \quad \text{(R6-10)}$$

However, the final oxidation products of $SO4^{\bullet-}$ and $HO^{\bullet}$ were similar [202-203]. 2-Propanol was a scavenger of $SO4^{\bullet-}$ ($k = 7.42\times10^7\ M^{-1}\ s^{-1}$) and $HO^{\bullet}$ ($k = 1.9\times10^9\ M^{-1}\ s^{-1}$) [156], while tert-Butanol (t-BuOH) reacted with $HO^{\bullet}$ ($k = 6.0\times10^8\ M^{-1}s^{-1}$) [177] at significantly higher rate than with $SO4^{\bullet-}$ ($k = 8.31\times10^5\ M^{-1}\ s^{-1}$). So 2-Propanol was considered to be the quencher for both $SO4^{\bullet-}$ and $HO^{\bullet}$, while t-BuOH was considered to be the quencher for $HO^{\bullet}$. The difference between the two scavengers was due to the

oxidation by $SO4^{\bullet-}$. Experiments to identify the role of $SO4^{\bullet-}$ and $HO^{\bullet}$ during the degradation of 4-t-BP were conducted with 2-Propanol and t-BuOH. 10 mM 2-Propanol (or t-BuOH) was introduced into the solution with 500 μM $S_2O_8^{2-}$ and 100 μM Fe(III)-EDDS. The effect of 2-Propanol and t-BuOH on 4-t-BP remaining in UV/Fe(III)-EDDS/$S_2O_8^{2-}$ system was displayed in Figure 6-13.

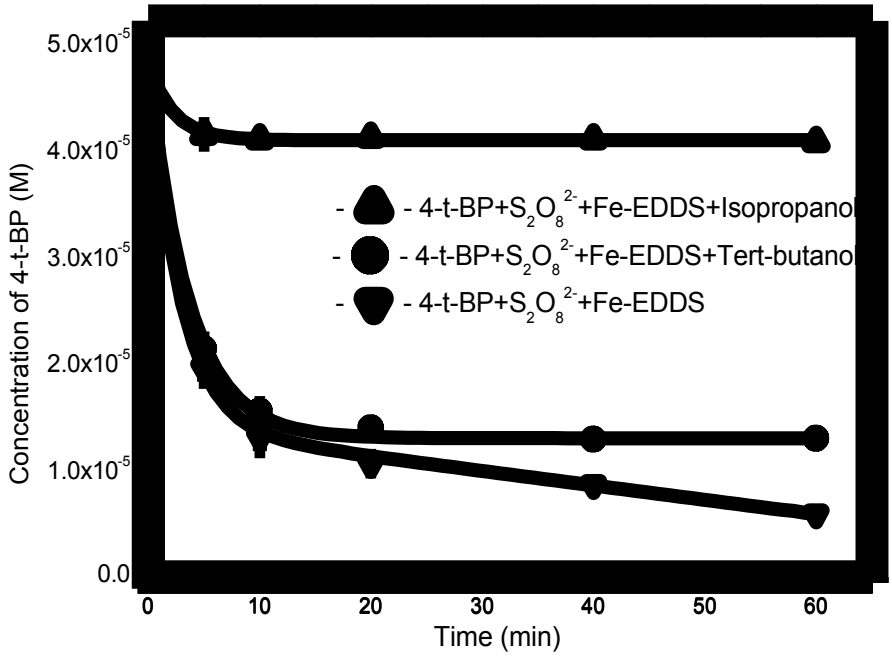

Figure 6-13 Effect of 2-Propanol and t-BuOH on the degradation of 4-t-BP

As shown in Figure 6-13, the inhibition of 4-t-BP degradation was about 70% in the presence of 2-Propanol, while it was only about 14% in the presence of t-BuOH,

which indicated that $SO4^{\bullet-}$ rather than $HO^{\bullet}$ was the major active free radical species in UV/Fe(III)-EDDS/$S_2O_8^{2-}$ system. It seems that these observations were the same as those in the system of $CoCl_2$ as catalyst [204].

6.7 Conclusion

In this chapter, the 4-t-BP degradation performance in UV/Fe(III)-EDDS/$S_2O_8^{2-}$ system was investigated with a series of experiments. The experiments were performed in a large range of pH which was a key parameter influencing the efficiency of the iron related oxidizing reaction and the effects of Fe(III)-EDDS concentration, $S_2O_8^{2-}$ concentration were also studied.

From this part of work, we could conclude that the UV/Fe(III)-EDDS/$S_2O_8^{2-}$ system performed higher efficiency than UV/Fe(III)/$S_2O_8^{2-}$ system. The high degradation efficiency of 4-t-BP was obtained in acid pH condition. However, the relatively lager pH range could be used in UV/Fe(III)-EDDS/$S_2O_8^{2-}$. The initial Fe(III)-EDDS and $S_2O_8^{2-}$concentrations had important influence on 4-t-BP removal rate. $R_{4\text{-t-BP}}$ increased with the increasing concentration of Fe(III)-EDDS and was inhibited when the Fe(III)-EDDS concentration was too high. $R_{4\text{-t-BP}}$ kept increasing when $S_2O_8^{2-}$ concentrations increased from 100 μM to 1 mM.

The transient laser flash photolysis experiments were performed to determine the second order reaction rate constant of the reactions between $SO_4^{\bullet-}$ and 4-t-BP/2-Propanol/t-BuOH. $k_{4\text{-t-BP, SO4}\bullet-}$, $k_{2\text{-Propanol, SO4}\bullet-}$ and $k_{\text{t-BuOH, SO4}\bullet-}$ were determined as 4.53×10^9 M^{-1} s^{-1}, 7.42×10^7 M^{-1} s^{-1} and 8.31×10^5 M^{-1} s^{-1}, respectively. In the UV/Fe(III)-

EDDS/$S_2O_8^{2-}$ system, $SO_4^{\bullet-}$ made the major contribution to 4-t-BP degradation, much larger than the contribution of $HO^{\bullet}$.

General conclusions

In this study, the advanced oxidation processes based on Fe(III)-EDDS were investigated. It included four processes as follow: photochemical process of Fe(III)-EDDS, Fenton-like process with Fe(III)-EDDS, photo Fenton-like process with Fe(III)-EDDS and UV/Fe(III)-EDDS/$S_2O_8^{2-}$ process. The 4-t-BP degradation rate was measured to evaluate the oxidation efficiency of these AOPs. The effect of several parameters such as pH values, Fe(III)-EDDS concentration, $H_2O_2/S_2O_8^{2-}$ concentration, oxygen concentration were studied.

First of all, the chemical properties of Fe(III)-EDDS and the 4-t-BP degradation efficiency in UV/Fe(III)-EDDS process were investigated. Fe(III)-EDDS was a stable

complex which was formed between Fe(III) and EDDS with the molar ratio 1:1. It could keep stable for one week. Theoretical and experimental approaches were used to investigate the form of Fe(III)-EDDS presented under different pH conditions. Fe(III)-EDDS is present under four different forms, FeL^-, $Fe(OH)L^{2-}$, $Fe(OH)_2L^{3-}$ and $Fe(OH)_4^-$. The presence of the different forms is due to the pH value and they had different sensitivity to the UV light. With the increasing concentration of Fe(III)-EDDS, 4-t-BP degradation rate increased but inhibited when the Fe(III)-EDDS concentration was too high. The photoredox process of Fe(III)-EDDS would produce $HO^{\bullet}$ to degrade pollutant, however, it also was the scavenger of $HO^{\bullet}$ with the high second-order reaction rate constant (4×10^8 M^{-1} s^{-1}). pH value had a significant effect on the degradation efficiency of 4-t-BP and it showed good degradation rate under neutral or alkaline conditions. This result was very encouraging for the application of Fe(III)-EDDS in Fenton and photo Fenton processes. pH value affected the Fe(III) and Fe(II) cycle. The formation of $HO_2^{\bullet}$ and $O_2^{\bullet-}$ (pKa= 4.86) as a function of pH was also one of the reasons. The $HO^{\bullet}$ was mainly responsible of 4-t-BP degradation but its formation was strongly depended of $O_2^{\bullet-}$ amount. On the other hand, it was observed that O_2 was an important parameter affecting the efficiency of this process. The significant impact of oxygen is due its important role play for the formation of $HO^{\bullet}$ and in the oxidation process of 4-t-BP.

Secondly, a series of experiments were performed to investigate the mechanism of Fe(III)-EDDS activating H_2O_2 and producing $HO^{\bullet}$, named Fenton-like process in this study. The results showed that the removal of 4-t-BP was relatively slow in

Fenton-like reaction. The initial degradation rate of 4-t-BP ($R_{4\text{-t-BP}}$) was calculated as $1.39 \pm 0.09\times10^{-9}$ M s^{-1}. With the increasing Fe(III)-EDDS or H_2O_2 concentration, $R_{4\text{-t-BP}}$ showed firstly increased and then decreased in the higher concentration. The reaction between Fe(III)-EDDS and H_2O_2 would produce $HO^{\bullet}$ which was the main reason for the 4-t-BP degradation. However, excessively high concentration of Fe(III)-EDDS or H_2O_2 would quench $HO^{\bullet}$ and the $R_{4\text{-t-BP}}$ decreased. When the pH value increased from 2.0 to 9.0, $R_{4\text{-t-BP}}$ showed increasing trend in Fenton-like process. It meant Fenton-like process could be used in neutral pH and alkaline condition which overcame the significant deficiency of the traditional Fenton reaction. This is the main advantage of this new iron complex. The 4-t-BP degradation rate also accelerated with the increasing of dissolved oxygen concentration.

Thirdly, the 4-t-BP degradation efficiency in UV/Fe(III)-EDDS/H_2O_2 (photo Fenton-like) process was investigated. Fe(II) was generated from the Fe(III)-EDDS photolysis and it could activate H_2O_2 and quickly produced $HO^{\bullet}$ to efficiently degrade organic pollutants. A series of experiments were performed to investigate the oxidation efficiency of UV/Fe(III)-EDDS/H_2O_2 system. The results showed that the 4-t-BP removal efficiency in photo Fenton-like reaction was much higher than that in Fenton-like reaction. The $R_{4\text{-t-BP}}$ was calculated as 1.48×10^{-7} M s^{-1}, nearly 100 times higher than Fenton-like process. With the increasing Fe(III)-EDDS concentration, R4-t-BP showed firstly increased and then decreased, similar mechanism as Fenton-like process. However, $R_{4\text{-t-BP}}$ kept increasing when the H_2O_2 concentration was increased. It was due to the photolysis of H_2O_2 which produced $HO^{\bullet}$. When the pH value

increased from 2.0 to 9.0, the highest $R_{4\text{-t-BP}}$ was obtained at pH 7.5 in photo Fenton-like reaction. The 4-t-BP degradation rate increased with the increase of the dissolved oxygen concentration.

Finally, the 4-t-BP degradation performance in UV/Fe(III)-EDDS/$S_2O_8^{2-}$ system was investigated with a series of experiments. The experiments were performed in a large range of pH which was a key parameter influencing the efficiency of the iron related oxidizing reaction and the effects of Fe(III)-EDDS concentration, $S_2O_8^{2-}$ concentration were also studied. The Fe(II) which produced by the photolysis of Fe(III)-EDDS activated $S_2O_8^{2-}$ and produced $SO_4^{\bullet-}$ to oxidize organic pollutant. The high degradation efficiency of 4-t-BP was obtained in acid pH condition. However, the relatively lager pH range (pH 2-8) could be used in UV/Fe(III)-EDDS/$S_2O_8^{2-}$ rather than UV/Fe(III)/$S_2O_8^{2-}$ system. $R_{4\text{-t-BP}}$ increased with the increasing concentration of Fe(III)-EDDS and was inhibited when the Fe(III)-EDDS concentration was too high. $R_{4\text{-t-BP}}$ kept increasing when $S_2O_8^{2-}$ concentrations increased from 100 μM to 1 mM. On the other hand, the transient laser flash photolysis experiments were performed to determine the second order reaction rate constant of the reactions between $SO_4^{\bullet-}$ and 4-t-BP/2-Propanol/t-BuOH. $k_{4\text{-t-BP, SO4}\bullet-}$, $k_{2\text{-Propanol, SO4}\bullet-}$ and $k_{\text{t-BuOH, SO4}\bullet-}$ were determined as 4.53×10^9 M^{-1} s^{-1}, 7.42×10^7 M^{-1} s^{-1} and 8.31×10^5 M^{-1} s^{-1}, respectively. In the UV/Fe(III)-EDDS/$S_2O_8^{2-}$ system, $SO_4^{\bullet-}$ made the major contribution to 4-t-BP degradation, rather than $HO^{\bullet}$.

References

Publication

[1]Yanlin Wu, Marcello Brigante, Wenbo Dong, Pascal de Sainte-Claire, Gilles Mailhot. Toward a Better Understanding of Fe(III)-EDDS Photochemistry: Theoretical Stability Calculation and Experimental Investigation of 4-tert-Butylphenol Degradation. Journal of Physical Chemistry A, 2014, 118 : 396-403.

[2]Yanlin Wu, Haixia Yuan, Guanran Wei, Shanduan Zhang, Hongjing Li, Wenbo Dong. Photodegradation of 4-tert-octylphenol in aqueous solution promoted by Fe(III). Environmental Science and Pollution Research, 2013, 20: 3-9.

[3]Yanlin Wu, Haixia Yuan, Xiaoxuan Jiang, Guanran Wei, Chunlei Li, Wenbo Dong. Photocatalytic degradation of 4-tert-octylphenol in a spiral photoreactor system. Journal of Environmental Sciences, 2012, 24(10): 1679-1685.

[4]Yanlin Wu, M. Passananti, Marcello Brigante, Wenbo Dong, Gilles Mailhot. Fe(III)-EDDS complex in Fenton and Photo-Fenton processes: from the radical formation to the degradation of a target compound. Environmental Science and Pollution Research. (online).

[5] Xiaoxuan Jiang, Yanlin Wu, Peng Wang, Hongjing Li, Wenbo Dong. Degradation of bisphenol A in aqueous solution by persulfate activated with ferrous ion. Environmental Science and Pollution Research, 2013, 20: 4947-4953.

[6] Peng Wang, Yanlin Wu, Jin Shi, Dan Liu, Wenbo Dong. Preparation of carbon-supported Bi/Ti composites and its catalytic activity under solar irradiation. Applied Surface Science, 2014, 292:1077-1082.

[7] Haixia Yuan, Huxiang Pan, Yanlin Wu, Jianfeng Zhao, Wenbo Dong. Laser Flash Photolysis Mechanism of Pyrenetetrasulfonate in Aqueous Solution. Acta Physico-Chimica Sinica, 2012, 28(04): 957-962.

[8] Jia Li, Yanlin Wu, Xiaoxuan Jiang, Wenbo Dong. A Study on the Degradation of Biphenyl in the Water with Persulfate by UV Light, Journal of Fudan University (Natural Science), 2013, 52(1):62-68. (CNKI)

1[] W.H. Glaze. Drinking water treatment with ozone. Environmental science & technology, 1987, 21(3), 224-230.

2[] W.H. Glaze, J.W. Kwang, D.H. Chapin. Chemistry of water treatment processes involving ozone, hydrogen peroxide and ultraviolet radiation. Ozone Science and Engineering, 1987, 9, 335-352.

3[] C.P. Huang, C.H. Dong, Z. Tang. Advanced chemical oxidation: its present role and potential future in hazardous waste treatment. Waste Management, 1993, 13, 361-377.

4[] R. Andreozzi, V. Caprio, A. Insola, R. Martota. Advanced oxidation proceses (AOP) for water purification and recovery. Catalysis Today, 1999, 53, 51-59.

5[] K. Rajeshwar. Photochemical strategies for abating environmental pollution. Chemistry and Industry, 1996, 12, 454-458.

6[] C.J. Somich, M.T. Muldoon, P.C. Kearney. On site treatment of pesticide waste and rinsate using ozone and biologically active soil. Environmenal Science and Technology, 1990, 24, 745-749.

7[] K. Ikehata, M.G. El-Din. Aqueous pesticide degradation by ozonation and ozonebased advanced oxidation processes: A review (Part I). Ozone: Science and Engneering 2005, 27, 83-114.

8[] B. Ning, N.J.D. Graham, Y.P. Zhang. Degradation of octylphenol and nonylphenol by ozone-Part I: Direct reaction. Chemosphere, 2007, 68, 1163-1172.

9[] J. De Laat, T.G. Lee, B. Legube. A comparative study of the effects of chloride, sulfate and nitrate ions on the rates of decomposition of H_2O_2 and organic compounds by Fe(II)/H_2O_2 and Fe(III)/H_2O_2. Chemosphere, 2004, 55, 715-723.

10[] G.F. Ijpelaar, R.T. Meijers, R. Hopman, J.C. Krivithot. Oxidation of herbicides in ground water by the Fenton process: A realistic alternative for O_3/H_2O_2. Ozone: Science and Engineering, 2000, 22(6), 607-616.

11[] M. Barbeni, C. Minero, E. Pelizzetti, E. Borgarello, N. Serpone. Chemical degradation of chlorophenols with Fenton's reagent (Fe^{2+}+H_2O_2). Chemosphere, 1987, 16(10-12), 2225-2237.

12[] W.G. Kuo. Decolorizing dye wastewater with Fenton's reagent. Water Research, 1992, 26(7),

881-886.

13[] M.M. Huber, S. Korhonen, T.A. Ternes, U. Gunten. Oxidation of pharmaceuticals during water treatment with chlorine dioxide. Water Research, 2005, 39(15), 3607-3617.

14[] J. Hoigné, H. Bader. Kinetics of reactions of chlorine dioxide (OClO) in water-I. Rate constants for inorganic and organic compounds. Water research, 1994, 28(1), 45-55.

15[] C. Comninellis, C. Pulgarin. Electrochemical oxidation of phenol for wastewater treatment using SnO_2 anodes. Journal of applied electrochemistry, 1993, 23, 108-112.

16[] L.C. Chiang, J.E. Chang, T.C. Wen. Indirect oxidation effect in electrochemical oxidation treatment of landfill leachate. Water Research, 1995, 29(2), 671-678.

17[] Z.C. Wu, M.H. Zhou. Partial degradation of phenol by advanced electrochemical oxidation process. Environmental Science and Technology, 2001, 35(13): 2698-2703.

18[] H.S. Joglekar, S.D. Samant, J.B. Joshi. Kinetics of wet air oxidation of phenol and substituted phenols. Water Research, 1991, 25(2), 135-145.

19[] P. Gallezot, N. Laurain, P. Isnard. Catalytic wet-air oxidation of carboxylic acids on carbon-supported platinum catalysts. Applied Catalysis B: Environmental, 1996, 9(1-4), L11-L17.

20[] H.E. Barner, C.Y. Huang, T. Johnson, G. Jacobs, M.A. Martch. Supercritical water oxidation: An emerging technology. Journal of Hazardous Materials, 1992, 31(1), 1-17

21[] P. Kritzer, E. Dinjus An assessment of supercritical water oxidation (SCWO): Existing problems, possible solutions and new reactor concepts. Chemical Engineering Journal, 2001, 83(3), 207-214.

22[] I. Hua, M.R. Hoffmann. Optimization of Ultrasonic Irradiation as an Advanced Oxidation Technology. Environmenal Science and Technology, 1997, 31 (8), 2237-2243.

23[] A. Kotronarou, G. Mills, M.R. Hoffmann. Ultrasonic irradiation of p-nitrophenol in aqueous solution. Journal of Physical and Chemistry, 1991, 95 (9), 3630-3638.

24[] Y. Ku, W.J. Su, Y.S. Shen. Decomposition of phenols in aqueous solution by a UV/O_3 process. Ozone: Science & Engineering: The Journal of the International Ozone Association, 1996, 18(5),

443-460.

25[] Y.S. Shen, Y. Ku. Decomposition of gas-phase chloroethenes by UV/O_3 process. Water Research, 1998, 32(9), 2669-2679.

26[] C.D. Adams, J.J. Kuzhikanni. Effect of UV/H_2O_2 preoxidation on the aerobic biodegradability of quaternary amine surfactants. Water Research, 2000，34(2), 668-672.

27[] B. Boyarri, J. Gimenez, D. Curco, S. Esplugas. Photocatalytic degradation of 2,4-dichlorophenol by TiO_2/UV: kinetics, actimometries and models. Catalysis Today, 2005, 101(3-4), 227-236.

28[] C. Guillard, P. Pichat, G. Huber, C. Hoang. The GC-MS analysis of organic intermediates from the TiO_2-UV photocatalytic treatment of water contaminated with lindane. Journal of Advanced Oxidation Technologies, 1996, 1, 53-60.

29[] A.E. Kinkennon, D.B. Green, B. Hutchinson. UV degradation of pyrymidinic herbicides using powder titanium dioxide suspensions. Chemosphere, 1995, 31(7), 3663-3671.

30[] R. Bauer, G. Waldner, H. Fallman, S. Hager, M. Klare, T. Krutzler, S. Malato, P. Maletzky. The photo-Fenton reaction and the TiO_2/UV process for waste water treatment-novel developments. Catalysis Today, 1999, 53, 131-144.

31[] Y. Sun, J.J. Pignatello. Organic intermediates in the degradation of 2,4-dichlorophenoxyacetic acid by Fe^{3+}/H_2O_2 and Fe^{3+}/H_2O_2/UV. Journal of Agricultural and Food Chemistry, 1993, 41, 1139-1142.

32[] Y. Sun, J.J. Pignatello. Photochemical reactions involved in the total mineralization of 2,4-D by Fe^{3+}/H_2O_2/UV. Environmental Science and Technology, 1993, 27, 304-310.

33[] G. Anipsitakis, D.D. Dionysiou. Degradation of organic contaminants in water with sulfate radicals generated by the conjunction of peroximonosufate with cobalt. Environmental Science and Technology, 2003, 37, 4790-4797.

34[] G. Anipsitakis, D.D. Dionysiou. Radical generation by the interaction of transition metals with common oxidants. Environmental Science and Technology, 2004, 38, 3705-3712.

35[] G. Anipsitakis, D.D. Dionysiou, M.A. Gonzalez. Cobalt mediated activation of peroxymonosulfate and sulfate radical attack on phenolic compounds. Implication of chloride ions. Environmental Science and Technology, 2006, 40, 1000-1007.

36[] Y.X. Lin, Photocatalysis of parabens by titanium dioxide under UV irradiation in aqueous solution, Université Claude Bernard-Lyon I, Lyon, 2009.

37[] I. Peternel, N. Koprivanac, H. Kusic. UV-based processes for reactive azo dye mineralization. Water Research, 2006, 40: 525-532.

38[] E. Rosales, O. Iglesias, M. Pazos, M.A. Sanromán. Decolourisation of dyes under electro-Fenton process using Fe alginate gel beads. Journal of Hazardous Materials, 2012, 213-214(30): 369-377.

39[] S.B. Abdelmelek, J. Greaves, K.P. Ishida, W.J. Cooper, W. Song. Removal of Pharmaceutical and Personal Care Products from Reverse Osmosis Retentate Using Advanced Oxidation Processes. Environmental Science and Technology, 2011, 45(8): 3665-3671.

40[] H. Shemer, Y.K. Kunukcu, K.G. Linden. Degradation of the pharmaceutical Metronidazole via UV, Fenton and photo-Fenton processes. Chemosphere, 2006, 63(2): 69-76.

41[] V. Homem, L. Santos. Degradation and removal methods of antibiotics from aqueous matrices - A review. Journal of Environmental Management, 2011, 92(10): 2304-2347.

42[] I. Oller, S. Malato, J.A. Sánchez-Pérez, M.I. Maldonado, R. Gassó. Detoxification of wastewater containing five common pesticides by solar AOPs–biological coupled system. Catalysis Today, 2007, 129(1-2): 69-78.

43[] E. Evgenidou, K. Fytianos. Photodegradation of Triazine Herbicides in Aqueous Solutions and Natural Waters. Journal of agricultural and food chemistry, 2002, 50(22): 6423-6427.

44[] E.M.R. Rocha, V.J.P. Vilar, A. Fonseca, I. Saraiva, R.A.R. Boaventura. Landfill leachate treatment by solar-driven AOPs. Solar Energy, 2011, 85(1): 46-56.

45[] J.P. Scott, D.F.Ollis. Integration of chemical and biological oxidation processes for water treatment: review and recommendations. Environmental Progress, 1995, 14(2), 88-103.

46[] J.P. Scott, D.F. Ollis. Engineering models of combined chemical and biological processes. Journal of Environmental Engineering, 1996, 122(12), 1110-1114.

47[] I. Oller, S. Malato, J.A. Sánchez-Pérez. Combination of Advanced Oxidation Processes and biological treatments for wastewater decontamination - A review. Science of the Total Environment, 2011, 409(20), 4141-4166.

48[] J. Hamilton-Taylor, M. Willis. A quantitative assessment of the sources and general dynamics of trace metals in a soft-water lake. Limnology and Oceanography, 1990, 35(4), 840-851.

49[] K. Kawamura, A Nissenbaum, High abundance of low molecular weight organic acids in hypersaline spring water associated with a salt diapir. Organic Geochemistry, 1992, 18(4): 469-476.

50[] S. Fuzzi, G. Orsi, G. Nardini, M.C. Facchini, S. McLaren, E. McLaren, M. Mariotti. Heterogeneous processes in the Po Valley radiation fog. Journal of Geophysical Research: Atmospheres, 1988, 93(D9): 11141–11151.

51[] A.G Clarke, M Radojevic. Oxidation of SO_2 in rainwater and its role in acid rain chemistry. Atmospheric Environment, 1987, 21(5): 1115-1123.

52[] J.W. Munger, D.J. Jacob, J.M. Waldman, M.R. Hoffmann. Fogwater chemistry in an urban atmosphere. Journal of Geophysical Research: Oceans, 1983, 88(C9): 5109-5121.

53[] H.J.H. Fenton. Oxidation of tartaric acid in presence of iron. Journal of the Chemical Society, Transactions, 1894, 65: 899-910.

54[] K. Ruel, J.P. Joseleau. Role of H_2O_2 in the degradation of wood polysaccharides by fungi[J]. Food Hydrocolloids, 1987, 1(5-6): 515-517.

55[] M. Barbeni, C. Minero, E. Pelizzetti, E. Borgarello, N. Serpone. Chemical degradation of chlorophenols with Fenton's reagent (Fe^{2+} + H_2O_2)[J]. Chemosphere, 1987, 16(10-12): 2225-2237.

56[] O. Koyama, Y. Kamagata, K. Nakamura. Degradation of chlorinated aromatics by fenton oxidation and methanogenic digester sludge[J]. Water Research, 1994, 28(4): 895-899

57[] J. Kiwi, C. Pulgarin, P. Peringer. Effect of Fenton and photo-Fenton reactions on the degradation and biodegradability of 2 and 4-nitrophenols in water treatment. Applied Catalysis B:

Environmental, 1994, 3(4): 335-350.

58[] W.G. Kuo. Decolorizing dye wastewater with Fenton's reagent. Water Research, 1992, 26(7): 881-886.

59[] K.H. Chan, W. Chu. Model applications and mechanism study on the degradation of atrazine by Fenton's system. Journal of Hazardous Materials, 2005, 118(1-3): 227-237.

60[] Y. Deng, J.D. Englehardt. Treatment of landfill leachate by the Fenton process. Water Research, 2006, 40, 3683-3694.

61[] Y. Deng. Physical and oxidative removal of organics during Fenton treatment of mature municipal landfill leachate. Journal of Hazardous Materials, 2007, 146(1-2): 334-340.

62[] C.Walling, A. Goosen. Mechanism of the ferric ion catalyzed decomposition of hydrogen peroxide. Effect of organic substrates. Journal of the American Chemical Society, 1973, 95(9): 2987-2991.

63[] C. Lee, J. Yoon. Temperature dependence of hydroxyl radical formation in the hv/Fe^{3+}/H_2O_2 and Fe^{3+}/H_2O_2 systems. Chemosphere, 2004, 56(10): 923-934.

64[] W. Huang. Homogeneous and heterogeneous Fenton and photo-Fenton processes: Impact of iron complexing agent EDDS. Aubiere: University Blaise Pascal, 2012: 35.

65[] H.J. Benkelberg, P. Warneck. Photodecomposition of iron(III) hydroxo and sulfato complexes in aqueous solution: wavelength dependence of OH and quantum yields. The Journal of Physical Chemistry, 1995, 99(14): 5214-5221.

66[] T.D. Waite. Challenges and opportunities in the use of iron in water and wastewater treatment. Review in environmental science and biotechnology, 2002, 1(1): 9-15.

67[] T.Y. Wei, Y.Y. Wang, C.C. Wan. Photocatalytic oxidation of phenol in the presence of hydrogen peroxide and titanium dioxide powders. Journal of Photochemistry and Photobiology A: Chemistry, 1990, 55(1): 115-126.

68[] C.Y. Kuo, S.L. Lo. Oxidation of aqueous chlorobiphenyls with photo-fenton process. Chemosphere, 1999, 38(9): 2041-2051.

69[] K. Wu, Y. Xie, J. Zhao, H. Hidaka. Photo-Fenton degradation of a dye under visible light irradiation. Journal of Molecular Catalysis A: Chemical, 1999, 144(1): 77-84.

70[] P.L. Huston, J.J. Pignatello. Degradation of selected pesticide active ingredients and commercial formulations in water by the photo-assisted Fenton reaction. Water Research, 1999, 33(5): 1238-1246.

71[] R.G. Zepp, B.C. Faust, J. Hoigne. Hydroxyl radical formation in aqueous reactions (pH 3-8) of iron(II) with hydrogen peroxide: the photo-Fenton reaction. Environmental science & technology, 1992, 26(2): 313-319.

72[] R. Bauer, H. Fallmann. The Photo-Fenton Oxidation - A cheap and efficient wastewater treatment method. Research on Chemical Intermediates, 1997, 23(4): 341-354.

73[] J.D. Laat, H. Gallard. Catalytic Decomposition of Hydrogen Peroxide by Fe(III) in Homogeneous Aqueous Solution: Mechanism and Kinetic Modeling. Environmental Science & Technology, 1999, 33(16): 2726-2732.

74[] E. Neyens, J. Baeyens. A review of classic Fenton's peroxidation as an advanced oxidation technique. Journal of Hazardous Materials, 2003, 98(1-3): 33-50.

75[] J.J. Pignatello. Dark and photoassisted Fe^{3+}-catalyzed degradation of chlorophenoxy herbicides by hydrogen peroxide. Environmental Science & Technology, 1992, 26(5): 944-951.

76[] K. Kawamura, S. Steinberg, I.R. Kaplan. Capillary GC determination of short-chain dicarboxylic acids in rain, fog, and mist. International Journal of Environmental Analytical Chemistry, 1985, 19(3): 175-188.

77[] A. Marinoni, P. Laj, K. Sellegri, G. Mailhot. Cloud chemistry at the Puy de Dôme: variability and relationships with environmental factors. Atmospheric Chemistry and Physics, 2004, 4: 715-728.

78[] M. Löflund, A. Kasper-Giebl, B. Schuster, H. Giebl, R. Hitzenberger, H. Puxbaum. Formic, acetic, oxalic, malonic and succinic acid concentrations and their contribution to organic carbon in cloud water. Atmospheric Environment, 2002, 36(9): 1553-1558.

79[] C. Lee, D.L. Sedlak. A novel homogeneous Fenton-like system with Fe(III)- phosphotungstate for oxidation of organic compounds at neutral pH values. Journal of Molecular Catalysis A: Chemical, 2009, 311(1-2): 1-6.

80[] N. Deng, F. Wu, F. Luo, Z. Liu. Photodegradation of Dyes in Aqueous Solutions Containing Fe(lII)-oxalato Complexes. Chemosphere, 1997, 35(11): 2697-2706.

81[] D. Zhou, F. Wu, N. Deng. Fe(III)-oxalate complexes induced photooxidation of diethylstilbestrol in water. Chemosphere, 2004, 57(4): 283-291.

82[] S.J. Hug, L. Canonica, M. Wegelin, D. Gechter, U.V. Gunten. Solar Oxidation and Removal of Arsenic at Circum neutral pH in Iron Containing Waters. Environmental Science & Technology, 2001, 35(10): 2114-2121.

83[] H. Katsumata, S. Kaneco, T. Suzuki, K. Ohta, Y. Yobiko. Photo-Fenton degradation of alachlor in the presence of citrate solution. Journal of Photochemistry and Photobiology A: Chemistry, 2006, 180(1-2), 38-45.

84[] M.R.A. Silva, A.G. Trovó, R.F.P. Nogueira. Degradation of the herbicide tebuthiuron using solar photo-Fenton process and ferric citrate complex at circumneutral pH. Journal of Photochemistry and Photobiology A: Chemistry, 2007, 191(2-3): 187-192.

85[] E. Lipczynska-Kochany, J. Kochany. Effect of humic substances on the Fenton treatment of wastewater at acidic and neutral pH. Chemosphere, 2008, 73(5): 745-750.

86[] M. Bucheli-Witschel, T. Egli. Environmental fate and microbial degradation of aminopolycarboxylic acids. FEMS Microbiology Review, 2001, 25(1): 69-106.

87[] T. Trott, R.W. Henwood, C.H. Langford. Sunliight photochemistry of ferric nitrilotriacetate complexes. Environmental Science & Technology, 1972, 6(4): 367-368.

88[] P. Natarajan, J.F. Endicott. Photoredox behavior of transition metal-ethylene diamine tetraacetate complexes, comparison of some group VIII metals. Journal of Physical Chemistry, 1973, 77(17): 2049-2054.

89[] J. Howsawkeng, R.J. Watts, D.L. Washington, A.L. Teel, T.F. Hess, R.L. Crawford. Evidence

for simultaneous abiotic-biotic oxidations in a microbial-Fenton's system. Environmental Science & Technology, 2001, 35(14): 2961-2966.

90[] A.C. Ndjou'ou, J. Bou-Nasr, D. Cassidy. Effect of Fenton reaction dose on coexisting chemical and microbial oxidation in soil. Environmental Science & Technology, 2006, 40(8): 2778-2783.

91[] Y.S. Kim, S.H. Kong. Treatment of 1-Hexanol and Carbon tetrachloride in modified Fenton's reagent using iron(III)-NTA complex. Journal of the Korean Industrial and Engineering, 2001, 12(7): 787-792.

92[] T. Zhou, Y. Li, F.S. Wong, X. Lu. Enhanced degradation of 2,4-dichlorophenol by ultrasound in a new Fenton like system (Fe/EDTA) at ambient circumstance. Ultrasonics Sonochemistry, 2008, 15(5): 782-790.

93[] B. Liu, S. Li, Y. Zhao, W. Wu, X. Zhang, X. Gu, R. Li, S. Yang. Enhanced degradation of 4-nitrophenol by microwave assisted Fe/EDTA process. Journal of Hazardous Materials, 2010, 176(1-3): 213-219.

94[] S. Metsärinne, T. Tuhkanen, R. Aksela. Photodegradation of ethylene diamine tetraacetic acid (EDTA) and ethylene diamine disuccinic acid (EDDS) within natural UV radiation range. Chemosphere, 2001, 45(6-7): 949-955.

95[] D. Schowanek, T.C.J. Feijtel, C.M. Perkins, F.A. Hartman, T.W. Federle, R.J. Larson. Biodegradation of [S,S], [R,R] and mixed stereoisomers of Ethylene Diamine Disuccinic Acid (EDDS), a transition metal chelator. Chemosphere, 1997, 34(11): 2375-2391.

96[] S. Tandy, A. Ammann, R. Schulin, B. Nowack. Biodegredation and speciation of residual S,S-ethylene diamine disuccinic acid (EDDS) in soil solution left after soil washing. Environmental Pollution, 2006, 142(2): 191-199.

97[] D.Y.S. Yan, I.M.C. Lo. Enhanced multi-metal extraction with EDDS of deficient and excess dosages under the influence of dissolved and soil organic matter. Environmental Pollution, 2011, 159(1): 78-83.

98[] L. Zhang, Z. Zhu, R. Zhang, C. Zheng, H. Zhang, Y. Qiu, J. Zhao. Extraction of copper from

sewage sludge using biodegradable chelant EDDS. Journal of Environmental Sciences, 2008, 20(8): 970-974.

99[] J. Li， G. Mailhot， F. Wu， N. Deng. Photochemical efficiency of Fe(Ⅲ)-EDDS complex: ·OH radical production and 17β-estradiol degradation. Journal of Photochemistry and Photobiology A: Chemistry, 2010, 212(1): 1-7.

100[] W. Huang, M. Brigante, F. Wu, C. Mousty, K. Hanna, G. Mailhot. Assessment of the Fe(III)-EDDS Complex in Fenton-Like Processes: From the Radical Formation to the Degradation of Bisphenol A. Environmental Science & Technology, 2013, 47(4): 1952-1959.

101[] W. Huang, M. Brigante, F. Wu, K. Hanna, G. Mailhot. Effect of ethylenediamine-N,N’-disuccinic acid on Fenton and photo-Fenton processes using goethite as an iron source: optimization of parameters for bisphenol A degradation. Environmental Science and Pollution Research, 2013, 20(1): 39-50.

102[] I.M. Kolthoff, I.K. Miller. The chemistry of persulfate I. The kinetics and mechanism of the decomposition of the persulfate ion in aqueous medium. Journal of the American Chemical Society, 1951, 73(7): 3055-3059.

103[] P.F. Killian, C.J. Bruell, C. Liang, M.C. Marley. Iron (II) activated persulfate oxidation of MGP contaminated soil. Soil Sediment Contamination: An International Journal, 2007, 16(6), 523-537.

104[] C.M. Zuo. Study on Degradation of dye Wastewater by Persulfate Oxidation Activated by Ferrous Ion Advanced Oxidation Technology, Chongqing University, Chongqing, China, 2012.

105[] M. Banerjee, R.S. Konar. Comment on the paper “Polymerization of acrylonitrile initiated by $K_2S_2O_8$-Fe(II) redox system. Journal of Polymer Science Part A: Polymer Chemistry, 1984(22): 1193-1195.

106[] R.H. Waldemer, P.G. Tratnyek, R.L. Johnson, J.T. Nurmi. Oxidation of chlorinated ethenes by heat activated persulfate: Kinetics and products. Environmental Science & Technology, 2007, 41(3): 1010-1015.

107[] K.C. Huang, Z. Zhao, G.E. Hoag, A. Dahmani, P.A. Block. Degradation of volatile organic compounds with thermally activated persulfate oxidation. Chemosphere, 2005, 61(4): 551-560.

108[] N. Zhang, M. Zhang, B. Sun. Preliminary study on processing methyl orange in the water with sulfate radical anion method. Journal of Harbin Institute of Technology, 2006, 38:636-638. (CNKI)

109[] J. Criquet, N.K.V. Leitner. Degradation of acetic acid with sulfate radical generated by persulfate ions photolysis. Chemosphere, 2009, 77(2): 194-200.

110[] X. Xu, X. Li. Degradation of azo dye Orange G in aqueous solutions by persulfate with ferrous ion. Separation and Purification Technology, 2010, 72(1): 105-111.

111[] G.P. Anipsitakis, D.D. Dionysiou. Degradation of organic contaminants in water with sulfate radicals generated by the conjunction of peroxymonosulfate with cobalt. Environmental Science & Technology, 2003, 37(20): 4790-4797.

112[] L. Zhang, X. Guo, F. Yan, M. Su, Y. Li. Study of the degradation behaviour of dimethoate under microwave irradiation. Journal of Hazardous Materials, 2007, 149(3): 675-679.

113[] Y.C. Lee, S.L. Lo, P.T. Chiueh, D.G. Chang. Efficient decomposition of perfluorocarboxylic acids in aqueous solution using microwave-induced persulfate. Water Research, 2009, 43(11): 2811-2816.

114[] P.A. Block, R.A. Brown, D. Robinson. Novel activation technologies for sodium persulfate in situ chemical oxidation. In: Proceedings of the Fourth International Conference on the Remediation of Chlorinated and Recalcitrant Compounds, Monterey, 2004.

115[] S. Yang, X. Yang, X. Shao, R. Niu, L. Wang. Activated carbon catalyzed persulfate oxidation of Azo dye acid orange 7 at ambient temperature. Journal of Hazardous Materials, 2011, 186(1): 659-666.

116[] T.K. Lau, W. Chu, N.J.D. Graham. The aqueous degradation of butylated hydroxyanisole by UV/$S_2O_8^{2-}$: study of reaction mechanisms via dimerization and mineralization. Environmental Science & Technology, 2007, 41(2): 613-619.

117[] Y.F. Huang, Y.H. Huang. Identification of produced powerful radicals involved in the

mineralization of bisphenol A using a novel UV-$Na_2S_2O_8$/H_2O_2-Fe(II, III) two-stage oxidation process. Journal of Hazardous Materials, 2009, 162(2-3): 1211-1216.

118[] G.P. Anipsitakis, D.D. Dionysiou. Radical Generation by the Interaction of Transition Metals with Common Oxidants. Environmental Science & Technology, 2004, 38(13): 3705-3712.

119[] C.J. Liang, Z.S. Wang, N. Mohanty. Influences of carbonate and chloride ions on persulfate oxidation of trichloroethylene at 20℃. Science of the Total Environment, 2006, 370(2-3): 271-277.

120[] Y.F. Ji, C. Ferronato, A. Salvador, X. Yang, J.M. Chovelon. Degradation of ciprofloxacin and sulfamethoxazole by ferrous-activated persulfate: Implications for remediation of groundwater contaminated by antibiotics. Science of The Total Environment, 2014, 472(15): 800-808.

121[] J. Zhao, Y. Zhang, X. Quan, Y. Zhao. Sodium Peroxydisulfate Activation by Heat and Fe(II) for the Degradation of 4-CP. Environmental Science, 2010, 31(5): 1233-1238. (CNKI)

122[] W. Zhen, X. Yang, J. Zhang, C. Zhang, L. Kong. Oxidation of As (Ⅲ) by Fe(II)/$K_2S_2O_8$. Environmental Science & Technology, 2007, 11: 41-42-57. (CNKI)

123[] Y.Q. Zhang, W.L. Huang, D.E. Fennell. In situ chemical oxidation of aniline by persulfate with iron(II) activation at ambient temperature. Chinese Chemical Letters, 2010, 21(8): 911-913.

124[] C.J. Liang, C.J. Bruell, M.C. Marley, K.L. Sperry. Persulfate oxidation for in situ remediation of TCE.II. Activated by chelated ferrous ion. Chemosphere, 2004, 55(9): 1225-1233.

125[]J. Zhang, X. Yang. Degradation of Diuron by Citric Acid-Fe(II)/$K_2S_2O_8$ in Slurry System. Environmental Protection Science, 2009, 35(1): 61-63. (CNKI)

126[] C.J. Liang, C.P. Liang, C.C. Chen. pH dependence of persulfate activation by EDTA/Fe(III) for degradation of trichloroethylene[J]. Journal of Contaminant Hydrology, 2009, 106(3-4): 173-182.

127[] http://www.chemicalbook.cn/ChemicalProductProperty_CN_CB1854749.htm

128[] B. Wu, J. Shen, H. Li, J. Feng. SYNTHESIS OF p-tert-BUTYLPHENOL OVER SUPPORTED HYDROGEN FLUORIDE/USY CATALYST. ,Speciality Petrochemicals, 2008, 25(2): 5-8. (CNKI)

129[] R.J. Kavlock. Overview of endocrine disruptor research activity in the United States. Chemosphere, 1999, 39(8): 1227-1236

130[] T. Colborn, D. Dumanoski, J.P. Myers. Our Stolen Future. Plume/Penguin Book: New York, 1996.

131[] USEPA． Special report on environmental endocrine disruption: An effects assessment and analysis． Washington D C:Environmental Protect Agency,1997．

132[] F. Li, Y. Jiang, L. Yao, Z. Li, L. Wang, Y. Zhan. The main species and pollution of environmental hormones in water. Chinese Fishery Quality and Standards, 2013, 3(1): 44-50. (CNKI)

133[] T.E. Haavisto, N.A. Adamssona, S.A. Myllymäki, J. Toppari, J. Paranko. Effects of 4-tert-octylphenol, 4-tert-butylphenol, and diethylstilbestrol on prenatal testosterone surge in the rat. Reproductive Toxicology, 2003, 17(5): 593-605.

134[] S. Myllymäki, T. Haavisto, M. Vainio, J. Toppari, J. Paranko. In vitro effects of diethylstilbestrol, genistein, 4-tert-butylphenol, and 4-tert-octylphenol on steroidogenic activity of isolated immature rat ovarian follicles. Toxicology and Applied Pharmacology, 2005, 204(1): 69-80.

135[] A.V. Barse, T. Chakrabarti, T.K. Ghosh, A.K. Pal, S.B. Jadhao. One-tenth dose of LC_{50} of 4-tert-butylphenol causes endocrine disruption and metabolic changes in *Cyprinus carpio*. Pesticide Biochemistry and Physiology, 2006, 86(3): 172-179.

136[] M. Fu. Distribution Characteristics of Alkylphenols in Coastal and Estuary Environment and the Ecological Risk Assessme. Qingdao: Ocean University of China, 2007: 60-61.

137[]G. Xue, C. Yao. 4-alkylpheno is Determination by GC /MS and its Water Pollution in Nanjing Section of Yangtze River. ENVIRONMENTAL SCIENCE AND MANAGEMENT, 2010, 35(6): 116-118. (CNKI)

138[]Z. Shao. Detection and Distribution of Phenolic in the organisms and Sediments of the Yellow Sea coast. Dalian: Dalian Maritime University, 2011: 37, 46.

139[] T. Tsuda, K. Suga, E. Kaneda, M. Ohsuga. Determination of 4-nonylphenol, nonylphenol

monoethoxylate, nonylphenol diethoxylate and other alkylphenols in fish and shellfish by high-performance liquid chromatography with fluorescence detection. Journal of Chromatography B: Biomedical Sciences and Applications, 2000, 746(2): 305-309.

140[] C. Uguz, I. Togan, Y. Eroglu, I. Tabak, M. Zengin, M. Iscan. Alkylphenol concentrations in two rivers of Turkey. Environmental Toxicology and Pharmacology, 2003, 14(1-2): 87-88.

141[] K. Inoue, Y. Yoshie, S. Kondo, Y. Yoshimura, H. Nakazawa. Determination of phenolic xenoestrogens in water by liquid chromatography with coulometric-array detection. Journal of Chromatography A, 2002, 946(1-2): 291-294.

142[] R.A. Rudel, D.E. Camann, J.D. Spengler, L.R. Korn, J.G. Brody. Phthalates, Alkylphenols, Pesticides, Polybrominated Diphenyl Ethers, and Other Endocrine-Disrupting Compounds in Indoor Air and Dust. Environmental Science & Technology, 2003, 37(20): 4543-4553.

143[] C. Basheer, H.K. Lee. Analysis of endocrine disrupting alkylphenols, chlorophenols and bisphenol-A using hollow fiber-protected liquid-phase microextraction coupled with injection port-derivatization gas chromatography-mass spectrometry. Journal of Chromatography A, 2004, 1057(1-2): 163-169.

144[] R.A. Rudel, S.J. Melly, P.W. Geno, G. Sun, J.G. Brody. Identification of Alkylphenols and Other Estrogenic Phenolic Compounds in Wastewater, Septage, and Groundwater on Cape Cod, Massachusetts. Environmental Science & Technology, 1998, 32(7): 861-869.

145[] C.G. Campbell, S.E. Borglin, F.B. Green, A. Grayson, E. Wozei, W.T. Stringfellow. Biologically directed environmental monitoring, fate, and transport of estrogenic endocrine disrupting compounds in water: A review. Chemosphere, 2006, 65(8): 1265-1280.

146[] M.I.H. Helaleh, S. Fujii, T. Korenaga. Column silylation method for determining endocrine disruptors from environmental water samples by solid phase micro-extraction. Talanta, 2001, 54 (6): 1039-1047.

147[] L. Wang, Y. Yu, H. Zhuang. Flow Injection Chemiluminescence Determination of p-tert-butylphenol with Luminol-H_2O_2. Water Purification Technology, 2006, 25(3): 68-70. (CNKI)

148[] A. Shibata, Y. Inoue, A. Katayama. Aerobic and anaerobic biodegradation of phenol derivatives in various paddy soils. Science of The Total Environment, 2006, 367(2-3): 979-987.

149[] Y. Ogata, T. Toyama, N. Yu, X. Wang, K. Sei, M. Ike. Occurrence of 4-tert-butylphenol (4-t-BP) biodegradation in an aquatic sample caused by the presence of Spirodela polyrrhiza and isolation of a 4-t-BP-utilizing bacterium. Biodegradation, 2013, 24(2): 191-202.

150[] V. Církva, J. Kurfürstová, J. Karban, M. Hájek. Microwave photochemistry III: Photochemistry of 4-tert-butylphenol. Journal of Photochemistry and Photobiology A: Chemistry, 2005, 174(1): 38-44.

151[] R. Li, N. Gao, B. Xu, J. Cao, L. Hu, L. Le. Removal of BP by UV/H_2O_2/Micro-aeration united use technique. China Environmental Science, 2007, 27(2): 160-164. (CNKI)

152[] X. Sun, N. Gao, B. Xu, X. Wang, R. Ning, S. Liu. Kinetics of Endocrine Disrupting Chemical 4-tert- butylphenol During Chlorination in Aqua. Environmental Science, 2007, 28(7): 1483-1489. (CNKI)

153[] D. Dulin, T. Mill. Development and evaluation of sunlight actinometers. Environmental science & technology, 1982, 16(11): 815-820.

154[] http://en.wikipedia.org/wiki/Quantum_yield

155[] http://en.wikipedia.org/wiki/Beer–Lambert_law

156[] O. Abida, G. Mailhot, M. Litter, M. Bolte. Impact of iron-complex (Fe(III)-NTA) on photoinduced degradation of 4-chlorophenol in aqueous solution. Photochemical & Photobiological Sciences, 2006, 5: 395-402.

157[] L. Huang, L. Li, W.B. Dong, Y. Liu, H.Q. Hou. Removal of Ammonia by OH Radical in Aqueous Phase. Environmental Science & Technology, 2008, 42(21): 8070-8075.

158[] C. George, J.M. Chovelon. A laser flash photolysis study of the decay of SO_4^- and Cl_2^- radical anions in the presence of Cl^- in aqueous solutions. Chemosphere, 2002, 47(4): 385-393.

159[] A.L. Lazrus, G.L. Kok, S.N. Gitlin, J.A. Lind, S.E. McLaren. Automated fluorimetric method for hydrogen peroxide in atmospheric precipitation. Analytical chemistry, 1985, 57(4): 917-922.

160[] G.G. Guilbault, P.J. Brignac Jr., M. Juneau. Substrates for the fluorometric determination of oxidative enzymes. Analytical chemistry, 1968, 40(8): 1256-1263.

161[] G.L. Kok, K. Thompson, A.L. Lazrus, S.E. McLaren. Derivatization Technique for the Determination of Peroxides in Precipitation. Analytical chemistry, 1986, 58(6): 1192-1194.

162[] L.L. Stookey. Ferrozine: a new spectrophotometric reagent for iron. Analytical chemistry, 1970, 42(7): 779-781.

163[] B.S. Berlett, R.L. Levine, P.B. Chock, M. Chevion, E.R. Stadtman. Antioxidant activity of ferrozine-iron-amino acid complexes. Proceedings of the National Academy of Sciences of the United States of America, 2001, 98(2): 451-456.

164[]http://www.wpi.edu/academics/cbc/General/jobsmethod.html

165[] P. Job. Formation and stability of inorganic complexes in solution. Annali di Chimica Applicata, 1928, 9(10): 113-203.

166[] C.Y. Huang. Determination of Binding Stoichiometry by the Continuous Variation Method: The Job Plot. Methods in Enzymology, 1982, 87, 509-525.

167[] Z.D. Hill, P. MacCarthy. Novel approach to Job's method: An undergraduate experiment. Journal of Chemical Education, 1986, 63(2), 162.

168[]http://en.wikipedia.org/wiki/Chemical_kinetics

169[] P.C. Vandevivere, H. Saveyn, W. Verstraete, T.C.J. Feijtel, D.R. Schowanek. Biodegradation of Metal-[S,S]-EDDS Complexes. Environmental Science & Technology, 2001, 35(9), 1765-1770.

170[] M. Oramaa, H. Hyvönena, H. Saarinen, R. Aksela. Complexation of [S,S] and mixed stereoisomers of N,N′-ethylenediaminedisuccinic acid (EDDS) with Fe(III), Cu(II), Zn(II) and Mn(II) ions in aqueous solution. Journal of the Chemical Society, Dalton Transactions, 2002, 24: 4644-4648.

171[] B. H. J. Bielski, D. E. Cabelli, R. L. Arudi, A. B. Ross. Reactivity of HO2/O2- Radicals in Aqueous Solution. Journal of Physical and Chemical Reference Data, 1985, 14:1041-1100.

172[] F. Haber, J. Weiss. The Catalytic Decomposition of Hydrogen Peroxide by Iron Salts[J].

Proceedings of the Royal Society of London A, 1934, 147(861): 332-351.

173[] W. G. Rothschild, A. O. Allen. Studies in the Radiolysis of Ferrous Sulfate Solutions: III. Air-Free Solutions at Higher pH. Radiation Research, 1958, 8(2): 101-110.

174[] G. G. Jayson, B. J. Parsons, A. J. Swallow. Oxidation of ferrous ions by perhydroxyl radicals. Journal of the Chemical Society, Faraday Transactions 1, 1973, 69: 236-242.

175[] J. D. Rush, B. H. J. Bielski. Pulse radiolytic studies of the reactions of HO_2/O_2^- with Fe(II)/Fe(III) ions. The reactivity of HO_2/O_2^- with ferric ions and its implication on the occurrence of the Haber-Weiss reaction. Journal of physical chemistry, 1985, 89(23): 5062-5066.

176[] J. Li. 17β-estradiol degradation photoinduced by iron complex, clay and iron oxide minerals: effect of the iron complexing agent ethylenediamine-N-N'-disuccinic acid. Aubiere: University Blaise Pascal, 2010: 78.

177[] G. V. Buxton, C. L. Greenstock, W. P. Helman, A. B. Ross. Critical Review of rate constants for reactions of hydrated electrons, hydrogen atoms and hydroxyl radicals ($^{\bullet}OH$ /$^{\bullet}O^-$) in Aqueous Solution. Journal of physical and chemical reference data, 1988, 17(2): 513-886

178[] M. Roder, L. Wojnarovits, G. Foldiak, S.S. Emmi, G. Beggiato, M. D'Angelantonio. Addition and elimination kinetics in OH radical induced oxidation of phenol and cresols in acidic and alkaline solutions. Radiation Physics and Chemistry, 1999, 54(5): 475-479.

179[] J.M. Kesselman, O. Weres, N.S. Lewis, M.R. Hoffmann. Electrochemical Production of Hydroxyl Radical at Polycrystalline Nb-Doped TiO_2 Electrodes and Estimation of the Partitioning between Hydroxyl Radical and Direct Hole Oxidation Pathways. The Journal of Physical Chemistry B, 1997, 101(14): 2637-2643.

180[] R. A. Torres, C. Pétrier, E. Combet, F. Moulet, C. Pulgarin. Bisphenol A mineralization by integrated ultrasound-UV-iron (II) treatment. Environmental Science & Technology, 2007, 41(1): 297-302.

181[] W. Huang, M. Brigante, F. Wu, K. Hanna, G. Mailhot. Development of a new homogenous photo-Fenton process using Fe(III)-EDDS complexes. Journal of Photochemistry and Photobiology

A, 2012, 239(1): 17-23

182[] G. Mailhot, L. Hykrdova, J. Jirkovsky, K. Lemr, G. Grabner, M. Bolte. Iron(III)-photoinduced degradation of 4-chloroaniline in aqueous solution. Applied Catalysis B: Environmental, 2004, 50(1): 25-35.

183[] H. Mestankova, G. Mailhot, J. F. Pilichowski, J. Krysa, J. Jirkovsky, M. Bolte. Mineralisation of Monuron photoinduced by Fe(III) in aqueous solution. Chemosphere, 2004, 57(10): 1307-1315.

184[] X.X. Jiang, Y.L. Wu, P. Wang, H.J. Li, W.B. Dong. Degradation of bisphenol A in aqueous solution by persulfate activated with ferrous ion. Environmental Science and Pollution Research, 2013, 20: 4947-4953.

185[] R. Woods, I.M. Kolthoff, E.J. Meehan. Arsenic(IV) as an intermediate in the induced oxidation of Arsenic(III) by the Iron(II)-persulfate reaction and the photoreduction of Iron(III). I. Absence of oxygen. Journal of the American Chemical Society, 1963, 85(16): 2385-2390.

186[] X.R. Xu, Z.Y. Zhao, X.Y. Li, J.D. Gu. Chemical oxidative degradation of methyl tert-butyl ether in aqueous solution by Fenton's reagent. Chemosphere, 2004(55): 73-79.

187[] W. Huang. Homogeneous and heterogeneous Fenton and photo-Fenton processes: Impact of iron complexing agent EDDS. Wuhan: Wuhan University, 2012: 61.

188[] A. Stefánsson, Iron(III) hydrolysis and solubility at 25℃. Environmental science & technology, 2007(41): 6117-6123.

189[] W. J. Mcelroy, S. J. Waygood. Kinetics of the reactions of the SO_4^- radical with SO_4^-, $S_2O_8^{2-}$, H_2O and Fe^{2+}. Journal of the Chemical Society, Faraday Transactions, 1990, 86(14): 2557-2564.

190[] P. Neta, R.E. Huie, A.B. Ross. Rate constants for reactions of inorganic radicals in aqueous solution. Journal of Physical and Chemical Reference Data, 1988, 17(3): 1027-1084.

191[] C.J. Liang, C.J. Bruell, M.C. Marley, K.L. Sperry. Persulfate oxidation for in situ remediation of TCE. I. Activated by ferrous ion with and without a persulfate-thiosulfate redox couple. Chemosphere, 2004, 55(9): 1213-1223.

192[] E. Heckel, A. Henglein, G. Beck. Pulsradiolytische Untersuchung des Radikalanions SO_4^-.

Berichte der Bunsengesellschaft für physikalische Chemie, 1966, 70(2): 149-154.

193[] E. Hayon, J. J. McGarvey. Flash photolysis in the vacuum ultraviolet region of SO_4^{2-}, CO_3^{2-}, and OH^- ions in aqueous solutions. The Journal of Physical Chemistry, 1967, 71(5): 1472-1477.

194[] H. P. Schuchmann, D. J. Deeble, G. Olbrich, C. Von Sonntag. The $SO_4^{\cdot -}$ induced chain reaction of 1, 3-dimethyluracil with peroxodisulphate. International Journal of Radiation Biology, 1987, 51(3): 441-453.

195[] I. Kraljić. Photolytic determination of SO_4^- rate constants. International Journal for Radiation Physics and Chemistry, 1970, 2(2): 59-68.

196[] E. Hayon, L. Dogliotti. Transient species produced in the photochemical decomposition of ceric salts in aqueous solution. Reactivity of NO_3 and HSO_4 free radicals. The Journal of Physical Chemistry, 1967, 71(18): 3802-3808.

197[] J. L. Redpath, R. L. Willson. Chain reactions and radiosensitization: Model enzyme studies. International Journal of Radiation Biology, 1975, 27(4): 389-398.

198[] E. Hayon, A. Treinin, J. Wilf. Electronic spectra, photochemistry, and autoxidation mechanism of the sulfite-bisulfite-pyrosulfite systems. SO_2^-, SO_3^-, SO_4^-, and SO_5^- radicals. Journal of the American Chemical, 1972, 94(1): 47-57.

199[] C.L. Clifton, R.E. Huie RE. Rate constants for hydrogen abstraction reactions of the sulfate radicals, $SO_4^{\cdot -}$ alcohols. International Journal of Chemical Kinetics, 1989, 21(8):677-687.

200[] H. Kusic, I. Peternel, S. Ukic, N. Koprivanac, T. Bolanca, S. Papic, A. Bozic. Modeling of iron activated persulfate oxidation treating reactive azo dye in water matrix. Chemical Engineering Journal, 2011, 172(1):109-121.

201[] Y.F. Huang, Y.H. Huang. Behavioral evidence of the dominant radicals and intermediates involved in bisphenol A degradation using an efficient Co^{2+}/PMS oxidation process. Journal of Hazardous Materials, 2009b, 167(1-3):418-426.

202[] P. Neta, V. Madhavan, H. Zemel, R.W. Fessenden. Rate constants and mechanism of reaction of $SO_4^{\cdot -}$ with aromatic compounds. Journal of the American Chemical Society, 1977, 99(1):163-

164.

203[] C. Walling, D.M. Camaioni. Aromatic hydroxylation by peroxydisulfate. Journal of the American Chemical Society, 1975, 97(6):1603-1604.

204[] M. Roger, T. Sabrine, C. Serge, B. Stéphane. Removal of carbamazepine from urban wastewater by sulfate radical oxidation. Environmental Chemistry Letters, 2011, 9(3):347-353.